8-2005

Geochemical Investigations of Ordinary Chondrites, Shergottites, and Hawaiian Basalts

Valerie Slater Reynolds
University of Tennessee - Knoxville

To the Graduate Council:

I am submitting herewith a dissertation written by Valerie Slater Reynolds entitled "Geochemical Investigations of Ordinary Chondrites, Shergottites, and Hawaiian Basalts." I have examined the final electronic copy of this dissertation for form and content and recommend that it be accepted in partial fulfillment of the requirements for the degree of Doctor of Philosophy, with a major in Geology.

Harry Y. McSween, Major Professor

We have read this dissertation and recommend its acceptance:

Larry Taylor, Ted Labotka, Craig Barnes

Accepted for the Council:
Dixie L. Thompson

Vice Provost and Dean of the Graduate School

(Original signatures are on file with official student records.)

To the Graduate Council:

I am submitting herewith a dissertation written by Valerie Slater Reynolds entitled "Geochemical Investigations of Ordinary Chondrites, Shergottites, and Hawaiian Basalts." I have examined the final electronic copy of this dissertation for form and content and recommend that it be accepted in partial fulfillment of the requirements for the degree of Doctor of Philosophy, with a major in Geology.

Harry Y. McSween, Jr.
Major Professor

We have read this dissertation
and recommend its acceptance:

Larry Taylor

Ted Labotka

Craig Barnes

Acceptance for the Council:

Anne Mayhew
Vice Chancellor and Dean
of Graduate Studies

(Original signatures are on file with official student records.)

GEOCHEMICAL INVESTIGATIONS OF ORDINARY CHONDRITES, SHERGOTTITES, AND HAWAIIAN BASALTS

A Dissertation
Presented for the
Doctorate of Philosophy Degree
The University of Tennessee, Knoxville

Valerie Slater Reynolds
August 2005

DEDICATION

This dissertation is dedicated to the most important people in my life: my husband and soul mate, Joshua Reynolds, and my daughter, Sierra Grace. Knowingly or unknowingly, they have taught me lessons about love and life that I will never forget. For that, and for all their smiles and hugs, I am forever thankful.

ACKNOWLEDGEMENTS

Completion of this degree would not have been possible without the financial support and guidance provided by my Advisor, Dr. Hap McSween. Additional financial support was provided by the Department of Earth and Planetary Sciences. I would like to thank my dissertation committee members Drs. Larry Taylor, Ted Labotka, and Craig Barnes for their support, and for taking the time during the summer to attend my dissertation defense. Dr. Jeff Ryan at the University of South Florida and Dr. Bill McDonough at the University of Maryland also contributed to this degree through the use of their geochemical laboratories and financial support. I would like to acknowledge the department secretaries for all the tasks they perform for graduate students that help with travel arrangements and manuscript submittal. Finally, I hope fellow graduate students Karen Stockstill, Tabbatha Cavendish, and Kathleen Lordo (and many others) realize my appreciation for their moral support during difficult times.

ABSTRACT

Part I: Quantifying peak temperatures achieved during metamorphism is critical for understanding the thermal histories of ordinary chondrite parent asteroids. I performed two-pyroxene geothermometry, using QUILF95, on the *same* Type 6 chondrites for which peak temperatures were estimated using the plagioclase geothermometer. Pyroxenes record a narrow, overlapping range of temperatures in H6 (865-926°C), L6 (812-934°C), and LL6 (874-945°C) chondrites. Lower plagioclase temperature estimates may not reflect peak metamorphic temperatures because chondrule glass probably recrystallized to plagioclase prior to reaching the metamorphic peak. The average temperature for H, L, and LL chondrites (~900°C) is at least 50°C lower than peak temperatures used in current asteroid thermal evolution models, which may require minor adjustments.

Part II: The light lithophile elements lithium, beryllium, and boron have been used successfully to indicate recycled crust or fluids derived from recycled crust in the source regions of island arc lavas. Radiogenic isotopes and other geochemistry of Mauna Kea lavas and Martian basalts (basaltic shergottites) suggest their source regions may contain a crustal component. The goal of this study is to determine whether Li, Be, and B indicate the presence of a crustal component in the source regions of Mauna Kea and Martian basalts and whether it was altered at low temperatures.

Mauna Kea: Although several samples show effects of alteration, our results suggest Li (3.9±0.9 ppm) and Be (0.47±0.09 ppm) preserve mantle compositions. In contrast, highly variable B/K ratios (0.0002-0.008) and B/Be ratios (1-25) suggest post-magmatic alteration has destroyed the mantle B signature. When examined with depth, Li and Be abundances increase in the uppermost portion of the core, in late main shield and post-shield samples, and correspond to decreasing degrees of partial melting as the volcano moved off the plume's center. Li and Be appear to be well mixed in the Hawaiian source region as evidenced by the lack of correlation between Li/Yb or Be/Nd

ratios and Pb isotopes or Nb/Zr ratios, which were previously used to identify geochemically distinct Mauna Kea lava groups. Such mixing probably also accounts for the lack of any crustal signature when Li/Yb or Be/Nd are compared with O isotopes. These elements do not appear to vary on the timescale of Hawaiian shield development, possibly reflecting the efficiency with which these elements are homogenized in the mantle.

Martian basalts: Although terrestrial alteration minerals (caliche) in Dhofar 019 apparently affected the primary Li and Be concentrations, the remaining basaltic shergottites contain Be (0.09-0.77 ppm) abundances similar to mid-ocean ridge basalts or ocean island basalts, whereas Li abundances (2.7-9.9 ppm) are slightly higher compared to these reservoirs. On diagrams of Li/Yb vs. Dy/Yb and K/Li vs. La/Yb, basaltic shergottites define trends similar to IAB, which are attributed to altered oceanic crust in the IAB source regions. However, the correlation between Li or Be and $\delta^{18}O$ for basaltic shergottites is weak, and $\delta^{7}Li$ values measured in two geochemically distinct basaltic shergottites, Zagami (+3.97‰) and EETA79001 (+4.37‰), are identical within error. Therefore, although the Martian assimilant appears to be enriched in Li and possibly Be, it either was not altered at low temperatures or the proportion of altered material in basaltic shergottite magmas is too small to be resolved using these crustal indicators.

TABLE OF CONTENTS

LIST OF TABLES

Table Page

LIST OF FIGURES

Figure Page

PART I

Introduction

This dissertation is divided into Parts that describe each component of my research. Part II summarizes my work on peak metamorphic temperatures recorded by ordinary chondrites. Chondrite meteorites are named for their most abundant component, *chondrules*, which are spherical in their unaltered state and consist primarily of magnesian olivine and low-calcium pyroxene with interstitial feldspathic glass. Chondrules are set in a mineralogically similar matrix that also contains Fe-Ni metal (kamacite and taenite), sulfides, and refractory (calcium-aluminum) inclusions. Chondrules contain some of the oldest and most primitive material from the solar system, and although their origin is complex, they appear to have experienced at least one melting event (and therefore display igneous textures) that occurred after nebular condensation (Wasson, 1993). Chondrites are divided into three *Classes*, one of which is the ordinary chondrites, which are identified by their unique oxygen isotope and bulk compositions (Clayton, 1993). Ordinary chondrites are further subdivided into three *Groups* (H, L, and LL) based primarily on variations in oxidation state (Rubin et al., 1988). The most reduced group is the H-chondrites, which contains the highest bulk Fe/FeO ratio and the highest Fe/Fe+Mg ratios in olivines and pyroxenes. LL-chondrites are the most oxidized group as evidenced by the lowest bulk Fe/FeO ratio and lower Fe/Fe+Mg ratios in olivines and pyroxenes. L-chondrites are between these two end-members. The differences among these groups suggest the H, L, and LL chondrites originated from three separate parent asteroids. Each of these groups is further divided into petrologic *Types* based on the type and degree of secondary processing that occurred after asteroid accretion (Van Schmus and Wood, 1967). Type 3 ordinary chondrites are unaltered and represent primary mineral compositions and textures. The effects of aqueous alteration observed in carbonaceous chondrites increase from Type 2 to Type 1. Ordinary chondrites did not experience aqueous alteration, but the heat produced by the decay of short-lived radionuclides (e.g. Al^{26}) resulted in a range of metamorphic conditions that are preserved in Type 4 through Type 6 chondrites.

The ordinary chondrite parent bodies, like most asteroids, are probably loosely consolidated and fragmented. There are two models, however, that have been proposed to explain the internal structure of these fragmented parent bodies. In the layered internal structure (i.e. onion shell) model, an asteroid initially concentrically zoned from unaltered (Type 3) material on the surface to highly metamorphosed (Type 6) material in the interior was bombarded and fragmented, but retained its primary metamorphic structure (Pellas and Fieni, 1988; Lipschutz et al., 1989). The fragmentation and assembly (i.e. rubble pile) model suggests that asteroids with an initial concentrically zoned structure fragmented and reassembled, which resulted in a disrupted metamorphic profile (Taylor et al., 1987). In H chondrites, Pu fission track densities in whitlockite were observed to increase with increasing metamorphic grade (Pellas and Fieni, 1988), and in unshocked H chondrites, metallographic cooling rates were observed to increase with decreasing metamorphic type (Lipschutz et al., 1989). Both of these observations support the layered internal structure model, which will be the framework for this study.

Ordinary chondrites that experienced the highest metamorphic grade (Type 6) are useful indicators of the peak temperatures reached in the interiors of asteroids during metamorphism, and the time interval over which these temperatures were maintained. However, the simple mineralogy of ordinary chondrites limits the applicability of many geothermometers commonly used in terrestrial metamorphic rocks. Therefore, this manuscript provides an assessment of previous peak temperature estimates and provides new estimates for peak metamorphic conditions experienced by the parent asteroids of Type 6 H, L, and LL chondrites.

Part III of this dissertation discusses how the light lithophile elements lithium, beryllium, and boron behave in basalts from Earth (i.e. the Mauna Kea volcano). Most active volcanoes on Earth are located at divergent or convergent lithospheric plate boundaries where regions of the mantle melt to produce mid-ocean ridge or arc basalts. Hawaiian volcanoes are known as intra-plate, or ocean island, volcanoes because they are

located within the interior of the Pacific plate, thousands of miles from the nearest plate boundary. Hawaiian volcanoes form on the Pacific plate as it passes over a stationary magma source (i.e. mantle plume or hot spot) that originates at the core-mantle boundary (Perfit and Davidson, 2000). As the plume ascends through the mantle, surrounding lower and upper mantle material becomes entrained in the outer portions of the plume, whereas the interior of the plume retains its primitive geochemical signature (Griffiths and Campbell, 1990, 1991; Griffiths, 1991; Hauri et al., 1994). As a result, the compositions of Hawaiian lavas vary as the volcano passes over and samples different regions of the underlying, compositionally zoned mantle plume (Kurz et al., 1996; Lassiter et al., 1996).

The recently acquired drill core from Phase 2 of the Hawaii Scientific Drilling Project consists of approximately 3,000 meters of continuous lava flows from the Mauna Kea volcano, which is located on the main island of Hawaii. Preserved as the most complete sample collection from any single intra-plate volcano, the HSDP-2 Mauna Kea lava flows represent ~400 kyr of eruptive history, nearly half of the volcano's lifespan of ~1 Myr (Stolper et al., 1996). The HSDP-2 drill core provides the first opportunity to study spatial heterogeneities of the Hawaiian mantle plume via geochemical variations of Mauna Kea lavas. In this chapter, we summarize the geochemical structure of the Hawaiian plume and examine how the light lithophile elements lithium, beryllium, and boron vary within Mauna Kea lavas. We also address whether these elements can be used to identify geochemically distinct components in the source region for Mauna Kea magmas.

Part IV of this dissertation compares the behavior of lithium, beryllium, and boron in basalts from Mars (i.e. basaltic shergottites) to those from Mauna Kea and other terrestrial oceanic magmatic environments. Basaltic shergottites are a subgroup of achondritic (i.e. without chondrules) meteorites of Martian origin known as the *S*hergottite-*N*akhlite-*C*hassignite, or SNC, meteorites. The majority of SNC meteorites

are shergottites, which are divided into basalts containing pyroxene and plagioclase and lherzolites containing pyroxene-olivine cumulates. Nakhlites consist of clinopyroxene cumulates, and the Chassignite group was defined by only one dunite (Chassigny) until another dunite, Northwest Africa 2737, was found in 2000. The meteorite Allan Hills 84001 is an orthopyroxene cumulate that does not fit into the "SNC" classification scheme. As a result, the term "Martian" has been proposed to replace "SNC" (Mittlefehldt, 1994).

SNC meteorites were first identified as a unique group by their oxygen isotopic compositions and young crystallization ages. Although Allan Hills 84001 has a crystallization age similar to most meteorites (~4.5 Gyr), the remaining SNC meteorites are much younger (1.3 Ga to 0.17 Gyr) (Clayton, 1989; McSween, 2002 and references therein). Such young crystallization ages require a parent body large enough to retain the amount of heat necessary to support igneous activity for an extended time period. Mars became the most likely candidate as the parent body for the SNC meteorites because it was large enough to sustain igneous activity to ≤1.3 Ga, and Martian soils measured by the Viking lander were compositionally similar to the type shergottite, Shergotty (Wood and Ashwal, 1981). Definitive evidence for a Martian origin for the SNC meteorites, however, was provided by Bogard and Johnson (1985) who measured trapped noble gases in shock-produced glass in the basaltic shergottite Elephant Morraine (EETA) 79001. Gas compositions measured in EETA79001 were nearly identical to Martian atmospheric compositions measured by the Viking lander. These authors suggested the gas could have been implanted into the meteorite during the impact event that ejected this sample from Mars.

Since the general acceptance of their Martian origin, the SNC meteorites have endured decades of meticulous scrutiny for any information related to interior (lithospheric) or surficial (atmospheric, hydrospheric, or biologic) processes on Mars. Systematic geochemical relationships observed among the basaltic shergottites suggest

they represent mixtures of at least two compositionally distinct components. However, the source for one of these components is disputable. In this chapter, we summarize the characteristics and possible source regions of each component. We also examine how the light lithophile elements lithium, beryllium, and boron are distributed among the basaltic shergottites. Finally, we compare the signatures of these elements in basaltic shergottites to those in terrestrial oceanic magmatic systems and discuss the implications these data have for the components' source regions.

PART II

Peak Metamorphic Temperatures in Type 6 Ordinary Chondrites: An Evaluation of Pyroxene and Plagioclase Geothermometry

This Part is revised from the manuscript with same title published in the journal *Meteoritics & Planetary Science* in 2005 by Valerie Slater-Reynolds and Harry Y. McSween, Jr. My responsibilities were data collection and interpretation as well as organization and presentation of the data in manuscript form. McSween provided support during data interpretation and suggested organization revisions for the finished manuscript.

Slater-Reynolds V. and McSween H. Y., Jr. (2005) Peak metamorphic temperatures in type 6 ordinary chondrites: An evaluation of pyroxene and plagioclase geothermometry. *Meteoritics & Planetary Science* (in print).

ABSTRACT

Quantifying peak temperatures achieved during metamorphism is critical for understanding the thermal histories of ordinary chondrite parent asteroids. Various geothermometers have been used to estimate equilibration temperatures for chondrites of the highest metamorphic grade (Type 6), but results are inconsistent and span hundreds of degrees. Because different geothermometers and calibration models were used with different meteorites, it is unclear whether variations in peak temperatures represent actual ranges of metamorphic conditions within Type 6 chondrites or differences in model calibrations. We addressed this problem by performing two-pyroxene geothermometry, using QUILF95, on the *same* Type 6 chondrites for which peak temperatures were estimated using the plagioclase geothermometer (Nakamuta and Motomura, 1999). We also calculated temperatures for published pyroxene analyses from other Type 6 H, L, and LL chondrites to determine the most representative peak metamorphic temperatures for ordinary chondrites. Pyroxenes record a narrow, overlapping range of temperatures in H6 (865-926°C), L6 (812-934°C), and LL6 (874-945°C) chondrites. Plagioclase temperature estimates are 96-179°C lower than pyroxenes in the same Type 6 meteorites. Plagioclase estimates may not reflect peak metamorphic temperatures because chondrule

glass probably recrystallized to plagioclase prior to reaching the metamorphic peak. The average temperature for H, L, and LL chondrites (~900°C), which agrees with previously published oxygen isotope geothermometry, is at least 50°C lower than peak temperatures used in current asteroid thermal evolution models. This difference may require minor adjustments to thermal model calculations.

1. INTRODUCTION

Peak metamorphic temperatures reached within the interiors of ordinary chondrite parent bodies, as well as chronology and cooling rates, are critical input parameters for asteroid thermal evolution models (McSween et al., 2002). Peak temperatures are measured by applying geothermometers to chondrites that experienced the highest metamorphic grade (Petrologic Type 6), as deduced from their re-crystallized textures and mineral equilibration (Van Schmus and Wood, 1967). Current peak temperature estimates for Type 6 H, L, and LL chondrites, based on a variety of geothermometers, span ranges of several hundred degrees, and temperature estimates for lower petrologic types are even less certain. These ranges are probably real, at least in part, because each petrologic type is gradational and includes chondrites metamorphosed over some temperature interval. McSween et al. (1988) attempted to estimate the upper and lower temperature limits for each petrologic type, but such estimates are poorly constrained because of the simple mineral assemblage in metamorphosed ordinary chondrites. Another factor is that the temperature ranges reflect the use of different geothermometers, many of which record blocking temperatures during cooling rather than peak metamorphism.

The most widely used geothermometer for ordinary chondrites is based on Ca exchange between coexisting clinopyroxene and orthopyroxene. The interpretation of pyroxene thermometry is complicated by differing results depending on the calibration used and by apparent disequilibrium between coexisting pyroxenes in many ordinary

chondrites (McSween and Patchen, 1989; Jones, 1997; Gastineau-Lyons et al., 2002). More recently, plagioclase geothermometry, based on Si-Al ordering, has been applied to ordinary chondrites (Nakamuta and Motomura, 1999). This method gives peak metamorphic temperature estimates that differ significantly from pyroxene thermometry. However, pyroxene thermometry and plagioclase thermometry have not been applied to the same specific chondrites, so the measured temperature differences might reflect real variations among Type 6 chondrites. To resolve this problem, we performed two-pyroxene geothermometry (using an improved numerical solution model of Andersen et al., 1993) on the same meteorites previously studied using plagioclase geothermometry. Our new data and an assessment of the various geothermometers used for chondrites suggest that temperatures recorded by pyroxene pairs, as calculated using QUILF95, provide the most accurate estimate of peak metamorphic temperatures. We also recalculated temperatures for published pyroxene analyses of other Type 6 chondrites to obtain the most representative peak metamorphic temperature estimates for the H, L, and LL chondrite parent bodies.

2. EVALUATION OF PREVIOUS PEAK TEMPERATURE ESTIMATES

2.1. Two-Pyroxene Geothermometry

The basis for pyroxene geothermometry is Ca partitioning between co-existing low-Ca (pigeonite or orthopyroxene) and high-Ca (augite) pyroxene. As temperature increases, the Ca content of high-Ca pyroxene decreases while the Ca content of low-Ca pyroxene increases until equilibrium compositions are established. Because geothermometers are thermodynamically based, a fundamental assumption is that both pyroxenes achieved equilibrium. Kretz (1982) constructed a geothermometer using only clinopyroxene because the slope of the solvus in the orthopyroxene region is steep, making it difficult to discern temperature differences graphically. The effect of non-quadrilateral components (i.e. minor elements) on temperature was assumed to be small,

and therefore was not considered. Lindsley's (1983) geothermometer was developed for both orthopyroxenes and clinopyroxenes and incorporated the effects of minor elements. Depending on the model used or the meteorite examined, estimates for peak metamorphic conditions in Type 6 ordinary chondrites vary considerably (Table A-1, all tables in Appendix A).

Olsen and Bunch (1984) estimated peak temperatures for clinopyroxenes in nine H6, eleven L6, and four LL6 chondrites using the Kretz (1982) and Lindsley (1983) two-pyroxene geothermometers. Both models predicted the same peak equilibration temperature for H6 meteorites. Although L6 and LL6 chondrites appear to have equilibrated at similar temperatures, the Kretz (1982) model predicted a higher temperature than the Lindsley (1983) model.

McSween and Patchen (1989) applied the same geothermometers to orthopyroxene-clinopyroxene pairs in three LL6 chondrites. Their results for clinopyroxene were higher than those calculated by Olsen and Bunch (1984) using both models. The Kretz (1982) data were dismissed because estimates exceeded the metal-sulfide eutectic melting temperature. McSween and Patchen (1989) also observed that temperatures estimated by the Lindsley (1983) model for orthopyroxene are 100-200°C lower than those for clinopyroxene in the same meteorite. The cause for such discrepancy is not known, but McSween and Patchen (1989) suggested that, following equilibration of both pyroxenes at peak metamorphic conditions, orthopyroxene may have re-equilibrated to a lower blocking temperature during cooling (Figure B-1a, all figures in Appendix B). As a result, these authors recommended clinopyroxene as a more reliable indicator of peak metamorphic conditions for LL chondrites.

Langenhorst et al. (1995) examined one H6 chondrite for evidence of shock and thermal metamorphism. These authors used the Lindsley (1983) geothermometer to calculate average temperatures for orthopyroxene and clinopyroxene. Although this study

did not focus on geothermometry of ordinary chondrites, it provided the only available orthopyroxene temperature estimate for H6 chondrites.

Jones (1997) measured temperatures recorded by orthopyroxene-clinopyroxene pairs in one LL6 chondrite using the Lindsley (1983) model. Temperatures estimated for orthopyroxenes were generally higher than associated clinopyroxene temperatures, which ranged significantly within the same meteorite. Jones (1997) observed greater variation in minor element abundances in and temperature estimates for clinopyroxenes, and concluded that orthopyroxenes equilibrated faster during prograde metamorphism (Figure B-1b). It is not obvious why clinopyroxenes record lower temperatures in this study, but the unvarying orthopyroxene temperatures estimated by Jones (1997) for Type 4-6 chondrites suggest these could be blocking temperatures rather than peak metamorphic temperatures.

2.2. Oxygen Isotope Thermometry

Oxygen diffusion between olivine, pyroxene, and plagioclase is the basis for oxygen isotope geothermometry in ordinary chondrites. Clayton (1993) used oxygen isotope thermometry to calculate peak temperature estimates for Type 6 H, L, and LL chondrites (Table A-1). Oxygen isotopes record an average peak metamorphic temperature similar to clinopyroxene estimates of McSween and Patchen (1989). The lack of hydrous phases in ordinary chondrites indicates thermal metamorphism occurred under relatively dry conditions. As a result, equilibration temperatures recorded by oxygen isotopes are not susceptible to exchange during retrograde reactions and thus provide potentially robust estimates of peak metamorphic conditions. Unfortunately, isotopic fractionation between these minerals is limited, thereby decreasing their sensitivity to temperature.

2.3. Olivine-Spinel Thermometry

Kessel et al. (2002) applied improved estimates of activities in multicomponent spinels to the thermodynamic model of Sack and Ghiorso (1991) to calculate equilibration temperatures using olivine-spinel pairs in four Type 4, four Type 5, and three Type 6 chondrites (Table A-1). The estimated temperatures are low, reflecting continued Fe-Mg exchange between olivine and spinel during cooling. According to these authors, the limited temperature variation between Types 4-6 chondrites could indicate that metamorphic type is not a function of peak temperature. However, we suspect that the similar (low) equilibration temperatures reflect blocking conditions of Fe-Mg exchange between olivine and spinel on cooling.

2.4. Plagioclase Geothermometry

Disagreement between McSween and Patchen (1989) and Jones (1997), two studies that used the same geothermometer for LL6 chondrites, exemplifies the problem with current pyroxene temperature estimates. Nakamuta and Motomura (1999) avoided this problem by applying a plagioclase geothermometer to six weakly shocked or unshocked Type 6 H, L, and LL chondrites. The plagioclase geothermometer is based on Si-Al ordering within the four tetrahedral sites of the crystal lattice. When plagioclase begins to crystallize from chondrule glass at low temperatures, during prograde metamorphism, Al is concentrated in only one of the four tetrahedral sites. This plagioclase is highly ordered. In plagioclase that crystallizes at progressively higher temperatures, Al is distributed more randomly among the four sites, and Si-Al partitioning becomes progressively more disordered. Slow diffusion rates of Si-Al in plagioclase, especially under dry conditions relevant to ordinary chondrites (Grove et al., 1984), suggest that the degree of order/disorder is locked in at the temperature at which a plagioclase grain crystallizes. Therefore, during prograde metamorphism, a range of

temperatures is recorded by different plagioclase grains in a single meteorite (Figure B-1c).

Nakamuta and Motomura (1999) estimated temperatures for several plagioclase crystals separated from each meteorite. They found that each chondrite contained plagioclase crystals recording a range of temperatures, and they assumed that the highest temperature crystals formed at peak metamorphic conditions. Results for plagioclase are closer to temperatures estimated previously for orthopyroxene in other Type 6 chondrites (McSween and Patchen, 1989; Langenhorst et al., 1995; Jones, 1997), leading Nakamuta and Motomura (1999) to conclude that the lower (orthopyroxene) temperatures are more representative of peak metamorphic conditions. Presumably, the higher clinopyroxene temperatures would be relics of igneous (chondrule melt) conditions.

The validity of plagioclase peak temperatures for Type 6 chondrites rests on an assumption that plagioclase continued to crystallize from chondrule glass through Type 6 conditions. Petrographic observations used to develop the current chondrite classification scheme suggest all chondrule glass crystallized to plagioclase by temperatures associated with Type 5 conditions (Van Schmus and Wood, 1967; Sears et al., 1980). This conclusion is supported by Gastineau-Lyons et al. (2002), who compared the normative and modal abundances of plagioclase in L4-L6 and LL4-LL6 chondrites. They assumed that normative plagioclase abundances predicted for ordinary chondrites represent the maximum amount of plagioclase that could crystallize from available chondrule glass. With progressive metamorphism, the actual (i.e. modal) abundance of plagioclase should increase, eventually approaching the normative abundance. When the modal and normative abundances converge, no further plagioclase crystallization can occur because all available plagioclase components in chondrule glass have recrystallized. These authors observed that the modal and normative abundances of plagioclase converged by Type 5 conditions for LL chondrites and by Type 6 for L chondrites. A similar study by Chamot (2000) did not observe a convergence for H chondrites. Presumably, this

indicates that plagioclase continued to crystallize through Type 6 conditions for H chondrites, suggesting plagioclase temperatures should be representative of peak metamorphic conditions for H6 chondrites. However, the lowest plagioclase temperatures are observed for H6 chondrites, and are the same or less than the minimum temperature predicted by olivine-spinel thermometry. If Si-Al ordering is locked in at the plagioclase crystallization temperature and plagioclase crystallization was complete before Type 6 conditions, then the lower temperatures recorded by plagioclase in Type 6 meteorites may not represent peak metamorphic conditions.

3. ANALYTICAL METHODS

Pyroxene geothermometry was performed on the same six chondrites (Table A-2) for which peak temperatures were estimated for plagioclase by Nakamuta and Motomura (1999). Pyroxene chemical analyses were collected using a Cameca SX-50 electron microprobe at the University of Tennessee. An accelerating voltage of 15 kV was used with a beam current of 30 nA, a beam size of 1 μm, and a counting time of 20 sec for all elements. Average pyroxene compositions for each meteorite were projected onto a temperature-contoured pyroxene quadrilateral (Lindsley 1983) so that temperatures could be compared directly with results from earlier studies. Temperatures were also estimated using QUILF95 (Andersen et al., 1993, modified for Windows in 1995), an updated computer solution model based on Lindsley's (1983) graphical approach. QUILF95 is superior to the Lindsley (1983) graphical method because it eliminates error associated with converting and plotting chemical analyses onto the pyroxene quadrilateral. QUILF95 also incorporates an improved experimental data set for pyroxene equilibrium, and eliminates difficulties associated with discerning temperature differences for orthopyroxene on the quadrilateral due to narrow temperature contours. The error associated with QUILF95 is ±50°C for single temperatures calculated for orthopyroxene-clinopyroxene pairs, but the error can be quite large if the pyroxenes are not in equilibrium. Therefore, we also calculated temperatures for individual pyroxenes by

fixing one pyroxene's composition and allowing the solution model to select an equilibrium composition for the other. The result is a temperature estimate for each pyroxene with no apparent uncertainty because the pyroxene composition chosen by the solution model fits exactly. This process was repeated for the other pyroxene to assess the true temperature difference between orthopyroxenes and clinopyroxenes. All temperature estimates assume a pressure of 1 bar.

4. RESULTS AND DISCUSSION

Average pyroxene analyses are presented in Table A-3, and peak temperature estimates for average pyroxene compositions using Lindsley (1983) and QUILF95 are shown in Table A-4. Plagioclase temperature estimates for the same meteorites (Nakamuta and Motomura, 1999) are shown in Table A-4 for comparison.

The graphical approach of Lindsley (1983) yields temperatures comparable to those determined previously for other Type 6 ordinary chondrites with narrower temperature differences between orthopyroxene and clinopyroxene (25-175°C) within the same meteorite. Using QUILF95, pyroxene pairs provide generally higher temperature estimates than the Lindsley (1983) model with reasonable errors ($\leq \pm 75$°C). When temperatures were calculated for individual pyroxenes, the difference between orthopyroxene and clinopyroxene (15-75°C) is even less than that determined graphically, reflecting the improved calibration of QUILF95. Our results for pyroxene pairs are 96-179°C higher than those for plagioclase Si-Al ordering in the same Type 6 meteorites (Nakamuta and Motomura, 1999). Results are summarized in Figure B-2.

4.1 Effect of Analytical Uncertainty on Temperature Estimates

Temperatures calculated for Type 6 chondrites using average pyroxene analyses provide reliable estimates with reasonable errors. However, the calculated error reflects

how well the pyroxene compositions fit the model, and does not account for error introduced by analytical uncertainty. To determine the maximum temperature range expected due to analytical uncertainty, we calculated two temperatures for each meteorite. Minimum temperatures were determined by increasing and decreasing the CaO content (the calibration is most sensitive to this component) an amount equal to 1 sigma (σ) standard deviation in clinopyroxene and orthopyroxene, respectively. Maximum temperatures were calculated by decreasing and increasing the CaO content 1σ standard deviation in clinopyroxene and orthopyroxene, respectively. The temperature range associated with analytical uncertainty was then compared with the temperature range calculated for each meteorite using average pyroxene compositions (Table A-4). The calculated temperature range using average pyroxene analyses encompasses the temperature range expected due to analytical uncertainty for all meteorites.

4.2. Pyroxene Equilibrium in Type 6 Chondrites

Peak metamorphic temperatures determined by two-pyroxene thermometry are reliable only if both pyroxenes attained chemical equilibrium during metamorphism. Previous studies concluded that pyroxene compositions in Type 6 chondrites represent disequilibrium conditions because temperatures recorded by orthopyroxene and clinopyroxene within the same meteorite differ by 100-200°C using Lindsley's (1983) graphical method. The narrower range of temperatures recorded by orthopyroxenes and clinopyroxenes in this study using both the Lindsley (1983) and QUILF95 models suggest pyroxenes in these meteorites are closer to equilibrium assemblages. However, rare clinopyroxenes in Holbrook and Dhurmsala contain a jadeite component that influences the estimated temperatures for these meteorites. If these analyses are considered, the individual clinopyroxene temperatures increase to 1017°C for Holbrook and 1012°C for Dhurmsala. The effect of these clinopyroxenes on pyroxene pair estimates is minimal (Holbrook 922°C; Dhurmsala 925°C). The effect of high alumina contents in pyroxenes on temperature estimates is consistent with that observed by

Lindsley (1983). Despite these rare clinopyroxenes, peak temperatures estimated using both pyroxenes are reliable and suggest that near-equilibrium assemblages are preserved in Type 6 ordinary chondrites.

4.3. Evaluation of Temperatures above the Metal-Sulfide Eutectic Melting Point

The jadeite-rich clinopyroxenes in Holbrook and Dhurmsala record temperatures that exceed the metal-sulfide eutectic melting temperature (988°C). As a test of the plausibility of peak temperatures greater than 988°C, we examined Holbrook (L6/S2) and Dhurmsala (LL6/S3) petrographically for evidence of metal-sulfide eutectic melting. We also examined Peekskill (H6/S2), in which clinopyroxene does not record temperatures higher than the metal-sulfide eutectic, for reference. If melting occurred, metal-sulfide melt veins, melt droplets, or plessite should be present. None of these textures were observed in any of these meteorites, suggesting eutectic melting has not occurred (Figure B-3). We suggest the jadeite component observed in rare clinopyroxenes in Holbrook and Dhurmsala is the cause for the higher temperature estimates in these meteorites.

4.4. Comparisons to Other Type 6 Meteorites

Our results demonstrate that orthopyroxene-clinopyroxene pairs and the QUILF95 calibration provide the best estimate of peak metamorphic conditions and suggest that plagioclase geothermometry records lower temperatures prior to the metamorphic peak. To determine the most representative estimate for Type 6 peak metamorphic conditions, we calculated temperatures for published pyroxene analyses of other chondrites in the literature (9 H6, 19 L6, and 9 LL6) using QUILF95 (Table A-5). Including analyses from this study, peak metamorphic temperatures for H6, L6, and LL6 chondrites overlap and comprise a narrow range from 812-945°C. We do not observe lower peak temperatures for H6 chondrites than for L6 or LL6 chondrites, as has been suggested previously (Olsen

and Bunch 1984; Nakamuta and Motomura 1999). Our results are consistent with those previously determined by Clayton (1993) using oxygen isotopes (900±50°C).

4.5. Peak Metamorphic Temperatures Applied to Asteroid Thermal Evolution Models

Current asteroid thermal evolution models (summarized in McSween et al., 2002; Ghosh et al., 2003) limit peak internal temperatures either to the metal-sulfide eutectic (988°C) or the peak temperature (950°C) estimated for Type 6 chondrites by McSween et al. (1988). The average peak temperatures estimated using pyroxene pairs for Type 6 H, L, and LL chondrites from this study (Table A-5) are 894°C, 877°C, and 908°C, respectively. Using this slightly lower peak temperature estimate (~900°C) may influence the results obtained for thermal evolution histories for ordinary chondrite parent asteroids, although the differences are expected to be minor.

5. SUMMARY AND CONCLUSIONS

We estimated peak metamorphic temperatures, using the QUILF95 pyroxene geothermometer, for the same six Type 6 chondrites for which plagioclase temperatures were previously determined by Nakamuta and Motomura (1999). We also calculated temperatures for published pyroxene analyses in other Type 6 meteorites to obtain a more representative estimate of peak metamorphic conditions experienced by ordinary chondrites. We conclude the following:

- Pyroxene pairs record similar, overlapping temperatures for H6 (865-926°C), L6 (812-934°C), and LL6 (874-945°C) chondrites.
- No evidence of metal-sulfide eutectic melting was observed in three of the studied meteorites, placing an upper limit of <988°C on the peak temperatures.

- Pyroxenes in Type 6 ordinary chondrites represent near-equilibrium assemblages. Previous suggestions for disequilibrium (McSween and Patchen, 1989; Jones, 1997) may be an artifact of the Lindsley (1983) graphical method.
- Two-pyroxene temperature estimates are 96-179°C higher than plagioclase in the same meteorite. We suspect the lower plagioclase temperatures reflect crystallization prior to the metamorphic peak.
- Our revised peak temperature estimates for ordinary chondrites (~900°C) are 50°C lower than current estimates used in asteroid thermal evolution models and may influence thermal model calculations for the parent asteroids.

ACKNOWLEDGEMENTS

This research was supported by NASA Cosmochemistry grant NAG5-12896 to H. Y. M. We thank Larry Taylor and Don Lindsley for helpful comments and suggestions during this research. Thin sections were provided by M. Wadhwa (Chicago Field Museum), G. Kurat (Naturhistorisches Museum, Vienna), and T. McCoy (Smithsonian National Museum of Natural History). This manuscript also benefited from reviews by L. Folco, R. Jones, and Y. Nakamuta.

PART III

Lithium, Beryllium, and Boron in Mauna Kea Basalts from Phase 2 of the Hawaii Scientific Drilling Project

This Part is revised from the manuscript with the same title prepared for submittal to the journal *Geochemistry, Geophysics and Geosystems (G-cubed)* by Valerie S. Reynolds, Jeffrey G. Ryan, and Harry Y. McSween, Jr. My primary responsibilities were data collection, interpretation, and compilation of results into a manuscript. Ryan contributed to data interpretation, and the manuscript benefited from suggestions for organization by both Ryan and McSween.

ABSTRACT

Determining mantle compositions of the light lithophile elements lithium, beryllium, and boron is important for understanding how these elements are processed and homogenized after subduction. The abundances of these elements in mid-ocean ridge basalts are assumed to represent mantle concentrations, but ocean island basalts are potential indicators of Li, Be, and B in the deeper mantle. Existing Li, Be, and B data for ocean islands are limited to exposed subaerial or dredged submarine samples, which represent only the last 5% to 10% of the volcano's total volume. The main drill core collected during the Hawaii Scientific Drilling Project (HSDP-2) provides the most complete collection of continuous lava flows from a hot spot volcano, representing approximately 400,000 years of Mauna Kea's volcanic history. We analyzed Li, Be, and B abundances in Mauna Kea basalts from the HSDP drill core to determine how these elements vary as the volcano passes over and samples different regions of the underlying mantle plume. Although several samples show effects of alteration, our results suggest Li (3.9±0.9 ppm) and Be (0.47±0.09 ppm) preserve mantle compositions. In contrast, highly variable B/K ratios (0.0002-0.008) and B/Be ratios (1-25) suggest post-magmatic alteration has destroyed the mantle B signature. When examined with depth, Li and Be abundances increase in the uppermost portion of the core, in late main shield and post-shield samples, and correspond to decreasing degrees of partial melting as the volcano moved off the plume's center. Li and Be appear to be well mixed in the Hawaiian source region as evidenced by the lack of correlation between Li/Yb or Be/Nd ratios and Pb

isotopes or Nb/Zr ratios, which were previously used to identify geochemically distinct Mauna Kea lava groups. Such mixing probably also accounts for the lack of any crustal signature when Li/Yb or Be/Nd are compared with O isotopes. These elements do not appear to vary on the timescale of Hawaiian shield development, possibly reflecting the efficiency with which these elements are homogenized in the mantle.

1. INTRODUCTION

The ability for the light lithophile elements lithium, beryllium, and boron to track crustal involvement in subduction zones has sparked interest in the role these elements assume in other volcanic environments. Upper mantle compositions are typically inferred from mid-ocean ridge basalts, but ocean island basalts provide invaluable insight into deeper mantle compositions and heterogeneity. Characterizing Li, Be, and B in ocean island volcanoes, however, is challenging because the greatest proportion of lavas produced by a single volcano are buried by younger lavas or are inaccessible due to subsidence accompanying volcano formation. As a result, the dataset for light lithophile elements in ocean island basalts is limited.

The recently acquired drill core from Phase 2 of the Hawaii Scientific Drilling Project (HSDP-2) provides the most comprehensive sampling of a hot spot volcano, representing 400,000 years of continuous lava flows from Mauna Kea. We analyzed Li, Be, and B abundances in selected Mauna Kea reference samples from the drill core and these data allow us to determine how these elements vary as the magmas sampled different regions of the underlying mantle plume. We examine the effects of seawater or (fresh) ground water interaction, mantle melting and heterogeneity, and the influence of a crustal component in the source region.

1.1. Formation and Geochemical Evolution of Hawaiian Hot Spot Volcanoes

Hawaiian volcanoes form as the Pacific plate passes over and samples different regions of the underlying mantle plume, producing compositionally distinct lavas (Figure B-4). Variations in the degree of partial melting and geochemical zonation of the plume cause the observed geochemical heterogeneity, and are attributed to a superimposed temperature gradient (Hauri et al., 1994). Heat generated from a point-source within the mantle forms an upwelling plume that is hotter and less viscous than surrounding mantle. As the plume ascends, it increases the temperature and decreases the viscosity of the surrounding mantle, which becomes entrained in the outer regions of the plume. The result is a zoned plume with a hot core of primitive plume material that is surrounded by cooler regions with entrained lower mantle and depleted upper mantle (Griffiths and Campbell, 1990, 1991; Griffiths, 1991; Hauri et al., 1994). The higher temperature of the plume's core allows for greater degrees of partial melting at shallower depths whereas the cooler peripheral regions experience lower degrees of partial melting at greater depths.

The geochemistry of hot spot lavas indicates the region of the plume over which the volcano is positioned, and corresponds to three stages of volcano growth (Figure B-4). During the pre-shield building stage, the youngest lavas originate from low degrees of partial melting at significant depths and typically comprise only 5% of the volcano's total volume. These lavas tend to be alkaline basalts, basanites, nephelinites, and other evolved compositions with a depleted geochemical signature typical of the upper mantle. As the young volcano passes over the core of the plume, the greatest volume of lavas (90%) are produced by higher degrees of partial melting at shallower depths. Main shield lavas are tholeiitic basalts characterized by a primitive geochemical signature indicative of the plume's source region. As the volcano moves away from the plume's center, magma production rates decline, and localized alkaline basalts and other evolved compositions (commonly ~5%) are produced by lower degrees of partial melting at greater depths during the final post-shield building stage. In addition to geochemical variations caused

by melting and temperature gradients in the Hawaiian plume, Mauna Kea lavas are further complicated by the potential for assimilated young oceanic crust or ancient subducted crustal components in the entrained mantle. Complications in light lithophile elements can also arise because of the fluid-mobile character of Li and B. Earlier flows are submarine and thus may have interacted with seawater. Also, the possibility of groundwater interactions after solidification must be considered.

Prior to the HSDP, samples collected from any hot spot volcano were limited to subaerially exposed or dredged submarine lavas, which represent only brief intermittent time intervals in the volcano's eruptive history (5% to 10%) (Stolper et al., 1996). The HSDP was designed to drill into the flank of a hot spot volcano and collect continuous core samples that represent its entire eruptive history. The HSDP-2 core consists of 245 m (~100 kyr) of main shield Mauna Loa lavas overlying 2853 m (~400 kyr) of Mauna Kea post-shield and main shield lavas, representing nearly 400,000 years of eruptive history (Hawaii Scientific Drilling Project-2, 2000; Sharp and Renne, 2005). Drilling efforts continue in hopes of reaching Mauna Kea's pre-shield lavas. Because it is the most complete evolutionary record of a hot spot volcano, the HSDP core provides the first opportunity to study the structure of a mantle plume via temporal trends of erupting lavas. The goal of the HSDP is to achieve a better understanding of the geochemistry of a hot spot volcano as it passes progressively over an upwelling mantle plume (Stolper et al., 1996; DePaolo et al., 2001).

1.2. Petrography and Geochemistry of Mauna Kea Lavas

Petrographically, Mauna Kea basalts are similar to those retrieved from the HSDP pilot hole (HSDP-1) (Baker et al., 1996; Garcia, 1996), and variations are not systematic with depth. The transition from subaerial to submarine lavas occurs at 1078 meters below sea level (mbsl) (Table A-6). Submarine samples consist of massive and pillow basalts, hyaloclastites, and intrusive units (Rhodes and Vollinger, 2004). Crystallinity ranges

from holocrystalline to vitrophyric, and vesicularity ranges from 0% to 25%. Texturally, samples can be subophitic or trachytic and contain quench features, such as skeletal plagioclase. Samples are typically porphyritic, with olivine as the dominant phenocryst, but clinopyroxene and plagioclase are common in the groundmass and are rare phenocrysts in several samples. Strained olivine phenocrysts, similar to those observed by Baker et al. (1996) in HSDP-1 lavas, are uncommon. Several olivine phenocrysts display resorption features, such as embayed borders. Although samples from the HSDP-2 drill core are relatively fresh, serpentine or iddingsite alteration of olivine is apparent in several samples, and completely replaces the mineral in some cases. Secondary mineralization is also apparent in vesicles of a few samples near the bottom of the drill core. Alteration appears to be localized within the core, and represents at least one known freshwater aquifer near the submarine/subaerial transition (Thomas et al., 1996).

Figure B-5 is a total alkalis-silica classification diagram (Le Bas et al., 1986) showing the compositions of samples analyzed in this study (data from Rhodes and Vollinger, 2004). Mauna Kea lavas are dominantly tholeiitic basalts, except for interlayered transitional and alkaline basalts in the uppermost region of the drill core (Rhodes and Vollinger, 2004). Several samples are picritic, reflecting the MgO-rich nature of Mauna Kea lavas. MgO contents range from 7% to 30%, but samples with MgO contents greater than approximately 14% to 18% contain olivine phenocrysts with forsterite contents too low to be in chemical equilibrium with their host melts (Figure B-6). Baker et al. (1996) observed the same correlation in Mauna Kea lavas from HSDP-1, and concluded that lavas with >12% MgO contain accumulated olivine.

The effects of olivine control in Hawaiian lavas are well-documented (Wright, 1971), and are apparent when major elements are compared with MgO (Figure B-7; Rhodes and Vollinger, 2004). However, trace element variations suggest Mauna Kea compositions were also affected by other processes, such as magma mixing (Figure B-7; Rhodes and Vollinger, 2004). Rhodes and Vollinger (2004) used SiO_2 contents and Zr/Nb

ratios to identify five geochemically distinct groups within the Mauna Kea samples. In addition to these geochemical discriminants, Huang and Frey (2003) used radiogenic isotopes and other incompatible element ratios to narrow the groups to three (Figure B-8, adapted from Huang and Frey, 2003).

The Postshield Group (Type 2 magmas of Rhodes and Vollinger (2004)) includes the uppermost Mauna Kea lavas (246-396 mbsl)) and is defined by low-SiO_2 contents, low $^{3}He/^{4}He$ and $^{206}Pb/^{204}Pb$ ratios, and a trend to high incompatible element abundance ratios. The geochemical signature of the Postshield Group indicates the degree of partial melting was decreasing and the proportions of source components changing from that of main shield lavas (Huang and Frey, 2003). Lassiter et al. (1996) attributed the same signature (i.e. low $^{87}Sr/^{86}Sr$ and low $^{3}He/^{4}He$) observed in HSDP-1 post-shield lavas to an increasing proportion of depleted upper mantle entrained in the outer region of the plume. The other two lava types are intercalated throughout the remaining core. Volumetrically, the core is dominated by the High-SiO_2 Shield Group (Type 1 magmas of Rhodes and Vollinger (2004)). These lavas (353-3068 mbsl) are distinguished by higher SiO_2 contents at a given MgO content, similar to Kilauea lavas. The Low-SiO_2 Shield Group (Type 3 magmas of Rhodes and Vollinger (2004)) includes low-SiO_2 lavas in the submarine portion of the core as well as one subaerial sample (834-2968 mbsl). Although both the Postshield Group and the Low-SiO_2 Shield Group have similar SiO_2 contents, the Low-SiO_2 Shield Group has higher $^{3}He/^{4}He$ ratios in addition to higher Ti/Zr and Nb/Zr ratios, similar to Loihi seamount lavas. The petrogenesis of the main shield lavas appears to be complex, requiring variations in degree of melting in addition to melting of different source regions or mixing of geochemically distinct magmas (Huang and Frey, 2003; Rhodes and Vollinger, 2004).

Figure B-9, adapted from Huang and Frey (2003), demonstrates that three admixed components are required to explain the Sm/Yb and Pb isotope (expressed as $\Delta^{208}Pb/^{204}Pb$ $(((^{208}Pb/^{204}Pb)_{SAMPLE} - (^{208}Pb/^{204}Pb)_{NHRL}) \times 100$ where NHRL is northern

hemisphere reference line (Hart, 1984)) values in Mauna Kea lavas. The sources for the three components are disputable, but lower than normal $\delta^{18}O$ values, negative Th and U anomalies, positive Sr anomalies, and high $^{187}Os/^{188}Os$ ratios support ancient recycled hydrothermally altered (crustal) gabbros as one (or part of one) component (Eiler et al., 1996; Hauri et al., 1996; Hofmann and Jochum, 1996; Wang et al., 2003).

2. LITHIUM, BERYLLIUM, AND BORON AS CRUSTAL INDICATORS

The abundances and isotopic values of Li, Be, and B in island arc lavas are indicators of subducted crust or fluids derived from subducted crust and/or pelagic sediments in the source region. Whole-rock Li and B abundances and isotopic concentrations are enriched and isotopically heavier in oceanic crust altered by seawater at low temperatures (Seyfried et al., 1984; Spivack and Edmond, 1987). Although Be concentrations in oceanic crust are unaffected by seawater interaction, pelagic sediments have high $^{10}Be/Be$ ratios because the cosmogenic isotope ^{10}Be is present in pelagic sediments, but not in altered oceanic crust (Tera et al., 1986; Morris, 1991). As oceanic crust and sediments are subducted, dehydration reactions transport the fluid-mobile B and Li (heavy isotopes preferred) into the overlying mantle wedge where melting occurs (Moran et al., 1992; Bebout et al., 1993). Beryllium is not soluble in H_2O-rich fluids and therefore remains in the subducted slab. However, if the sediment component itself melts, arc lavas will contain high $^{10}Be/Be$ values. Isotopic fractionation does not occur during igneous melting or crystallization, thereby preserving the crustal signature imposed on the region of the mantle that melts to produce the erupted lavas (Tomascak et al., 1999). The subducted slab returns to the mantle depleted and isotopically light with respect to Li and B, whereas Be contents remain relatively unchanged. Ratios of elements with similar partitioning coefficients (B/K, B/Nb, Be/Nd, Li/V, and Li/Yb) are not fractionated during magma generation and crystallization and therefore can be useful indicators of contributions by slab-derived components in the source region (Tera et al., 1986; Ryan and Langmuir, 1987, 1988, 1993; Morris et al., 1990; Ryan et al., 1996).

3. SAMPLING AND ANALYTICAL METHODS

Powdered samples of 14 subaerial Mauna Kea alkaline and tholeiitic basalts and 22 submarine Mauna Kea tholeiitic basalts were selected from the HSDP-2 geochemical reference suite (Table A-6). Sample numbers (e.g. SR121-4.40) represent the core run number (SR121) and the depth, in feet, below the top of the run (4.40). Here samples are discussed using only the run number (SR121). Sample crushing techniques are described in Rhodes (1996). Whole-rock Li, Be, and B data were acquired using an ARL model SpectraSpan 7 direct coupled plasma atomic emission spectrometer (DCP-AES) at the University of South Florida. The DCP-AES was tuned to 670.7 nm for Li, 313.04 nm for Be, and 249.77 nm for B. Analytical precision for the techniques is ±5% or less for Be and Li and ±20% for B concentrations <10 ppm (Ryan and Langmuir, 1987; 1988; Ryan et al., 1996).

Samples were prepared using methods detailed in Ryan and Langmuir (1987). For B analysis, 0.5g of sample was mixed with 2g of Na_2CO_3 flux in Pt crucibles, which were covered and placed in a cold muffle furnace. The furnace was heated gradually to 1000°C, turned off, and the crucibles were allowed to cool in the furnace. The cooled crucibles were immersed in B-free water, sealed in Teflon beakers, and placed on a hotplate at 100-120°C for 12 hours. The fusion cakes were scraped from the crucibles into the B-free water and returned to the hotplate at 150° to dry. The dry samples were resuspended in B-free water, placed in centrifuge tubes and centrifuged three times, decanting the clear solutions after each centrifuge. The clear solutions were allowed to dry, then resuspended in 20 ml of B-free water and 5-10 ml of Ultra pure HNO_3 was added until solutions were neutralized. Samples were diluted to 50 ml with B-free water. For Li and Be analysis, 0.5g of sample was combined with 5 ml HF and 1.5 ml $HClO_4$ in Teflon beakers, which were sealed and placed on a 130° hotplate for at least 12 hours. The samples were allowed to dry, and then resuspended in HNO_3 to obtain clear

solutions. Once clear solutions were obtained, 10 ml HNO_3 was added and solutions were diluted to 50 ml with deionized (DI) water. Whole-rock Li, Be, and B concentrations for Mauna Kea basalts and standards are presented in Tables A-6 and A-7, respectively.

4. OLIVINE CORRECTION

Olivine accumulation and fractionation played a significant role in the formation of HSDP lavas (Baker et al., 1996; Huang and Frey, 2003; Rhodes and Vollinger, 2004). To correct for these processes, olivine (Fo_{85}) was added or subtracted until whole-rock compositions (Rhodes and Vollinger, 2004) were in equilibrium with Fo_{85}. For trace element corrections, distribution coefficients ($D^{min\text{-}melt}$) were assumed to be 0 for all incompatible elements except Li. To test this correction, we compared Be vs. Zr for uncorrected and corrected compositions (Figure B-10). Because Be and Zr are incompatible, they should vary similarly with olivine correction. Main shield lavas show minimal effects of olivine correction, but post-shield lavas change substantially. During Mauna Kea's post-shield stage, magma production rates were declining. As a result, magmas resided longer in crustal reservoirs where they interacted with crustal materials and evolved beyond olivine control (i.e. fractionated clinopyroxene and/or plagioclase). Therefore, correcting only for olivine may be too simplistic an approach for these samples.

Corrections for Li required a partitioning coefficient ($D_{Li}^{ol\text{-}melt}$) because Li partitions into olivine. The value for D_{Li} in olivine ranges significantly. Experimentally determined D_{Li} values by Brenan et al. (1998) range from 0.13 to 0.35. Chan and Frey (2003) measured Li concentrations in olivine/matrix pairs in two Koolau samples and calculated an average D_{Li} value of 0.45. We evaluated the effects of varying D_{Li} from 0.2-0.45 and determined the difference is minimal (Figure B-11). Increasing the D_{Li} value from 0.2 to 0.35 to 0.45 increases the average Li concentration from 3.86 ppm to 3.88 ppm to 3.90 ppm, respectively. Results from this study are reported using a value of

D_{Li}=0.35. All other major and trace element data are from Rhodes and Vollinger (2004) unless stated otherwise.

5. RESULTS AND DISCUSSION

5.1. Influence of Seawater and/or Groundwater

Assessing sample preservation is essential when studying the fluid-mobile elements Li and B. These elements are enriched in basalt altered by seawater, but leached when altered by fresh ground- or rainwater (Seyfried et al., 1984). Beryllium is insoluble in H_2O-rich fluids, and the consistent values (0.47±0.09 ppm) throughout the HSDP-2 core suggest igneous abundances were preserved.

All post-shield samples in this study, except SR121, have low K_2O/P_2O_5 values (0.55-1.2) and high K/Rb values (600-2594), suggestive of post magmatic alteration. However, Li correlates well with Zr, Nb, and Yb (Figure B-12), suggesting Li was not substantially mobilized with alteration in this interval. However, Li does not show a strong correlation with incompatible elements in Mauna Kea main shield lavas (Figure B-12), indicating post-magmatic Li modification. The average Li concentration for Mauna Kea lavas is 3.9±0.9 ppm, but selected samples from ~1000 to 2000 mbsl (SR413, SR472, SR531, SR664, and SR723) have higher than average Li concentrations (Figure B-13). Samples SR413 and SR723 appear unaltered, whereas the remaining samples have iddingsite or serpentine alteration of olivine and may or may not have anomalously high K/Rb or low K_2O/P_2O_5 ratios. The altered samples are all submarine and may have interacted with Li-rich seawater. Samples SR413 and SR472 straddle the submarine/subaerial transition, where a freshwater aquifer has been identified (Thomas et al., 1996). However, Li in basalts altered by freshwater tends to be unaffected or lowered. Two samples that have lower Li contents are SR916 and SR939 and are visibly altered with secondary mineralization in vesicles. A freshwater aquifer has not been identified at

this depth interval, but we suggest this may be the cause for such alteration. Sample SR850 has a slightly higher Li content, but it is unaltered and was described by Huang and Frey (2003) as having anomalously high abundances of many other incompatible elements.

Boron abundances in Mauna Kea lavas are highly variable (0.6-9.1), resulting in anomalous B/Be ratios (1-25) and B/K ratios (0.0002-0.008) (Figure B-14). Optical and geochemical evidence suggest many HSDP-2 lavas have been altered. B and Nb are not fractionated during melting and crystallization, and are good indicators of possible alteration-induced variation of B because B is easily mobilized in H_2O-rich fluids whereas Nb is not (Ryan and Langmuir, 1993). When examined with depth (Figure B-15), B/Nb ratios mimic B abundances, suggesting alteration is the cause for variable B values rather than source region heterogeneity. Variations in B abundances do not necessarily correlate with other alteration indicators, and probably reflect the highly fluid-mobile nature of this element.

5.2. Variations in Li, Be, and B with Mantle Melting and Heterogeneity

Differences in element abundances or element ratios within the HSDP-2 core potentially record changes in degree of melting and source region heterogeneity within the Hawaiian mantle plume. Alteration appears to have influenced B concentrations in Mauna Kea lavas to such an extent that mantle compositions are no longer preserved. Although the range in B is similar to other ocean islands, the lack of correlations of B with Be, K, or Nb (Figure B-14) render the B values unreliable.

The trend to higher Li abundances in post-shield lavas (Figure B-13) is similar to that observed for other incompatible elements, reflecting Mauna Kea's gradual shift from the shield building to post-shield stages (Huang and Frey, 2003). Ryan and Langmuir (1987) determined that Li behaves similarly to V and Dy during melting and to Yb during

low-pressure fractionation. With depth, Li/Dy, Li/V, and Li/Yb (Figure B-16) follow similar trends as Li abundance (Figure B-11), suggesting the anomalous Li abundances are a result of alteration and not source region variation.

Beryllium behaves incompatibly in Mauna Kea lavas, as indicated by regular correlations of Be with MgO, Zr and Nd (Figure B-17). Be concentrations are constant (0.45 ppm) from the bottom of the core to approximately 800 mbsl where values gradually increase to 0.55 ppm in the high-SiO_2 and post-shield lavas (Figure B-18). The shift to higher Be values corresponds to a similar shift in other incompatible element ratios (i.e. La/Yb), interpreted to represent the transition from Mauna Kea's main shield to post-shield stages (Lassiter et al., 1996; Huang and Frey, 2003; Rhodes and Vollinger, 2004). During this transition, Mauna Kea magmas were generated by lower degrees of partial melting at greater depths and these magmas resided longer in shallower reservoirs where they were influenced by a depleted (upper mantle?) source. To test whether Be variations reflect changing melting conditions, we compared Be with Nd and Zr, two elements with similar partitioning behaviors as Be during melting and crystallization (Figure B-18) (Ryan, 2002). Constant Be/Nd (0.03±0.006) and Be/Zr (0.0035±0.0007) values with depth suggest variations in the conditions of melt segregation, rather than source region compositional variation, caused the increase in Be values in the uppermost high-SiO_2 and post-shield lavas.

Three geochemically distinct components in the source region for Mauna Kea lavas were identified by Huang and Frey (2003) based on SiO_2 contents, radiogenic isotopes, and incompatible element ratios. We examined how Li and Be vary with respect to these geochemical groups by comparing Li/Yb and Be/Nd to Nb/Zr, $^{208}Pb/^{204}Pb$, and $^{206}Pb/^{204}Pb$ (Figure B-19). Be/Nd and Li/Yb ratios overlap and do not define distinct compositional groups. The light lithophile elements appear to be homogeneous with respect to the source components identified by other geochemical indicators.

5.3. Evidence for a Crustal Component in the Hawaiian Mantle Plume

Mauna Loa and Mauna Kea lavas retrieved from both HSDP-1 and HSDP-2 display geochemical signatures indicative of a crustal influence. Elevated $^{187}Os/^{188}Os$ ratios in Mauna Loa lavas and negative Th and U anomalies in Mauna Kea and Mauna Loa lavas suggest the Hawaiian plume contains entrained recycled oceanic gabbros (Hauri et al., 1996; Hofmann and Jochum, 1996). Unusually low $\delta^{18}O$ values in Mauna Kea lavas also support entrained recycled (hydrothermally altered) oceanic crust in the source region, but other interpretations are possible. Olivine phenocrysts in Mauna Kea lavas indicate distinctly lower $\delta^{18}O$ values in subaerial lavas (4.7‰) when compared to submarine lavas (5.0‰). However, smaller olivine phenocrysts (termed *micro*phenocrysts by Wang et al., 2003) that crystallized after the larger olivine phenocrysts in the submarine section of the core record similarly low $\delta^{18}O$ values as subaerial samples. Wang et al. (2003) suggested the subaerial lavas could have sampled portions of the volcanic edifice that were hydrothermally altered, but the lower values of the submarine microphenocrysts point to addition of an ^{18}O depleted component (i.e. assimilated or entrained hydrothermally altered crust) over time. The means for creating a low ^{18}O component, regardless of the mechanism for incorporating it into the plume, must be high temperature alteration (Gregory and Taylor, 1981).

Chan and Frey (2003) measured Li isotopes in HSDP-2 lavas and concluded that low-SiO_2 and post-shield lavas have similarly low δ^7Li values of 4‰ (similar to mid-ocean ridge basalts (MORB)), whereas high-SiO_2 lavas have slightly higher δ^7Li values of 5‰ to 6‰, indicating the presence of recycled oceanic crust. These authors noted the small variation in δ^7Li values and suggested only a small proportion of recycled crust is in the Hawaiian plume. The higher δ^7Li values reported by Chan and Frey (2003) are not limited to the submarine high-SiO_2 lavas. Subaerial high-SiO_2 and post-shield lavas (~1000-500 mbsl) show similar enrichments in δ^7Li, within analytical error. Because isotopic fractionation of Li is temperature dependent, higher δ^7Li values indicate the

crustal component must have experienced low-temperature alteration (Seyfried et al., 1984). This conclusion is in contrast to oxygen isotope data, however, which require a deeper gabbroic crustal component altered at high temperatures (Eiler et al., 1996; Wang et al., 2003). Although it is possible that both shallow and deep portions of the crust were recycled into the mantle, Li and O isotopes should correlate because their fractionation behaviors are similar at high and low temperatures. The depth interval where heavier Li isotopes were reported (~1700-1200 mbsl) does not correlate with heavier O isotopes. In fact, higher than normal (i.e. mantle) $\delta^{18}O$ values are not observed throughout the core, suggesting the oceanic crust present in the Hawaiian mantle plume was not altered at low temperatures.

Variations in Li, Be, and B abundance data from this study are minimal with depth within the HSDP-2 core, suggesting these elements are well homogenized among the geochemical groups defined by SiO_2 contents, He and Pb isotopes, and Nb/Zr and Ti/Zr ratios. If Be and Li preserve a signature of oceanic crust altered by seawater at low temperatures, Be/Nd and Li/Yb ratios should correlate with O isotopes. The lack of correlation for any of the identified geochemical groups (Figure B-20) suggests Li and Be abundances do not record a crustal signature. The efficiency with which Li is stripped from the subducting slab, and the lower fluid-melt partition coefficient for Be, most likely limits their sensitivity as crustal indicators in ocean island environments. Despite the greater potential Li isotopes have as an indicator of subducted oceanic crust altered at low temperatures, variations in ocean island settings may be too small (i.e. within error of current analytical methods) to be detected.

5.4. Comparisons to Other Oceanic Magmatic Environments

As discussed in previous sections, B in Mauna Kea lavas probably reflects variable degrees of alteration rather than primary magmatic compositions. Our results for Li abundances (3.8 ppm) compare well with Li concentrations determined by Chan and

Frey (2003) for Mauna Kea (3.6 ppm) and are similar to results for other ocean island basalts reported by Ryan and Langmuir (1987), who characterized Li contents of basalts and more evolved compositions from mid-ocean ridges, ocean islands, and island arcs. These authors determined that basalts from all of these environments have similar Li abundances of 3-10 ppm. The more fractionated compositions (i.e. dacites, andesites, and trachytes) from mid-ocean ridges and ocean islands have similar, but slightly higher Li contents of ~8-15 ppm. Silica-rich compositions in island arc environments can contain in excess of 60 ppm Li. Li/Yb ratios for Mauna Kea lavas (2.3) fall into the previously reported range for ocean islands, which are higher than MORB (1.7), and similar to arc tholeiitic basalts (Figure B-12) (Ryan and Langmuir, 1987). Higher Li/Yb ratios in OIB compared to MORB probably reflects the presence of garnet in the source region. The higher Li/Yb ratios observed in IAB are attributed to additional Li in the source region from devolatilized subducted slabs (Ryan and Langmuir, 1987).

Beryllium contents of Mauna Kea basalts (0.47±0.09 ppm) are at the low end of the OIB range reported by Ryan (2002) (0.5-1 ppm), but are higher than primitive MORB glasses (~0.15 ppm). Fe-Ti basalts from mid-ocean ridges and alkaline basalts from ocean islands contain higher Be abundances (1-10 ppm), which correlate with higher abundances of the light rare earth elements (i.e. Nd) and high field strength elements (i.e. Zr). Ryan and Langmuir (1988) originally suggested OIB and MORB had similar Be/Nd ratios of ~0.05, but Ryan (2002) observed slightly lower ratios for OIB (0.045) when compared to MORB (0.05) using an expanded dataset. Results from this study further lower the Be/Nd ratio, at least for Mauna Kea lavas, to 0.03 (Figure B-17). Similarly, Be/Zr ratios for Mauna Kea lavas from this study (0.003) are lower than MORB (0.0047), in contrast to data presented by Ryan (2002) for ocean island lavas (Be/Zr=0.006). However, the Be/Zr ratio determined for OIB by Ryan (2002) includes MORB differentiates (i.e. andesites and FeTi basalts) and alkaline basalts, which were not analyzed in this study. Therefore, our lower Be/Nd and Be/Zr ratios are better estimates

for tholeiitic basalts from ocean islands. Clearly, more data are necessary to constrain the ratios for more fractionated compositions.

6. SUMMARY AND CONCLUSIONS

Thirty-six Mauna Kea basalts from the HSDP-2 drill core, representing 400,000 years of Mauna Kea post-shield and main shield lavas, were analyzed for whole-rock Li, Be, and B abundances to determine how these elements vary within the underlying Hawaiian mantle plume. Although material retrieved from the drill core appears fresh, interaction with seawater and groundwater is apparent in several samples. Highly variable B abundances (0.6-9.1 ppm), B/K ratios (0.0002-0.008) and B/Be ratios (1-25) suggest this highly fluid-mobile element was influenced by alteration to such a degree that mantle compositions were not preserved. Average Li contents (3.9±0.9 ppm) and Li/Yb ratios (2.3) are typical for ocean island basalts, but alteration has resulted in anomalously low (2.4 ppm) and high (5.9 ppm) values in some samples. Beryllium abundances (0.47±0.09 ppm) are slightly lower than previously reported values for OIB, resulting in lower Be/Nd ratios (0.03) and Be/Zr ratios (0.0035). However, differentiated compositions analyzed in previous studies probably account for the higher reported Be measurements, and the larger dataset from this study places firmer constraints on Be/Nd and Be/Zr ratios for tholeiitic OIB.

Using SiO_2 contents, radiogenic isotopes, and incompatible element ratios, Huang and Frey (2003) identified three geochemical groups in the Mauna Kea lavas. Low-SiO_2 subaerial lavas (i.e. post-shield) have low $^{3}He/^{4}He$ and $^{206}Pb/^{204}Pb$ ratios, and were generated by lower degrees of partial melting at greater depths as Mauna Kea moved off the plume's center. High-SiO_2 lavas are most voluminous in the core and, with higher SiO_2 contents at a given MgO content, they are similar to Kilauea lavas and represent the "Kea" component of the plume. Low-SiO_2 submarine lavas have higher $^{3}He/^{4}He$ ratios and Ti/Zr and Nb/Zr ratios than low-SiO_2 subaerial lavas, similar to lavas produced at the

Loihi seamount. These geochemical groups are indistinguishable when Li/Yb and Be/Nd are compared with Pb isotopes and Nb/Zr ratios, suggesting mantle compositions of Li and Be do not vary on the time scale of Hawaiian shield development.

In addition to the groups identified by Huang and Frey (2003), lower than normal $\delta^{18}O$ values, negative Th and U anomalies, positive Sr anomalies, and high $^{187}Os/^{188}Os$ ratios suggest a component of hydrothermally altered oceanic gabbros (i.e. crust) is present in the Hawaiian plume (Eiler et al., 1996; Hauri et al., 1996; Hofmann and Jochum, 1996; Wang et al., 2003). Li isotopes were used to identify a component of recycled crust altered at *low* temperatures in the Hawaiian plume (Chan and Frey, 2003). When Li/Yb and Be/Nd ratios were compared with O isotopes, no correlation was observed. Therefore, despite the ability for Li, Be, and B to identify crustal signatures in in IAB source regions, these elements do not record a low-temperature altered crustal component in the Hawaiian mantle plume. Recycling processes have probably served to homogenize these elements too well to be useful identifiers in ocean island settings.

ACKNOWLEDGEMENTS

Thin sections and powdered samples from the HSDP-2 geochemical reference suite were provided by M. Garcia and E. Stolper.

PART IV

Using Lithium and Beryllium to Evaluate the Enriched and Depleted Components in Basaltic Shergottites

This chapter is revised from the manuscript with the same title prepared for submittal to the journal *Geochimica et Cosmochimica Acta* by Valerie S. Reynolds, Harry Y. McSween, Jr., William F. McDonough, and Jeff G. Ryan. My responsibilities were data collection, interpretation, and compilation of results into a manuscript. McDonough assisted with data collection, and Ryan and McSween contributed to data interpretation and manuscript organization.

ABSTRACT

Geochemically depleted and enriched reservoirs, formed early in Mars' history, have been preserved in the absence of plate tectonics, the mechanism responsible for mixing primitive and evolved compositions on Earth. The depleted reservoir is reduced and light rare earth element depleted, with high ε^{143}Nd and low initial $^{87}Sr/^{86}Sr$ values, similar to the terrestrial mantle. The enriched reservoir is oxidized, enriched in light rare earth elements, with low ε^{143}Nd and high initial $^{87}Sr/^{86}Sr$ values, similar to the terrestrial crust or to metasomatised mantle. Geochemical trends among the basaltic shergottites, a subgroup of Martian meteorites, suggest mixing occurred between these two compositionally distinct end-members. On Earth, crust-mantle interactions are recorded at subduction zones, where the light lithophile element lithium and beryllium (and boron) record a component of altered oceanic crust in the source regions of island arc basalts. We analyzed Li and Be abundances and Li isotopes in selected Martian meteorites to determine whether the enriched Martian assimilant was altered at low-temperatures, similar to the oceanic crust. Although terrestrial alteration minerals (caliche) in Dhofar 019 apparently affected the primary Li and Be concentrations, the remaining shergottites contain Be (0.09-0.77 ppm) abundances similar to mid-ocean ridge basalts or ocean island basalts, whereas Li abundances (2.7-9.9 ppm) are slightly higher compared to these reservoirs. On diagrams of Li/Yb vs. Dy/Yb and K/Li vs. La/Yb, basaltic shergottites define trends similar to arc basalts, which are attributed to altered oceanic crust in their source regions. However, the correlation between Li or Be and $\delta^{18}O$ for

basaltic shergottites is weak, and δ^7Li values measured in two geochemically distinct basaltic shergottites, Zagami (+3.97‰) and EETA79001 (+4.37‰), are identical within error. Therefore, although the Martian assimilant appears to be enriched in Li and possibly Be, it either was not altered at low temperatures or the proportion of altered material in basaltic shergottite magmas is too small to be resolved using these crustal indicators. It is not obvious, using Li and Be, whether the enriched assimilant on Mars originated as crust or metasomatised mantle.

1. INTRODUCTION

Planetary-scale melting and differentiation early in Mars' history resulted in the formation of both depleted (mantle) and enriched (crustal) reservoirs (McLennan, 2003). Igneous activity continued on Mars for at least 2 Gy, but primitive isotopic signatures in Martian meteorites suggest rigorous mantle convection did not occur after the initial fractionation event, preserving the geochemical distinctions of these reservoirs (Lee and Halliday, 1997; Spohn et al., 2001). Radiogenic isotopes, light rare earth element partitioning, and oxidation states of basaltic shergottites, a subgroup of Martian meteorites, suggest these meteorites experienced mixing between at least two components (Jones, 1989; Longhi, 1991; Wadhwa, 2001; Borg, 2002; Herd et al., 2002). One component is reduced, depleted in light rare earth elements, and contains a high ε^{143}Nd value and a low initial ^{87}Sr/^{86}Sr ratio, similar to the terrestrial mantle. The other component is oxidized, enriched in light rare earth elements, and contains a low ε^{143}Nd value and a high initial ^{87}Sr/^{86}Sr ratio. Although this component is similar to the terrestrial crust, it may also represent an enriched mantle source (e.g. Borg, 2002). The basaltic shergottites Shergotty/Los Angeles and Queen Alexandra Range (QUE) 94201 represent the enriched and depleted end-members, respectively, and the remaining basaltic shergottites define a mixing trend between them (Figure B-21). The depleted component is normally assumed to represent the post-differentiation mantle source for

shergottites, and the enriched component represents material assimilated by these magmas.

On Earth, the light lithophile elements lithium, beryllium, and boron record crust-mantle interactions at subduction zones. As altered, hydrous oceanic crust enriched in Li and B is subducted, dehydration reactions transport these fluid mobile elements (heavy isotopes preferred) into the overlying mantle wedge where melting occurs, leaving Be relatively unchanged (Moran et al., 1992; Bebout et al., 1993). The lack of isotopic fractionation during melting and crystallization preserves this crustal signature as higher δ^7Li and δ^{11}B in island arc basalts (IAB) compared to mid-ocean ridge basalts (MORB) (Moriguti and Nakamura, 1998; Tomascak et al., 1999a; Straub and Layne, 2002).

The oxidized nature of the assimilant in basaltic shergottites (Figure B-21c) suggests it may have been hydrated, introducing the possibility that it may have experienced low-temperature alteration. Oxygen and hydrogen isotopes measured in alteration minerals in Martian meteorites indicate that surface/crustal water reservoirs once present on Mars were enriched in δ^{18}O and δD (Karlsson et al., 1992; Leshin Watson et al., 1994; Boctor et al., 2003). Oxygen isotope variations in bulk basaltic shergottites provide a hint that the enriched component was hydrated (McSween, 2002), but the variations are not as systematic as for radiogenic isotopes. The presence of isotopically heavy oxygen and hydrogen isotopes suggests a reservoir may also have been enriched in Li and/or δ^7Li, potentially providing a Li-enriched component as an assimilant.

Previous studies of light lithophile elements in Martian meteorites focused on in-situ analyses of pyroxenes in basaltic shergottites and nakhlites (Lentz et al., 2001; Beck et al., 2004; Herd et al., 2005). The results from these studies reached similar conclusions, invoking magma degassing to explain lower Li and B abundances and higher δ^7Li in shergottite pyroxene rims versus pyroxene cores. Whole-rock Li, Be, and

B data for Martian meteorites are limited due to the difficulty associated with measuring these elements in such low abundances. Our goal is to examine bulk Li and Be abundances and Li isotopes in selected Martian meteorites to determine how they relate to the assimilant. We also re-evaluate the degassing theory proposed for basaltic shergottites in the context of these new data.

2. REVIEW OF LIGHT LITHOPHILE ELEMENT BEHAVIOR AND PREVIOUS STUDIES ON LI, BE, B IN MARTIAN METEORITES

2.1. How Lithium, Beryllium, and Boron Develop a Crustal Signature

The success of Li, Be, and B as crustal indicators in terrestrial island arc environments is based on the "crustal" signature that develops in oceanic crust altered by seawater at low temperatures. Fresh basalt generated at mid-ocean ridges (MORB) contains low concentrations and isotopic compositions of these incompatible elements (Ryan and Langmuir, 1987; Spivack and Edmond, 1987; Ryan, 2002). Seawater is enriched in Li and B and, at low temperatures, these elements fractionate into the crust, resulting in noticeably higher concentrations and heavy isotopic abundances (Seyfried et al., 1984; Spivack and Edmond, 1987; Chan et al., 1992). Beryllium concentrations remain relatively constant, but the cosmogenic isotope ^{10}Be is present in pelagic sediments, which may play a role during subduction (Tera et al., 1986; Morris, 1991). As altered oceanic crust (and sediment) is subducted, metamorphic reactions dehydrate the slab, and soluble Li and B are carried with the fluid into the overlying mantle wedge that melts to produce the erupted lavas (Moran et al., 1992; Bebout et al., 1993). Beryllium is insoluble in H_2O-rich fluids and remains in the subducted slab. The lack of isotopic fractionation during igneous melting and crystallization preserves this crustal signature (Tomascak et al., 1999a). Ryan and Langmuir (1987, 1988, 1993) determined that ratios of elements with similar partitioning behavior (e.g. Li/Yb, Be/Nd, and B/Nb) do not vary

with magma generation and crystallization, and therefore can be used to identify source region heterogeneity, which may result from the addition of subducted oceanic crust.

2.2. Previous Li, Be, and B Studies on Martian Meteorites

The current database for Li and Be in basaltic shergottites is presented in Table A-8. Although bulk Li and Be analyses are available for several meteorites, whole-rock B data is limited to Nakhla and Chassigny, and previous studies using these elements focused on variations measured by ion microprobe between pyroxene cores and rims. Lentz et al. (2001) measured Li, Be, and B abundances in pyroxene cores and rims and in plagioclase in two basaltic shergottites (Shergotty and Zagami) and two nakhlites (Nakhla and Lafayette) using secondary ionization mass spectrometry (SIMS). These authors observed that abundances of all three elements increase, as expected for incompatible elements, from pyroxene cores to rims in Nakhla and Lafayette. In Shergotty and Zagami, however, Be behaved as an incompatible element, but B and Li decreased from core to rim. These authors suggested the higher solubility of Li and B may have resulted in the loss of these elements during devolatilization upon ascent or eruption of the shergottite lavas.

Herd et al. (2005) also performed in-situ analyses of Li, Be, and B in pyroxenes in Shergotty and Zagami, and although these authors observed a similar decrease in Li from pyroxene cores to rims, a decrease in B was not apparent. Using mineral-melt partitioning coefficients for Li in pyroxene, Herd et al. (2005) determined that Li in pyroxene cores is too high to be in equilibrium with bulk Li compositions. This discrepancy can not occur solely as a result of igneous processes, and implicates a role for a fluid phase during crystallization.

Beck et al. (2004) analyzed Li isotopes in pyroxenes from the basaltic shergottite Northwest Africa (NWA) 480 using SIMS and observed an increase from -17‰

(compared to L-SVEC standard) in pyroxene cores to +10‰ in pyroxene rims with little or no change in Li concentration (~3.5 ppm). These authors attributed the variable isotopic compositions to magmatic degassing.

3. SAMPLE SELECTION AND ANALYTICAL METHODS

Martian meteorites were selected to represent the range of reported geochemical heterogeneity in basaltic shergottites. For Li isotope analyses, the enriched end-member is represented by Zagami and, although the Antarctic find QUE 94201 was the preferred depleted end-member, limited sample quantity precluded its availability for analysis. Therefore, we selected the dunite Chassigny to represent the mantle end-member. We also selected an intermediate composition, Elephant Morraine (EETA) 79001, for comparison. Whole-rock Li and Be abundance data were collected for these meteorites in addition to Shergotty, Los Angeles, and the Oman desert find Dhofar (Dho) 019, despite known terrestrial alteration in the latter (Taylor et al., 2002).

Samples were digested and analyzed at University of Maryland's Geochemistry Laboratory using techniques described by Tomascak et al. (1999b). Rock chips of Zagami, EET A79001, Dhofar 019, and Chassigny were ground to powders using an agate mortar and pestle. Approximately 25 mg of sample were combined with 1 mL each HF and HNO_3 in Teflon beakers, which were sealed and placed on a hotplate at ~120°C for at least 12 hours. Once samples were digested, the solutions were allowed to dry, and then resuspended in 1 mL high purity 2% HNO_3. Clear solutions were returned to the hotplate to dry, and then resuspended in concentrated HCl. Clear solutions were dried again on the hotplate and either resuspended in 1 mL high purity 2% HNO_3 for Li and Be analyses or resuspended in 1 mL 4M HCl for Li isotope column chromatography. Column procedures are modified from Tomascak et al. (1999b) and serve to separate Li from remaining ions in the solution. Samples were run through three cation exchange columns that were equilibrated with either Milli-Q H_2O or HCl. Samples were added to

first columns (12 mL columns of BioRad AG50W-x12) in 1 mL 4M HCl, and Li was eluted with 9 mL 2.5M HCl. Samples were dried, resuspended in 1.5 mL 0.15M HCl, run through second columns, and Li was eluted with 30 mL 0.15 HCl. Samples were dried, resuspended in 1 mL 0.15M HCl, added to third columns, and Li was eluted with 16 mL of 4M HCl mixed with 30% ethanol (CH_3OH). Samples were dried and resuspended in 1.5 mL 0.15M HCl for analysis.

Li and Be abundances were analyzed using the Element2 single collector inductively coupled plasma mass spectrometer (ICP-MS). Precision is ~5-10% for Li and Be. Li isotopes were analyzed using the NuPlasma multi-collector ICP-MS. Unknown samples were bracketed by analyses of the L-SVEC (Li_2CO_3) standard (Flesch et al., 1973), and in-house standards (Li-UMD-1 and IRMM-016) were run at the beginning and end of the analytical session. The standard BCR-1 was also analyzed for comparison. δ^7Li was calculated using $\{(^7Li/^6Li_{SAMPLE}/(^7Li/^6Li_{L\text{-}SVEC(1)} + {}^7Li/^6Li_{L\text{-}SVEC(2)})/2)\text{-}1\}*1000$. Analytical precision for δ^7Li is ±1‰ 2σ, for n=100 over a two-year period. Results for samples and standards are presented in Tables A-9 and A-10, respectively.

4. RESULTS AND DISCUSSION

4.1. Li and Be in Martian Meteorites

Beryllium concentrations for the analyzed meteorites range from 0.04 ppm to 0.77 ppm. Our abundances are slightly higher than the previously measured value for Dho 019 (0.03 ppm, Neal et al., 2001), the only sample previously analyzed for Be. Lithium compositions range from 1.8 ppm to 9.9 ppm, comparable to previous analyses for Chassigny and EETA79001. Our result for Li in Dho 019 is higher than previously reported (2.7 ppm, Neal et al., 2001), and we attribute the increased Li concentration to substantive amounts of alteration material (caliche) present in the sample. Lithium contents measured in Shergotty and Zagami are also higher than previous measurements.

Although both of these meteorites contain minor amounts of secondary alteration minerals (e.g. gypsum, Wentworth and Gooding, 2000), correlations between Li and Be (Figure B-22) suggest our estimates are representative of igneous conditions for these and other meteorites, except Dho 019. Li and Be values for Chassigny plot opposite the oxidized meteorites (Zagami, Shergotty, and Los Angeles), apparently representing Martian mantle Li and Be concentrations. Dho 019 plots in different regions of classification diagrams discussed in the following text, depending on the data source. Results for Li and Be from this study are higher in Dho 019 compared to Neal et al. (2001), and the Li vs. Be plot demonstrates this effect. Rather than explain the differences for Dho 019 in each comparison, we use the chemical data reported by Neal et al. (2001) in following sections.

Results for δ^7Li are identical for Zagami (+4‰) and EETA79001 (+4.4‰), within analytical error, whereas the value for Chassigny (+17‰) is significantly higher. Whole-rock δ^7Li values are comparable to the range of in-situ mineral analyses reported by Chaussidon (1999) for Zagami (+2.5‰ to +6.5‰) and EETA79001 (+2.5‰ to +3.8‰). Chaussidon (1999) measured a significantly lower δ^7Li value for olivine in Chassigny (+10.5‰) compared to our whole-rock result. Although the Li concentration in Chassigny does not appear anomalous, the higher δ^7Li value may be attributed to secondary gypsum and carbonates present in the sample (Wentworth and Gooding, 1994).

4.2. Evidence for Assimilation of a Li-Enriched Component

4.2.1. Li and Be Compositions of Chondrites and Earth's Mantle

Earth's primary (lower mantle) Li and Be concentrations are presumably represented by their concentrations in chondritic meteorites. Hanon et al. (1999) measured Li and Be abundances in chondrules from ordinary chondrites (LL3.0-LL3.1,

L3.7, and H3.6) and Allende (CV3.2) and determined average values of 0.83 ppm for Li and 0.043 ppm for Be. The concentration of Li calculated for mantle-derived peridotites (1-1.5 ppm), using Li concentrations and modal mineral abundances, is similar to chondritic values (Seitz and Woodland, 1999). Paquin et al. (2004) used a similar method to calculate Be abundances in mantle peridotite (~0.01 ppm) that are also similar to chondritic values.

4.2.2 Martian Meteorites Compared to Terrestrial Basalts

Lithium (1.8 ppm) and Be (0.04 ppm) concentrations in Chassigny are similar to chondrites and terrestrial (lower) mantle rocks. Terrestrial dunites typically show Li abundances in the range of 2.0±0.4 ppm (Lundstrom et al., 2005). Be is highly incompatible in olivine ($D_{Be}^{ol\text{-}melt}$=0.001-0.003, Brenan et al., 1998) and therefore is not well characterized in dunites. The range of Be abundances in basaltic shergottites (0.18-0.77 ppm) is similar to the range for MORB (0.1-1 ppm) and OIB (0.5-1 ppm) (Ryan, 2002; Ryan and Langmuir, 1987). Lithium concentrations, however, appear to be elevated in basaltic shergottites (2.7-9.9 ppm) when compared to MORB and OIB reservoirs. The ranges for Li in MORB and OIB are both ~3-8 ppm, although differentiated compositions in all volcanic environments commonly have higher values for both Li and Be. Lavas produced above subduction zones, however, show the greatest variation in Li abundances due to incorporation of subducted, Li-enriched material in the source region. IAB lavas typically contain10-30 ppm Li, whereas Be values are similar to MORB (0.1-1 ppm).

Ryan and Langmuir (1988) determined that Be behaves similarly to incompatible Nd and Zr during melting and crystallization, and Be/Nd and Be/Zr ratios can be used to define different terrestrial oceanic magmatic environments. Figure B-23 compares Be to Nd and Zr for the Martian meteorites analyzed in this study. Slopes representing terrestrial MORB (dashed), OIB (bold), and IAB (and differentiates) are shown for

comparison. Despite considerable scatter in the data, Be/Nd ratios in basaltic shergottites define a general trend similar to island arc calc-alkaline differentiates. When viewed individually, Dho 019 shows a slightly more MORB-like signature, whereas Zagami and Shergotty are similar to more differentiated compositions. Using Be/Zr ratios, the data as a whole cluster around OIB compositions. However, Dho 019 and EETA79001 appear more like MORB, whereas Zagami and Shergotty are similar to IAB.

A similar comparison can be made using Li/Yb ratios, because Li behaves similarly to the heavy rare earth elements (HREE) during melting and crystallization (Ryan and Langmuir, 1987). Figure B-24 shows Li/Yb ratios for the Martian meteorites, with MORB (dashed), OIB (shaded region), and arc differentiates shown for comparison. Dho 019, EETA79001 and Los Angeles define a trend similar to terrestrial OIB. Shergotty and Zagami clearly plot in the IAB field. We further investigate the relationship between Li and other REE in the shergottite source regions by comparing Li/Yb ratios to Dy/Yb ratios (Figure B-25). Because Li behaves similarly to the REE, higher Li abundances due to igneous processes such as melting and differentiation should result in similar increases in the REE concentrations (i.e. Dy). This relationship is observed for OIB, which are represented on Figure B-25 by the shaded region. In contrast, IAB (arrow) show a linear increase in Li/Yb without a corresponding increase in Dy/Yb. This suggests that the IAB source region must contain a component enriched in Li but not REE. On this plot, basaltic shergottites define a trend nearly identical to that of IAB, but Shergotty and Zagami represent the highest Li/Yb ratios and Dho 019, EETA79001 and Los Angeles plot closer to OIB.

Ryan and Langmuir (1987) evaluated the source for higher Li contents in arc volcanics using a plot of K/Li vs. La/Yb (Figure B-26). As in the Li/Yb vs. Dy/Yb plot, variations in K, Li, and REE due to igneous processes result in the trend defined by MORB (shaded region) and OIB (bold). Arc volcanics, however, define a steeper slope, indicating the presence of a component enriched in K, and to a lesser extent Li, but not

REE. On Earth, altered oceanic crust (box) is enriched in K compared to Li, but has limited La/Yb values. Adding a component of recycled altered oceanic crust to the IAB source region, therefore, results in the observed trend. Basaltic shergottites mimic the trend for IAB, extending from MORB-like compositions into the field for altered oceanic crust. The degree of K enrichment in Martian meteorites, however, is significantly less than that observed for arc lavas. The similar, near-vertical slope of the trend defined by basaltic shergottites suggests the K/Li and La/Yb ratios may have been influenced by a process similar to that observed in subduction zone environments. The lower K/Li ratios of basaltic shergottites compared to IAB probably reflect an overall lower abundance of K in the Martian reservoir available for assimilation.

On Earth, unaltered terrestrial basalts have ~5000 ppm K (Mason and Moore, 1982), which increases as secondary alteration phases enriched in K form in oceanic basalt weathered in a submarine environment (Pichler et al., 1999). Martian soils and rocks analyzed by Pathfinder have higher K contents compared to basaltic shergottites (Wänke et al., 2001), suggesting weathering may have caused similar enrichments in altered Martian basalts. Using soil and rock compositions from Pathfinder and Phobos-2 orbital gamma-ray spectroscopy, McClennan (2001) estimated that approximately 0.5% (5000 ppm) K resides in the Martian crust. If unaltered crust was assimilated into shergottitic magmas, the lower K content compared to terrestrial altered basalts may explain the range of K/Li values in basaltic shergottites. However, it is uncertain how high the K content would be in altered Martian crust.

4.3. Li and Be as Crustal Indicators on Mars

If the assimilant in basaltic shergottites parent magmas was enriched in Li and Be, these elements should correlate with previously determined geochemical indicators of the assimilant. We compared Li and Be to $\varepsilon^{143}Nd$, $^{87}Sr/^{86}Sr$, and La/Yb ratios (Figure B-27). The correlations are not strong, and Li and Be abundances in Los Angeles appear

anomalous when compared to La/Yb ratios, but the general trends suggest Li and Be are concentrated in the assimilant.

The similarities between basaltic shergottites and terrestrial arc lavas using Li/Yb, Be/Nd, and K/Li ratios suggest the assimilant may be similar in trace element composition to altered oceanic crust. The crustal signature identified in terrestrial arc source regions originates by alteration of oceanic crust by seawater at low-temperatures (<350°C, Seyfried et al., 1984). In addition to elevated Li contents, oceanic crust altered at low temperatures also carries an enriched δ^7Li and δ^{18}O signature (Gregory and Taylor, 1980; Chan et al., 1992). Bridges et al. (2001) suggested that the most likely environment of formation for the secondary alteration minerals (siderite, gypsum, calcite, magnesite, halite, and other chlorides and sulfates) identified in basaltic shergottites and other Martian meteorites was evaporation of brines at low temperatures (25-150°C). Although isotopically heavy surface waters most likely enriched the rocks with which they interacted, the depth of alteration was probably limited to the near surface. Alteration minerals in Martian meteorites are typically limited to fractures or shock-induced cracks, suggesting large-scale replacement or secondary mineralization did not occur (Bridges et al., 2001 and references therein). The depth of hydrothermal alteration on Mars is unknown, but oxygen isotope studies on terrestrial ophiolite sequences indicate that high temperature (300-600°C) hydrothermal alteration occurs in the upper 4-8 km of oceanic crust. However, low-temperature alteration (200-300°C) is limited to the upper 1-2 km (Gregory and Taylor, 1981; Cocker et al., 1982; Cartwright and Barnicoat, 1999).

We compared Li and Be abundances with oxygen isotope data for basaltic shergottites to determine whether these meteorites possess a low-temperature altered signature (Figure B-28). There is more scatter in the Li data compared to Be, and the trends are not distinct in either case. The δ^{18}O value for Dho 019 appears exceptionally high and the Li and Be values for Los Angeles also appear anomalous (similar to

comparison to La/Yb). However, the remaining meteorites define a rough correlation with $\delta^{18}O$, as might be expected for low-temperature altered crust. As a second test for a low-temperature signature, we evaluated the Li isotopic data. Low-temperature altered oceanic crust has higher $\delta^{7}Li$ and $\delta^{18}O$ values compared to normal mantle (MORB) values. Although we analyzed $\delta^{7}Li$ in only three meteorites, their geochemical heterogeneity is apparent in a variety of comparisons. The two basaltic shergottites analyzed in this study, Zagami (+3.97‰) and EETA79001 (+4.37‰), have Li isotopic compositions identical to each other and to MORB (+4‰). The higher $\delta^{7}Li$ value measured for Chassigny (+17‰) suggests a hydrated reservoir on Mars was enriched in $\delta^{7}Li$, but this reservoir apparently did not interact with the Martian assimilant to an extent that it is recognizable in shergottitic lavas. This is not surprising, as the Martian crust is much thicker (~30-80 km) than Earth's crust (Wieczorek and Zuber, 2004). As shergottite magmas ascend through the crust, the signature of the lower (unaltered) interval of this crust most likely overwhelms any signature imposed by the shallowest interval.

4.4. Magmatic Degassing in the Context of New Li and Be Data

Whole-rock Li and Be abundances for basaltic shergottites are consistent with an assimilant containing greater abundances of these incompatible elements compared to Martian mantle (Chassigny) values. In all geochemical comparisons, except K/Li vs. La/Yb, Shergotty and Zagami define more evolved compositions, presumably representing greater proportions of the assimilated component. However, these results are in contrast to in-situ pyroxene Li, Be, and B abundance data that suggest Li and B were lost from Shergotty and Zagami magmas during degassing upon ascent (Lentz et al., 2001; Herd et al., 2005). Beck et al. (2004) also attributed the increase in Li isotopes measured in NWA 480 from core (-17‰) to rim (+10‰) to magmatic degassing.

Using pyroxene-melt partitioning data for Li ($D_{Li}^{pyroxene\text{-}melt}$=0.20, Herd et al., 2004), Herd et al. (2005) determined that the Li concentrations in Shergotty pyroxene cores (4.5 ppm) and rims (1.5 ppm) require melt compositions of 22 ppm and 7.5 ppm, respectively. Our revised results for Li in Shergotty (8 ppm) satisfy the requirement for melt compositions in equilibrium with pyroxene rims, but not pyroxene cores. Therefore, despite new Li and Be data for Shergotty and Zagami, the mechanism responsible for creating the observed Li, Be, and B trends in basaltic shergottite pyroxenes remains unclear. Detailed examination of light lithophile element behavior in basaltic shergottites is limited, and Shergotty and Zagami, two very similar meteorites, have received the most attention. The obvious difference between these and other basaltic shergottites is the presence of (Li-rich) cumulus pyroxene in both Shergotty and Zagami (Stolper and McSween, 1979; McCoy et al., 1992). If an amount of Li equal to that contained in cumulus pyroxene cores of Shergotty (4.5 ppm*13% cumulus pyroxene; Hale et al., 1999) is subtracted from the bulk composition measured in this study (8 ppm), the Li concentration decreases slightly to 7.4 ppm. Although lower, this Li concentration remains enriched compared to the other basaltic shergottites and does not change the observed geochemical relationships previously discussed. Therefore, magmatic degassing remains the most plausible scenario to explain the in-situ Li data in basaltic shergottites. However, the conflicting trends for whole-rock and in-situ pyroxene Li data should not be ignored.

4.5. What is the Source for the Enriched Component?

Although the depleted end-member identified in basaltic shergottites appears to represent the Martian mantle, the origin of the enriched component is disputable. Borg and Draper (2003) successfully modeled the basaltic shergottites as mixtures of mafic cumulates and late-stage crystallization products of a Martian magma ocean to explain observed differences in major and trace element abundances and radiogenic isotopes. Treiman (2003) observed that highly incompatible elements and moderately incompatible

elements do not correlate in basaltic shergottites. Age relationships suggest these element groups were decoupled prior to melt generation. Therefore, the observed enrichment is better explained by mantle metasomatism prior to melt genesis rather than "crustal" assimilation after melt formation.

Lithium and Be further support the presence of enriched and depleted Martian reservoirs, which were mixed in various proportions to form the basaltic shergottites. However, these elements do not provide definitive evidence that the enriched component is crust or metasomatised mantle. The similarities basaltic shergottites share with IAB suggest the scenario of Borg and Draper (2003) may be more appropriate, at least for these elements. The absence of isotopically heavy Li or O suggests the assimilant was not altered at low temperatures. However, alteration at the high temperatures expected for mantle metasomatism typically liberates Li from basalt compositions and results in isotopically light $\delta^{18}O$ and $\delta^{7}Li$ (Gregory and Taylor, 1981; Cocker et al., 1982; Chan et al., 1992, 2002; Cartwright and Barnicoat, 1999; Foustoukos et al., 2004; Seyfried et al., 1998). In contrast, we observe a positive correlation between Li (and Be) and other indicators of the enriched component (Figure B-27). Although the $\delta^{18}O$ values for basaltic shergottites are slightly below Earth's mantle average (+5.7±0.4‰, Gregory and Taylor, 1981), the consistent $\delta^{18}O$ and $\delta^{7}Li$ values for basaltic shergottites (+4.7 ±0.4‰ and +4.2 ±0.3‰, respectively) suggest the O and Li isotopic signatures of the enriched component did not differ significantly from Earth's (and presumably Mars') mantle.

5. SUMMARY AND CONCLUSIONS

Geochemical relationships among basaltic shergottites, a subgroup of meteorites from Mars, suggest variable amounts of an enriched (crust-like) component were assimilated into mantle derived (depleted) magmas (Jones, 1989; Longhi, 1991; Wadhwa, 2001; Borg, 2002; Herd et al., 2002). On Earth, the light lithophile elements Li, Be, and B preserve a component of altered oceanic crust in the source regions of OIB lavas (Ryan

and Langmuir, 1987, 1988, 1993). The crustal signature develops in oceanic crust altered at low temperatures, and differences in fluid-rock partitioning behavior of Li, Be, and B result in higher abundances and heavier isotopic concentrations of Li and B, whereas Be is unchanged. During subduction, dehydration reactions transfer the crustal signature recorded by fluid-mobile Li and B to the overlying mantle wedge where melting occurs.

The enriched component in basaltic shergottites may have been hydrated (McSween, 2002), and isotopically heavy oxygen and hydrogen measured in alteration minerals in Martian meteorites (Karlsson et al., 1992; Leshin Watson et al., 1994; Boctor et al., 2003) suggests this reservoir may also have been enriched in Li. We measured Li and Be abundances and Li isotopes in basaltic shergottites that encompass the reported range of geochemical heterogeneity. Shergotty, Zagami, and Los Angeles represent the enriched end-member, EETA79001 is an intermediate composition, and Dho 019 and Chassigny represent the depleted end-member.

Chassigny appears to represent Martian mantle Li (1.8 ppm) and Be (0.04 ppm) abundances, which are similar to values measured in chondrites and terrestrial mantle rocks. Terrestrial alteration minerals in the sample of Dho 019 analyzed in this study apparently modified the primary bulk Li and Be concentrations. Beryllium concentrations in the remaining basaltic shergottites (0.09-0.77 ppm) are similar to MORB and OIB, but Li concentrations (2.7-9.9 ppm) are enriched compared to these reservoirs. Using Be/Nd, Be/Zr, and La/Yb ratios, Shergotty and Zagami are similar to IAB compositions whereas the remaining shergottites resemble MORB or OIB. Basaltic shergottites define trends similar to IAB when Li/Yb is compared to Dy/Yb and K/Li is compared to La/Yb. In IAB source regions, subducted altered oceanic crust is responsible for increasing K and Li while maintaining relatively constant REE values (Ryan and Langmuir, 1987). Although the assimilant in basaltic shergottites appears to be enriched in Li (and possibly Be), the weak correlation when Li and Be are compared to $\delta^{18}O$ suggests the assimilant was not altered at low temperatures. Furthermore, Li isotopes in two meteorites with

presumably different amounts of assimilated material, Zagami (+3.97‰) and EETA79001 (+4.37‰), are identical within analytical error and are also similar to average MORB (+4‰). Therefore, it is not clear, using Li and Be, whether the enriched component observed in basaltic shergottites originated as metasomatised mantle or was assimilated as evolved crust.

Our results for Shergotty and Zagami suggest these two meteorites assimilated a greater proportion of the enriched component. However, these data are in contrast to previous studies using in-situ pyroxene analyses, which suggest Li and B were lost during magmatic degassing (Lentz et al., 2001; Beck et al., 2004; Herd et al., 2005). Although these meteorites contain cumulus pyroxene, adjusting the bulk composition by an amount equal to that represented by the cumulus pyroxene does not change the observed correlations among basaltic shergottites.

ACKNOWLEDGEMENTS

This research was supported by NASA Cosmochemistry grant NAG5-12896 to H. Y. M.

LIST OF REFERENCES

Andersen D. J., Lindsley D. H., and Davidson P. M. (1993) QUILF: A Pascal program to assess equilibria among Fe-Mg-Mn-Ti oxides, pyroxenes, olivine, and quartz. *Computers & Geosciences* **19**, 1333-1350.

Baker M. B., Alves S., and Stolper E. M. (1996) Petrography and petrology of the Hawaii Scientific Drilling Project lavas: Inferences from olivine phenocryst abundances and compositions. *J. Geophys. Res.* **101,** 11,715-11,727.

Barrat J. A., Jambon A., Bohn M., Gillet Ph. Sautter V., Gopel C., Lesourd M., Keller F., and Petit E. (2002a) Petrology and chemistry of the Picritic Shergottite North West Africa 1068. *Geochim. Cosmochim. Acta* **66**, 3505-3518.

Barrat J. A., Gillet Ph., Sautter V., Jambon A., Javoy M., Gopel C., Lesourd M., Keller F., and Petit E. (2002b) Petrology and chemistry of the basaltic shergottite North West Africa 480. *Meteorit. Planet. Sci.* **37**, 487-499.

Baryshnikova G. V., Stakheyeva S. A., Ignatenko K. I., and Lavrukhina A. K. (1985) Pyroxenes in H- and L-group ordinary chondrites. *Geokhimiya* **1**, 20-34.

Bebout G. E., Ryan J. G., and Leeman W. P. (1993) B-Be systematics in subduction-related metamorphic rocks: Characterization of the subducted component, *Geochim. Cosmochim. Acta.* **57**, 2227-2237.

Beck P., Barrat J. A., Chaussidon M., Gillet Ph., and Bohn M. (2004) Li isotopic variations in single pyroxenes from the Northwest Africa 480 shergottite (NWA 480): a record of degassing of Martian magmas? *Geochim. Cosmochim. Acta* **68**, 2925-2933.

Bennett M. E. and McSween H. Y. Jr. (1996) Shock features in iron-nickel metal and troilite of L-group ordinary chondrites. *Meteorit. Planet. Sci.* **31**, 255-264.

Blichert-Toft J., Weis D., Maerschalk C., Agranier A., and Albarede F. (2003) Hawaiian hot spot dynamics as inferred from the Hf and Pb isotope evolution of Mauna Kea volcano. *Geochem. Geophys. Geosyst.* ***4 (2),*** 8704, doi:10.1029/2002GC000340.

Boctor N. Z., Alexander C. M. O'D., Wang J., and Hauri E. (2003) The sources of water in Martian meteorites: clues from hydrogen isotopes. *Geochim. Cosmochim. Acta* **67**, 3971-3989.

Borg L. E., Nyquist L. E., Taylor L. A., Wiesmann H., and Shih C-Y. (1997) Constraints on Martian differentiation processes from Rb-Sr and Sm-Nd isotopic analyses of the basaltic shergottite QUE 94201. *Geochim. Cosmochim. Acta* **61**, 4915-4931.

Borg L. E., Nyquist L. E., Wiesmann H., Reese Y., and Papike J. J. (2000) Sr-Nd isotopic systematics of martian meteorite DaG476 (abstr.). *Lunar Planet. Sci. Conf.* **XXXI** #1036.

Borg L. E., Nyquist L. E., Reese Y., Wiesmann H., Shih C-Y., Ivanova M., Nazarov M. A., and Taylor L. A. (2001) The age of Dhofar 019 and its relationship to the other martian meteorites (abstr.). *Lunar Planet. Sci. Conf.* **XXXII** #1144.

Borg L. E. (2002) Exploring trace element and isotopic mixing relationships in the martian meteorite suite (abstr.). *Workshop on Unmixing the SNCs* #6004.

Borg L. E. and Draper D. S. (2003) A petrogenetic model for the origin and compositional variation of the martian basaltic meteorites. *Meteorit. Planet. Sci.* **38**, 1713-1731.

Brenan J. M., Neroda E., Lundstrom C. C., Shaw H. F., Ryerson F. J., and Phinney D. L. (1998) Behaviour of boron, beryllium, and lithium during melting and crystallization:

Constraints from mineral-melt partitioning experiments. *Geochim. Cosmochim. Acta* **62**, 2129-2141.

Bridges J. C., Catling D.C., Saxton J. M., Swindle T. D., Lyon I. C., and Grady M. M. (2001) Alteration assemblages in martian meteorites: implications for near-surface processes. *Space Sci. Rev.* **96**, 365-392.

Bunch T. E., Mall A. P., and Lewis C. F. (1972) The Seoni chondrite. *Meteoritics* **7,** 87-95.

Cartwright I. and Barnicoat A. C. (1999) Stable isotope geochemistry of Alpine ophiolites: a window to ocean-floor hydrothermal alteration and constraints on fluid-rock interaction during high-pressure metamorphism. *Int. Jour. Earth Sciences* **88**, 219-235.

Chamot J. (2000) Modal mineralogy of the H-group chondrites: Progressive effects of metamorphism. M.S. thesis, University of Tennessee, Knoxville, Tennessee, USA.

Chan L. H., Edmond J. M., Thompson G., and Gillis K. (1992) Lithium isotopic composition of submarine basalts: implications for the lithium cycle in the oceans. *Earth Planet. Sci. Lett.* **108**, 151-160.

Chan L. H., Alt J.C. and Teagle D. A. H. (2002) Lithium and lithium isotope profiles through the upper oceanic crust: a study of seawater-basalt exchange at ODP Sites 504b and 896a. *Earth Planet. Sci. Lett.* **201**, 187-201.

Chan L.-H. and Frey F. A. (2003) Lithium isotope geochemistry of the Hawaiian plume: Results from the Hawaii Scientific Drilling Project and Koolau Volcano, *Geochem. Geophys. Geosyst., 4 (3)*, 8707, doi:10.1029/2002GC000365.

Chaussidon M. and Robert F. (1999) $^{7}Li/^{6}Li$ and $^{11}B/^{10}B$ ratios of SNC meteorites. *Lunar Planet. Sci. Conf.* ***XXX***, #1592.

Clayton R. N. (1993) Oxygen isotopes in meteorites. *Annual Review of Earth and Planetary Science* **21**, 115-149.

Cocker J. D., Griffin B. J., and Muehlenbachs K. (1982) Oxygen and carbon isotope evidence for seawater-hydrothermal alteration of the Macquarie Island ophiolite. *Earth Planet. Sci. Lett.* **61**, 112-122.

DePaolo D. J., Stolper E., and Thomas D. M. (2001) Deep drilling into a Hawaiian Volcano. *Eos* ***82,*** 149-160.

Dodd R. T. and Jarosewich E. (1981) Chemical variations among L-group chondrites, III. Major element variation in L6 chondrites. *Meteoritics* **16,** 93-111.

Donnely T. W., Thompson G., and Salisbury M. H. (1980) The chemistry of altered basalts at site 417, Deep Sea Drilling Project leg 51. In *Init. Repts. DSDP 51-53* (eds. R. Powell and F. Laughter), 1319-1330.

Eiler J. M., Valley J. W., and Stolper E. M. (1996) Oxygen isotope ratios in olivine from the Hawaii Scientific Drilling Project. *J. Geophys. Res.* **101***,* 11,807-11,813.

Feigenson M. D., Bolge L. L., Carr M. J., and Herzberg C. T. (2003) REE inverse modeling of HSDP2 basalts; evidence for multiple sources in the Hawaiian plume. *Geochem. Geophys. Geosyst.* ***4 (2),*** 8706, doi:10.1029/2001GC000271.

Ferraris C., Folco L., and Mellini M. (2002) Chondrule thermal history from unequilibrated H chondrites: A transmission and analytical electron microscopy study. *Meteoritics & Planetary Science* **37,** 1299-1321.

Flesch G. D., Anderson A. R. J., Svec H. J. (1973) A secondary isotopic standard for $^{6}Li/^{7}Li$ determinations. *Int. Jour. Mass Spectrom. Ion Process.* **12**, 265-272.

Folco L. and Mellini M. (2000) Enstatite chemical composition and microstructures in the La Villa H4 chondrite. *Meteorit. Planet. Sci.* **35,** 733-742.

Folco L., Franchi I.A., D'Orazio M., Rocchi S. and Schultz L. (2000) A new Martian meteorite from the Sahara: the shergottite Dar al Gani: 489. *Meteorit. Planet. Sci.* **35**, 827–839.

Foustoukos D. I., James R. H., Berndt M. E., Seyfried W. E. (2004) Lithium isotopic systematics of hydrothermal vent fluids at the Main Endeavour Field, Northern Juan de Fuca Ridge. *Chem. Geol.* **212**, 17-26.

Garcia M. O. (1996) Petrography and olivine and glass chemistry of lavas from the hawaii Scientific Drilling Project. *J. Geophys. Res.* **101***,* 11,701-11,713.

Gastineau-Lyons H. K., McSween H.Y., Jr., and Gaffey M. J. (2002) A critical evaluation of oxidation versus reduction during metamorphism of L and LL group chondrites, and implications for asteroid spectroscopy. *Meteorit. Planet. Sci.* **37**, 75-89.

Gee L. L. and Sack R.O. (1988) Experimental petrology of melilite nephelinites. *J. Petrol.* **29***,* 1233-1255.

Ghosh A., Weidenschilling S. J., McSween Jr. H. Y. (2003) Importance of the accretion process in asteroidal thermal evolution: 6 Hebe as an example, *Meteoritics & Planetary Science* 38: 711-724.

Gregory R. T. and Taylor, Jr. H. P. (1981) An oxygen isotope profile in a section of Cretaceous oceanic crust, Samail ophiolite, Oman: Evidence for $\delta^{18}O$ buffering of the oceans by Deep (> 5km) seawater-hydrothermal circulation. *J. Geophys. Res.* **86***,* 2737-2755.

Griffiths R. W. and Campbell I. H. (1990) Stirring and structure in mantle starting plumes. *Earth Planet. Sci. Lett.* **99***,* 66-78.

Griffiths R. W. (1991) Entrainment and stirring in viscous plumes. *Physics of Fluids A-Fluid Dynamics* **3**, 1233-1242.

Griffiths R. W. and Campbell I. H. (1991) On the dynamics of long-lived plume conduits in the convecting mantle. *Earth Planet. Sci. Lett.* **103**, 214-227.

Grove T. L., Baker M. B., and Kinzler R. J. (1984) Coupled CaAl-NaSi diffusion in plagioclase feldspar: Experiments and applications to cooling rate speedometry. *Geochim. Cosmochim. Acta* **48**, 2113-2121.

Hale V. P. S., McSween H. Y., Jr., and McKay G. A. (1999) Re-evaluation of intercumulus liquid composition and oxidation state for the Shergotty meteorite. *Geochim. Cosmochim. Acta* **63**, 1459-1470.

Hanon P., Chaussidon M., and Robert F. (1999) Distribution of lithium, beryllium, and boron in meteoritic chondrules. *Meteorit. Planet. Sci.* **34**, 247-258.

Hart S. R. (1984) A large-scale isotope anomaly in the Southern Hemisphere mantle. *Nature* **309***,* 753-757.

Hauri E. H., Whitehead J. A., and Hart S. R. (1994) Fluid dynamic and geochemical aspects of entrainment in mantle plumes. *J. Geophys. Res.* **99***,* 24,275-24,300.

Hauri E. H., Lassiter J. C., and DePaolo D. J. (1996) Osmium isotope systematics of drilled lavas from Mauna Loa, Hawaii. *J. Geophys., Res.* **101***,* 11,793-11,806.

Hawaii Scientific Drilling Project-2, Core logs and summarizing data (2000) edited by C. A. Seaman, M. O. Garcia, and E. M. Stolper, California Institute of Technology.

Herd C.D.K. and Papike J.J. (2000) Oxygen fugacity of the martian basalts from analysis of iron-titanium oxides: implications for mantle-crust interaction on Mars (abstr.). *Meteorit. Planet. Sci. Supp.* **35**, A70.

Herd C. D. K., Borg L. E., Jones J. H., and Papike J. J. (2002) Oxygen fugacity and geochemical variations in the martian basalts: Implications for martian basalt petrogenesis and the oxidation state of the upper mantle of Mars. *Geochim. Cosmochim. Acta* **66**, 2025-2036.

Herd C. D. K., Trieman A. H., McKay G. A., and Shearer C. K. (2004) The behavior of Li and B during planetary basalt crystallization. *Am. Mineral*. **89**, 832-840.

Herd C. D. K., Trieman A. H., McKay G. A., and Shearer C. K. (2005) Light lithophile elements in martian basalts: Evaluating the evidence for magmatic water degassing. *Geochim. Cosmochim. Acta* **69**, 2431-2440.

Heyse J.V. (1978) The metamorphic history of LL-group ordinary chondrites. *Earth Planet. Sci. Lett.* **40,** 365-381.

Hofmann A. W. and Jochum K. P. (1996) Source characteristics derived from very incompatible trace elements in Mauna Loa and Mauna Kea basalts, Hawaii Scientific Drilling Project. *J. Geophys. Res,* **101,** 11,831-11,839.

Huang S. and Frey F. A. (2003) Trace element abundances of Mauna Kea basalt from phase 2 of the Hawaii Scientific Drilling project: Petrogenetic implications of correlations with major element content and isotopic ratios. *Geochem. Geophys. Geosyst.,* **4 (6),** 8711, doi:10.1029/2002GC000322.

Jaques A. L., Lowenstein P. L., Green D. H., Kiss E., Nance W. B., Taylor S. R., and Ware N. G. (1975) The Ijopega chondrite: A new H6 fall. *Meteoritics* **10**, 289-301.

Jambon A., Barrat J. A., Sautter V., Gillet Ph., Gopel C., Javoy M., Joron J. L., and Lesourd M. (2002) The basaltic shergottite Northwest Africa 856: Petrology and chemistry. *Meteorit. Planet. Sci.* **37**, 1147-1164.

Jones J. H. (1989) Isotopic relationships among the shergottites, the Nakhlites and Chassigny. *Proc. Lunar Planet. Sci.* **19**, 465-474.

Jones R. H. (1997) Equilibration of pyroxenes in Type 4-6 LL chondrites (abstract). *Proceedings, 28th Lunar and Planetary Science Conference*. pp. 681-682.

Karlsson H. R., Clayton R. N., Gibson E. K., and Mayeda T. K. (1992) Water in SNC Meteorites: Evidence for a Martian hydrosphere. *Science* **255**, 1409-1411.

Keil K., Lange D., Ulbrich M. N. C., Gomes C. B., Jarosewich E., Roisenberg A., and Souza M. J. (1978) Studies of Brazilian meteorites XIII. Mineralogy, petrology, and chemistry of the Putinga, Rio Grande Do Sul, chondrite. *Meteoritics* **13**, 165-175.

Kessel R. and Stolper E. M. (2002) The thermal history of equilibrated ordinary chondrites and the relationship between textural maturity and temperature. *Lunar Planet. Sci. Conf.* **XXXII,** #1420.

Kretz R. (1982) Transfer and exchange equilibria in a portion of the pyroxene quadrilateral as deduced from natural and experimental data. *Geochim. Cosmochim. Acta* **46,** 411-422.

Lange D. E., Moore C. B., and Rhoton K. (1973) The Willowbar meteorite. *Meteoritics* **8**, 201-256.

Langenhorst F., Joreau P., and Doukhan J. C. (1995) Thermal and shock metamorphism of the Tenham chondrite: A TEM examination. *Geochim. Cosmochim. Acta* **59**, 1835-1845.

Lassiter J. C., DePaolo D. J., and Tatsumoto M. (1996) Isotopic evolution of Mauna Kea volcano: Results from the initial phase of the Hawaii Scientific Drilling Project. *J. Geophys. Res.* **101,** 11,769-11,780.

Le Bas M. J., Le Maitre R. W., Streckeisen A., and Zanettin B. (1986) A chemical classification of volcanic rocks based on the total alkali-silica diagram. *Jour. Petrol.* **27,** 745-750.

Lee C-D and Halliday A. (1997) Core formation on Mars and differentiated asteroids. *Nature* **388**, 854-857.

Lentz R. C. F., McSween H. Y., Jr., Ryan J. G., and Riciputi L. R. (2001) Water in martian magmas: Clues from light lithophile elements in shergottite and nakhlite pyroxenes. *Geochim. Cosmochim. Acta* **65**, 4551-4565.

Leshin Watson L., Hutcheon I. D., Epstein S., and Stolper E. M. (1994) Water on Mars: Clues from Deuterium/Hydrogen and Water Contents of Hydrous Phases in SNC Meteorites. *Science* **265**, 86-90.

Lindsley D. H. (1983) Pyroxene thermometry. *American Mineral.* **68**, 477-493.

Lipschutz M. E., Gaffey M. J., and Pellas P. (1989) Meteoritic parent bodies: nature,number, size and relation to present-day asteroids. In *Asteroids II* (eds. Binzel R. P., Gehrels T., Mathews M. S.) University of Arizona Press, Tucson, 740-777.

Lodders K. (1998) A survey of shergottite, nakhlite and chassigny meteorites whole-rock compositions. *Meteorit. Planet. Sci.* **33**, A183-A190.

Longhi J. (1991) Magmatic processes on Mars: Insights from SNC meteorites. *Proc. Lunar Planet. Sci.* **21**, 695-709.

Longhi J., Knittle E., Holloway J. R., and Wänke H. (1992) The bulk composition, mineralogy and internal structure of Mars. In *Mars* (eds. H. H. Keiffer, B. M. Jakosky, C. W. Snyder, and M. S. Matthews), University of Arizona Press, Tuscon, 184-208.

Lundstrom C. C., Chaussidon M., Hsui A. T., Kelemen P., and Zimmerman M. (2005) Observations of Li isotopic variations in the Trinity Ophiolite: Evidence for isotopic fractionation by diffusion during mantle melting. *Geochim. Cosmochim. Acta* **69**, 735-751.

Macdonald G. A. and Katsura T. (1964) Chemical composition of Hawaiian lavas. *Jour. Petrol.* **5***,* 82-133.

Mason B. and Moore C. B. (1982) *Principles of Geochemistry*, 4th ed., Wiley, New York, pp. 46-47 and 176-177.

McCoy T. J., Taylor G. J., and Keil K. (1992) Zagami: Product of a two-stage magmatic history. *Geochim. Cosmochim. Acta* **56**, 3571-3582.

McLennan S. M. (2001) Crustal heat production and the thermal evolution of Mars. *Geophys. Res. Lett.* **28**, 4019-4022.

McLennan S. M. (2003) Large-ion lithophile element fractionation during the early differentiation of Mars and the composition of the martian primitive mantle. *Meteorit. Planet. Sci.* **38**, 895-904.

McSween H. Y., Jr. (2002) The rocks of Mars, from far and near. *Meteorit. Planet. Sci.* **37**, 7-25.

McSween H. Y. Jr., Sears D. W. G., and Dodd R. T. (1988) Thermal metamorphism. In *Meteorites and the Early Solar System* (eds. Kerridge J. F. and Matthews M.S.) University of Arizona Press, Tucson, 102-113.

McSween H. Y. Jr. and Patchen A. D. (1989) Pyroxene thermobarometry in LL-group chondrites and implications for parent body metamorphism. *Meteoritics* **24**, 219-226.

McSween H. Y. Jr. (2002) The rocks of Mars, from far and near. *Meteorit. Planet. Sci.* **37**, 7-25.

McSween H. Y. Jr., Ghosh A., Grimm R. E., Wilson L., and Young E. D. (2002) Thermal evolution models of asteroids. In *Asteroids III,* edited by Bottke W. F., Cellino A., Paolicchi P., and Binzel R. P. Tucson: University of Arizona Press. pp. 559-571.

Mittlefehldt D. W. (1994) ALH84001, a cumulate orthopyroxenite member of the SNC meteorite group. *Meteoritics* **29**, 214-221.

Moran A. E., Sisson V. B. and Leeman W. P. (1992) Boron depletion during progressive metamorphism: Implications for subduction processes. *Earth Planet. Sci. Lett.* **111**, 331-349.

Moriguti T. and Nakamura E. (1998) Across-arc variation of Li isotopes in lavas and implications for crust/mantle recycling at subduction zones. *Earth Planet. Sci. Lett.* **163**, 167-174.

Morris J. D. (1991) Applications of cosmogenic ^{10}Be to problems in the earth sciences. *Ann. Rev. Earth Planet. Sci.* **19**, 313-350.

Morris J. D., Leeman W. P., and Tera F. (1990) The subduction component in island arc lavas: constraints from barium isotopes and B-Be systematics. *Nature* **344,** 31-36.

Nakamuta Y. and Motomura Y. (1999) Sodic plagioclase thermometry of type 6 ordinary chondrites: Implications for the thermal histories of parent bodies. *Meteorit. Planet. Sci.* **34**, 763-772.

Neal C. R., Taylor L. A., Ely J. C., Jain J. C., and Nazarov M. A. (2001) Detailed geochemistry of new shergottite, Dhofar 019. *Lunar Planet. Sci. Conf. **XXXII**,* #1671.

Nyquist L. E., Wooden J., Bansal B., Wiesmann H., McKay G., and Bogard D. D. (1979) Rb-Sr age of the Shergotty achondrite and implications for metamorphic resetting of isochron ages. *Geochim. Cosmochim. Acta* **43**, 1057-1074.

Nyquist L. E., Reese Y. D., Wiesmann H., Shih C-Y., and Schwandt C. (2000) Rubidium-strontium age of the Los Angeles shergottite (abstr.). *Meteorit. Planet. Sci. Supp.* **35**, A121-A122.

Nyquist L. E., Reese Y. D., Wiesmann H., and Shih C-Y. (2001) Age of EET79001B and implications for shergottite origins (abstr.). *Lunar Planet. Sci. Conf.* **XXXII**, #1407.

Olsen E. J. and Bunch T. E. (1984) Equilibration temperatures of the ordinary chondrites: A new evaluation. *Geochim. Cosmochim. Acta* **48**, 1363-1365.

Paquin J., Altherr R., and Ludwig T. (2004) Li-Be-B systematics in the ultrahigh-pressure garnet peridotite from Alpe Arami (Central Swiss Alps): implications for slab-to-mantle wedge transfer. *Earth Planet. Sci. Lett.* **218**, 507-519.

Perfit M. R. and Davidson J. P. (2000) Plate tectonics and volcanism. In *Encyclopedia of Volcanoes* (eds. Sigurdsson H., Houghton B. F., McNutt S. R., Rymer H., and Stix J.) Academic Press, 89-113.

Pichler T., Ridley W. I., and Nelson E. (1999) Low-temperature alteration of dredged volcanics from the Southern Chile Ridge: additional information about early stages of seafloor weathering. *Marine Geol.* **159**, 155-177.

Pellas P. and Fieni C. (1988) Thermal histories or ordinary chondrite parent asteroids. *Lunar Planet. Sci. Conf.* **XIX**, 915-916.

Rhodes J. M. (1996) Geochemical stratigraphy of lavas flows sampled by the Hawaii Scientific Drilling Project. *J. Geophys. Res.* **101,** 11,729-11,746.

Rhodes J. M. and Vollinger M. J. (2004) Composition of basaltic lavas sampled by phase-2 of the Hawaii Scientific Drilling Project: Geochemical stratigraphy and magma types. *Geochem. Geophys. Geosyst.* **5,** Q03G13, doi: 10.1029/2002GC000434.

Rubin A. E., Fegley B., and Brett R. (1988) Oxidation state in chondrites. In *Meteorites and the Early Solar System* (eds. J. F. Kerridge, M. S. Matthews) The University of Arizona Press, Tucson, 488-511.

Rubin A. E., Warren P. H., Greenwood J. P., Verish R. S., Leshin L. A., Hervig R. L., Clayton R. N., and Mayeda T. K. (2000) Los Angeles: The most differentiated basaltic martian meteorite. *Geology* **28**, 1011-1014.

Ryan J. G. and Langmuir C.H. (1987) The systematics of lithium abundances in young volcanic rocks. *Geochim. Cosmochim. Acta* **51**, 1727-1741.

Ryan J. G. and Langmuir C.H. (1988) Beryllium systematics in young volcanic rocks: Implications for ^{10}Be. *Geochim. Cosmochim. Acta* **52**, 237-244.

Ryan J. G. and Langmuir C. H. (1993) The systematics of boron in young volcanic rocks. *Geochim. Cosmochim. Acta* **57,** 1489-1498.

Ryan J. G., Leeman W. P., Morris J. D., and Langmuir C. H. (1996) The boron systematics of intraplate lavas: Implications for crust and mantle evolution. *Geochim. Cosmochim. Acta* **60,** 415-422.

Ryan J. G. (2002) The trace-element behavior of beryllium in terrestrial materials. In *Beryllium: Mineralogy and Geochemistry. Reviews of Mineralogy and Geochemistry* (ed. E. Grew) **50**, pp. 121-145

Sack R. O and Ghiorso M. S. (1991) Chromian spinels as petrogenetic indicators: Thermodynamics and petrological applications. *American Mineral.* **76**, 827-847.

Sears D. W. G., Grossman J. N., Melcher C. L., Ross L. M., and Mills A. A. (1980) Measuring metamorphic history of unequilibrated ordinary chondrites. *Nature* **287**, 791-795.

Seitz H-M. and Woodland A. B. (1999) The distribution of lithium in peridotitic and pyroxenitic mantle lithologies—an indicator of magmatic and metasomatic processes. *Chem. Geol.* **166**, 47-64.

Seyfried W. E., Jr., Janecky D. R., and Mottl M. J. (1984) Alteration of the oceanic crust: Implications for geochemical cycles of lithium and boron. *Geochim. Cosmochim. Acta* **48,** 557-569.

Sharp W. D. and Renne P. R. (2005) The $^{40}Ar/^{39}Ar$ dating of core recovered by the Hawaii Scientific Drilling Project (phase 2), Hilo, Hawaii. *Geochem. Geophys. Geosyst.* **6,** Q04G17, doi:10.1029/2004GC000846.

Spivack A. J. and Edmond J. M. (1987) Boron isotope exchange between seawater and the oceanic crust. *Geochim. Cosmochim. Acta* **51,** 1033-1043.

Stolper E. M., DePaolo D. J., and Thomas D. M. (1996) Introduction to special section: Hawaii Scientific Drilling Project. *J. Geophys. Res.* **101,** 11,593-11,598.

Shervais J. W., Taylor L. A., Cirlin E-H., Jarosewich E., and Laul J. C. (1986) The Maryville meteorite: A 1983 fall of an L6 chondrite. *Meteoritics* **21**, 33-45.

Sighinolfi G. P., Garuti G., and Morais E. (1991) The Jolomba, Angola LL6 chondrite. *Meteoritics* **26**, 27-29.

Slater V. P. and McSween H. Y. Jr. (2001) Testing the applicability of the plagioclase and two-pyroxene geothermometers in Guarena, a H6 chondrite (abstract). *Meteorit. Planet. Sci.* **36**, A193.

Spivack A. J. and Edmond J. M. (1987) Boron isotope exchange between seawater and the oceanic crust. *Geochim. Cosmochim. Acta* **51**, 1033-1043.

Spohn T., Acuña M. H., Breuer D., Golombek M., Greeley R., Halliday A., Hauber E., Jaumann R., and Sohl F. (2001) Geophysical constraints on the evolution of Mars. *Space Sci. Rev.* **96**, 231-262.

Stöffler D., Keil K., and Scott E. R. D. (1991) Shock metamorphism of ordinary chondrites. *Geochim. Cosmochim. Acta* **55**, 3845-3867.

Stolper E. and McSween H. Y., Jr. (1979) Petrology and origin of the shergottite meteorites. *Geochim. Cosmochim. Acta* **43**, 1475-1498.

Straub S. M. and Layne G. D. (2002) The systematics of boron isotopes in Izu arc front volcanic rocks. *Earth Planet. Sci. Lett.* **198**, 25-39.

Taylor S. R., Maggiore P., Scott E. R. D., RuinA. E., and Keil K. (1987) original structures and fragmentation and reassembly histories of asteroids: Evidence from meteorites. *Icarus* **69**, 1-13.

Taylor L. A., Nazarov M. A., Shearer C. K., McSween H. Y., Jr., Cahill J., Neal C. R., Ivanova M. A., Barsukova L. D., Lentz R. C., Clayton R. N., and Mayeda T. K. (2002) Martian meteorite Dhofar 019: A new shergottite. *Meteorit. Planet. Sci.* **37**, 1107-1128.

Tera F., Brown L., Morris J., Sacks I. S., Klein J., and Middleton R. (1986) Sediment incorporation in island-arc magmas: Inferences from ^{10}Be. *Geochim. Cosmochim. Acta.* **50**, 535-550.

Thomas D. M., Paillet F. L., and Conrad M. E. (1996) Hydrogeology of the Hawaii Scientific Drilling Project borehole KP-1 2. Groundwater geochemistry and regional flow patterns. *J. Geophys. Res.* **101,** 11,683-11,694.

Tomascak P. B., Tera F., Helz R. T., and Walker R. J. (1999a) The absence of lithium isotope fractionation during basalt differentiation: New measurements by multicollector sector ICP-MS. *Geochim. Cosmochim. Acta.* **63**, 907-910.

Tomascak P. B., Carlson R. W., and Shirey S. B. (1999b) Accurate and precise determination of Li isotopic compositions by multi-collector sector ICPMS. *Chem. Geology* **158**, 145-154.

Treiman A.H. (2003) Chemical composition of martian basalts (shergottites): Some inferences on basalt formation, mantle metasomatism, and differentiation in Mars.

Van Schmus W. R. and Wood J. A. (1967) A chemical-petrologic classification for the chondritic meteorites. *Geochim. Cosmochim. Acta* **31,** 747-765.

Wadhwa M. (2001) Redox state of Mars' upper mantle and crust from Eu anomalies in shergottite pyroxenes. *Science* **291**, 1527-1530.

Wang D. and Rubin A. E. (1987) Petrology of nine ordinary chondrite falls from China. *Meteoritics* **22**, 97-104.

Wang Z., Kitchen N. E., and Eiler J. M. (2003) Oxygen isotope geochemistry of the second HSDP core. *Geochem. Geophys. Geosyst. **4 (8),*** 8712, doi:10.1029/2002GC000406.

Wänke H., Brückner J., Dreibus G., Reider R., and Ryabchikov I. (2001) Chemical composition of rocks and soils at the Pathfinder site. *Space Sci. Rev*. **96**, 317-330.

Wasson J. T. (1993) Constraints on chondrule origins. *Meteoritics* **28**, 14-28.

Wentworth S. J. and Gooding J. L. (1994) Carbonates and Sulfates in the Chassigny Meteorite: Further Evidence for Aqueous Chemistry on the SNC Parent Planet. *Meteoritics* **29**, 861-863.

Wentworth S. J. and Gooding J. L. (2000) Weathering and Secondary Minerals in the Martian Meteorite Shergotty. *Lunar Planet. Sci. Conf.* **XXXI**, #1888.

Wieczorek M. A. and Zuber M. T. (2004) Thickness of the Martian crust: Improved constraints from geoid-to-topography ratios. *Jour. Geophys. Res. Planets* **109**, Article No. E01009.

Wood C. A. and Ashwal L. D. (1981) SNC meteorites: Igneous rocks from Mars? *Proc. Lunar Planet. Sci.* **128**, 1359-1375.

Wooden J. L., Shih C-Y., Nyquist L. E., Bansal B. M., Wiesmann H., and McKay G. (1982) Rb-Sr and Sm-Nd isotopic constraints on the origin of EETA 79001: A second Antarctic shergottite (abstr.). *Lunar Planet. Sci. Conf.* **XIII**, 879-880.

APPENDICES

APPENDIX A

Table A-1. Previously determined peak temperatures (°C) for Type 6 ordinary chondrites.

	Olsen and Bunch (1984)		McSween and Patchen (1989)		Langenhorst et al. (1995)		Jones (1997)		Clayton (1993)	Kessel et al. (2002)
	Cpx	**Opx**	**Cpx**	**Opx**	**Cpx**	**Opx**	**Cpx**	**Opx**	**Plag-Ol**	**Ol-Spinel**
H6	820-830 [a,b]	-	-	-	870 [b]	810 [b]	-	-	900±50	740
L6	920-930 [a] 860-870 [b]	-	-	-	-	-	-	-	900±50	700
LL6	920-930 [a] 860-870 [b]	-	1040-1112 [a] 900-960 [b]	790-900 [b]	-	-	650-800 [b]	800 [b]	900±50	720

[a] Estimates using the Kretz (1982) geothermometer.

[b] Estimates using the Lindsley (1983) geothermometer.

Table A-2. Meteorites examined in this study.

		Shock Classification (Nakamuta and Motomura, 1999)	**Source**	**Section Number**
Peekskill	H6	S2	USNMNH	6543-1
Mulga (north)	H6	S2	USNMNH	3414
Great Bend	H6	S1-S2	Field Museum/ Naturhistorisches Museum Vienna	Me3017/L8853
Holbrook	L6	S2	USNMNH	437-1
Owasco	L6	S3	Field Museum/ Naturhistorisches Museum Vienna	Me3039/1153a
Dhurmsala	LL6	S3	USNMNH	82-1

Table A-3. Average compositions for pyroxenes analyzed in this study (1 sigma standard deviation).

	Peekskill H6		Mulga (north) H6		Great Bend H6		Holbrook L6		Owasco L6		Dhurmsala LL6	
Oxide Wt. %	**Cpx [8][a]**	**Opx [5]**	**Cpx [7]**	**Opx [12]**	**Cpx [6]**	**Opx [16]**	**Cpx [3]**	**Opx [2]**	**Cpx [6]**	**Opx [16]**	**Cpx [6]**	**Opx [4]**
SiO_2	53.8 (4)	56.2 (2)	54.0 (1)	56.0 (6)	53.7 (3)	55.6 (2)	53.6 (4)	55.0 (1)	53.6 (2)	55.1 (9)	53.8 (5)	54.9 (8)
TiO_2	0.48 (4)	0.19 (3)	0.47 (3)	0.19 (2)	0.43 (3)	0.17 (1)	0.39 (3)	0.14 (0)	0.42 (2)	0.17 (2)	0.37 (4)	0.16 (2)
Al_2O_3	0.53 (3)	0.18 (3)	0.54 (2)	0.19 (3)	0.49 (3)	0.15 (1)	1.01 (102)	0.13 (1)	0.47 (2)	0.19 (2)	1.17 (102)	0.15 (2)
Cr_2O_3	0.86 (11)	0.14 (4)	0.77 (6)	0.11 (3)	0.73 (6)	0.12 (2)	0.76 (4)	0.11 (0)	0.68 (4)	0.21 (5)	0.60 (4)	0.08 (3)
MgO	16.9 (2)	30.0 (1)	17.1 (1)	31.1 (2)	16.6 (2)	29.0 (2)	16.1 (7)	28.4 (1)	16.8 (1)	28.8 (5)	16.2 (10)	28.0 (5)
CaO	22.0 (3)	0.81 (8)	22.6 (2)	0.68 (11)	22.3 (3)	0.89 (14)	21.2 (5)	0.90 (10)	22.0 (2)	1.03 (19)	21.2 (11)	0.93 (3)
MnO	0.22 (4)	0.46 (4)	0.24 (3)	0.48 (3)	0.21 (2)	0.44 (3)	0.22 (3)	0.43 (3)	0.21 (4)	0.44 (3)	0.21 (3)	0.47 (4)
FeO	4.05 (64)	11.5 (3)	3.70 (24)	11.7 (9)	4.90 (41)	13.6 (2)	4.87 (48)	14.0 (1)	4.97 (22)	14.0 (10)	5.15 (72)	15.4 (8)
Na_2O	0.56 (5)	0.01 (1)	0.55 (3)	0.04 (1)	0.51 (4)	0.02 (1)	0.80 (47)	0.04 (0)	0.45 (3)	0.03 (1)	0.74 (41)	0.02 (1)
Total	99.4	99.5	99.98	100.5	99.9	100	98.9	99.1	99.6	100	99.4	100.1
a.f.u./6 oxygens												
Si	1.98	2	1.98	1.98	1.97	1.99	1.98	1.99	1.97	1.98	1.98	1.98
Ti	0.01	0	0.01	0	0.01	0	0.01	0	0.01	0	0.01	0
Al	0.02	0.01	0.02	0.01	0.02	0.01	0.04	0	0.02	0.01	0.05	0.01
Cr	0.02	0	0.02	0	0.02	0	0.02	0	0.02	0.01	0.02	0
Mg	0.93	1.59	0.93	1.63	0.91	1.54	0.89	1.53	0.92	1.54	0.89	1.5
Ca	0.87	0.03	0.88	0.02	0.88	0.03	0.84	0.03	0.87	0.04	0.84	0.03
Mn	0.01	0.01	0.01	0.01	0.01	0.01	0.01	0.01	0.01	0.01	0.01	0.01
Fe	0.12	0.34	0.11	0.34	0.15	0.41	0.15	0.42	0.15	0.42	0.16	0.46
Na	0.04	0	0.04	0	0.04	0	0.06	0	0.03	0	0.05	0
Sum	4	3.98	4	3.99	4.01	3.99	4	3.98	4	4.01	4.01	3.99

[a] [ ] Number of grains averaged.

Table A-4. Temperatures (°C) calculated for average pyroxene compositions using QUILF95 and Lindsley (1983) compared with peak temperatures recorded by plagioclase. Maximum and minimum temperatures were determined by adjusting CaO contents in pyroxene pairs ±1 sigma (σ) standard deviation.

		QUILF95					Lindsley (1983)		Nakamuta and Motomura (1999)
		Cpx	**Opx**	**Pyroxene Pairs**	**Maximum T** **Cpx-1σ CaO** **Opx+1σ CaO**	**Minimum T** **Cpx+1σ CaO** **Opx-1σ CaO**	**Cpx**	**Opx**	**Plagioclase**
Peekskill	H6	988	913	914±47	943±39	880±59	975	800	735
Mulga (north)	H6	901	881	865±57	900±52	826±60	850	800	725
Great Bend	H6	878	901	874±57	909±57	836±64	750	800	740
Holbrook	L6	984	916	918±37	936±41	898±34	850	750	810
Owasco	L6	910	982	934±73	960±64	879±64	875	900	820
Dhurmsala	LL6	937	922	896±75	933±58	859±120	850	900	800

Table A-5. Temperatures (°C) calculated for published chondrite pyroxene analyses.

Meteorite	Type	Two-Pyroxenes	Cpx	Opx	Reference
Canon City	H6	918±29	980	914	Chamot (2000)
Canyonlands	H6	926±47	895	919	Lange et al. (1974)
Chiang Khan	H6	876±64	977	876	Chamot (2000)
Great Bend	H6	874±57	878	901	This Study
Guarena	H6	893±38	988	878	Slater and McSween (2001)
Ijopega	H6	889±24	1000	871	Jaques et al. (1975)
Mulga (north)	H6	865±57	901	881	This Study
Peekskill	H6	914±47	988	913	This Study
Seoni	H6	887±20	996	867	Bunch et al. (1972)
Aumale	L6	865±42	954	860	Dodd and Jarosewich (1981)
Chantonnay	L6	873±48	1028	855	Dodd and Jarosewich (1981)
Girgenti	L6	904±36	991	896	Gastineau-Lyons et al. (2002)
Guangnan	L6	-	-	932	Wang and Rubin (1987)
Holbrook	L6	918±37	984	916	This Study
Kyushu	L6	812±150	891	887	Baryshnikova et al. (1985)
L'Aigle	L6	881±50	996	872	Dodd and Jarosewich (1981)
Maryville	L6	-	-	797	Shervais et al. (1986)
Nan Yang Pao	L6	-	-	895	Wang and Rubin (1987)
Owasco	L6	934±73	910	982	This Study
Putinga	L6	-	-	894	Keil et al. (1978)
Raoyang	L6	-	-	931	Wang and Rubin (1987)
Sheyang	L6	-	-	908	Wang and Rubin (1987)
Suizhou	L6	-	-	907	Wang and Rubin (1987)
Tourinnes-la-Grosse	L6	869±52	1013	854	Dodd and Jarosewich (1981)
Tuan Tuc	L6	861±39	1026	839	Dodd and Jarosewich (1981)
Vouille	L6	858±57	975	852	Dodd and Jarosewich (1981)
Willowbar	L5/L6	879±80	940	902	Lange et al. (1973)
Zhaodong	L6	-	-	712	Wang and Rubin (1987)
Appley Bridge	LL6	-	1001	-	McSween and Patchen (1989)
Chicora	LL6	934±68	936	968	Heyse (1978)
Dhurmsala	LL6	896±75	937	922	This Study
Jolomba	LL6	-	-	969	Sighinolfi et al. (1991)
Mangwendi	LL6	-	-	916	McSween and Patchen (1989)
Mangwendi	LL6	930±41	1010	926	Heyse (1978)
Nyirabrany	LL6	945±42	984	952	Heyse (1978)
Saint Mesmin A	LL6	910±43	964	914	Heyse (1978)
Saint Mesmin B	LL6	877±24	1011	856	Heyse (1978)
Saint-Severin A	LL6	897±104	1037	904	Heyse (1978)
Saint-Severin B	LL6	874±32	882	885	Heyse (1978)
Saint-Severin	LL6	888±42	945	891	Gastineau-Lyons et al. (2002)
Varvik	LL6	925±106	987	962	Heyse (1978)

Table A-6. Sample description and results for Li, Be, and B from this study.

	Geochemical Group[a]	Rock Type[b]	Top Depth (mbsl)	B (ppm)	1s[c]	Be (ppm)	1s	Li (ppm)	1s
SR0121-4.40	post shield	subaerial	246.2	7.9		0.9		4.9	
SR0125-6.25	post shield	subaerial	256.5	3.6	0.42 (2)	0.7		4.7	
SR0129-5.20	post shield	subaerial	267.5	1.1	0.70 (3)	0.7		3.6	0.35 (2)
SR0133-8.20	post shield	subaerial	281.3	3.8		0.5		2.7	
SR0141-7.90	high SiO_2	subaerial	305.8	2.0		1.0		4.1	
SR0193-0.00	high SiO_2	subaerial	443.6	0.6		0.6		3.2	
SR0240-3.30	high SiO_2	subaerial	563.5	2.8		0.5	0.05 (2)	4.0	
SR0256-0.95	high SiO_2	subaerial	589	2.3	0.36 (3)	0.7		4.0	
SR0276-7.85	high SiO_2	subaerial	636	6.9		0.4		4.9	0.07 (2)
SR0300-6.50	high SiO_2	subaerial	695.9	3.5	1.06 (2)	0.6		4.5	
SR0340-1.00	high SiO_2	subaerial	793.6	5.5	1.00 (3)	0.3		3.7	
SR0354-7.75	low SiO_2	subaerial	833.9	0.7		0.4		3.5	
SR0372-2.80	high SiO_2	subaerial	871.2	5.1		0.6		3.3	
SR0413-3.10	high SiO_2	subaerial	984.2	5.2		0.4		5.1	
(submarine transition at 1078 mbsl)									
SR0472-1.00	high SiO_2	massive	1123.2	3.4		0.5		5.0	0.21 (2)
SR0490-1.50	high SiO_2	hyaloclastite	1229.6	2.9		0.4		3.2	
SR0531-4.40	low SiO_2	hyaloclastite	1352.6	6.5		0.3		5.3	
SR0545-8.35	low SiO_2	hyaloclastite	1395	3.6	0.99 (2)	0.4		3.5	
SR0574-1.90	high SiO_2	hyaloclastite	1474.7	1.0	1.27(2)	0.4		3.8	0.14 (2)
SR0603-8.90	high SiO_2	hyaloclastite	1548.2	2.8	1.15 (3)	0.5		3.5	
SR0655-4.00	high SiO_2	hyaloclastite	1678.7	2.5		0.4		3.5	
SR0664-5.10	high SiO_2	hyaloclastite	1705.5	5.1		0.5	0.09 (2)	6.1	
SR0694-9.00	high SiO_2	massive	1794.8	6.1	1.38 (3)	0.5		3.1	
SR0723-13.70	high SiO_2	hyaloclastite	1933.8	3.0	0.89 (3)			4.8	
SR0732-1.10	low SiO_2	hyaloclastite	1973.8	1.7		0.6	0.01 (2)	3.6	
SR0741-7.90	low SiO_2	pillow	2009.8	3.1		0.2		3.6	
SR0768-11.20	high SiO_2	hyaloclastite	2157.4	1.9		0.5		3.2	
SR0776-17.70	high SiO_2	hyaloclastite	2209.5	6.3	2.65 (3)	0.4		3.4	
SR0826-20.60	high SiO_2	pillow	2414.1	3.2	1.56 (3)	0.6		3.4	
SR0850-5.95	high SiO_2	hyaloclastite	2550.9	6.1		0.5		4.4	
SR0860-8.10	high SiO_2	pillow	2615	2.3		0.5		3.4	
SR0871-13.00	low SiO_2	pillow	2654.1	3.0	1.06 (2)	0.5	0.01 (2)	4.4	
SR0907-1.65	high SiO_2	pillow	2789.9	3.9	0.14 (2)	0.5		3.2	
SR0916-1.15	high SiO_2	pillow	2837.6	1.9		0.4	0.04 (2)	2.5	
SR0939-18.10	high SiO_2	pillow	2961	2.6		0.4		2.6	
SR0956-18.35	high SiO_2	intrusive	3019	4.1	0.07 (2)	0.7		3.3	
SR0967-2.75	high SiO_2	pillow	3068.9	3.7	0.53 (3)	0.4		3.2	

[a] Huang and Frey (2003)

[b] descriptions from Rhodes and Vollinger (2004)

[c] ( ) number of analyses

Table A-7. Results for standards analyzed in this study and their reported concentrations.

	Measured Concentration	Actual Concentration[a]
Li	(ppm)	(ppm)
BHVO-1	4.2	4.6 (1.5)
BCR-2	8.0	9.0 (2)
Be		
BIR-1	0.5	0.6
B (ppm)		
BHVO-1	2.4	2.5 (0.6)
BHVO-1	2.8	

[a] USGS recommended and information values

Table A-8. Previously determined bulk Li and Be data for basaltic shergottites and Chassigny.

Meteorite	Li ppm	Be ppm
Chassigny[a]	1.4 (0.2)	na[a]
DaG 476	na	na
DaG 489[b]	2.6	<0.04
Dho 019[c]	2.7	0.03
Dho 378	na	na
EETA79001[a]	4.5	na
EETB79001[a]	2.2	na
Los Angeles	na	na
NWA 1068[d]	4.3	0.35
NWA 1195	na	na
NWA 1669	na	na
NWA 2046	na	na
NWA 480[e]	2.9	0.21
NWA 856[f]	4.1	0.36
QUE 94201	na	na
SAU 005	na	na
Shergotty[a]	4.5 (0.9)	na
Y 980459	na	na
Zagami[a]	2.9 (1.3)	na

* ( ) 1 sigma precision

[a] Lodders (1998)

[b] Folco et al. (2000)

[c] Neal et al. (2001)

[d] Barrat et al. (2002a)

[e] Barrat et al. (2002b)

[f] Jambon et al. (2002)

Table A-9. Results for Li and Be analyses from this study.

Meteorite	δ^7Li (‰)	Li (ppm)	Be (ppm)
Chassigny	17.8	1.8 (0.11)[b]	0.04 (0.007)
Dhofar 019	na[a]	8.3 (0.14)	0.18 (0.006)
EETA79001	4.37	2.7 (0.20)	0.09 (0.008)
Los Angeles	na	9.9 (0.24)	0.77 (0.020)
Shergotty	na	8.0 (0.36)	0.46 (0.020)
Zagami	3.97	6.7 (0.38)	0.42 (0.018)

[a] na=not analyzed

[b] 2σ standard deviation

APPENDIX B

Figure B-1. Cartoons illustrating the difference between clinopyroxene, orthopyroxene, and plagioclase as peak metamorphic temperature indicators. Clinopyroxene and orthopyroxene identify the ultimate phases, even though orthopyroxene inverted from other structural states (e.g. protoenstatite, clinoenstatite) on cooling (Folco and Mellini, 2000; Ferraris et al., 2002). In (a), clinopyroxene and orthopyroxene achieved equilibrium at peak metamorphic conditions (T_{eq}), but only clinopyroxene records T_{eq} because orthopyroxene re-equilibrated to a lower temperature during cooling. In (b), neither pyroxene necessarily records peak metamorphic conditions because both pyroxenes did not equilibrate, although several authors have suggested that orthopyroxene compositions were reset at the metamorphic peak (T_{eq}). In (c), plagioclase crystals record crystallization (from chondrule glass) temperatures up to the metamorphic peak (T_{eq}).

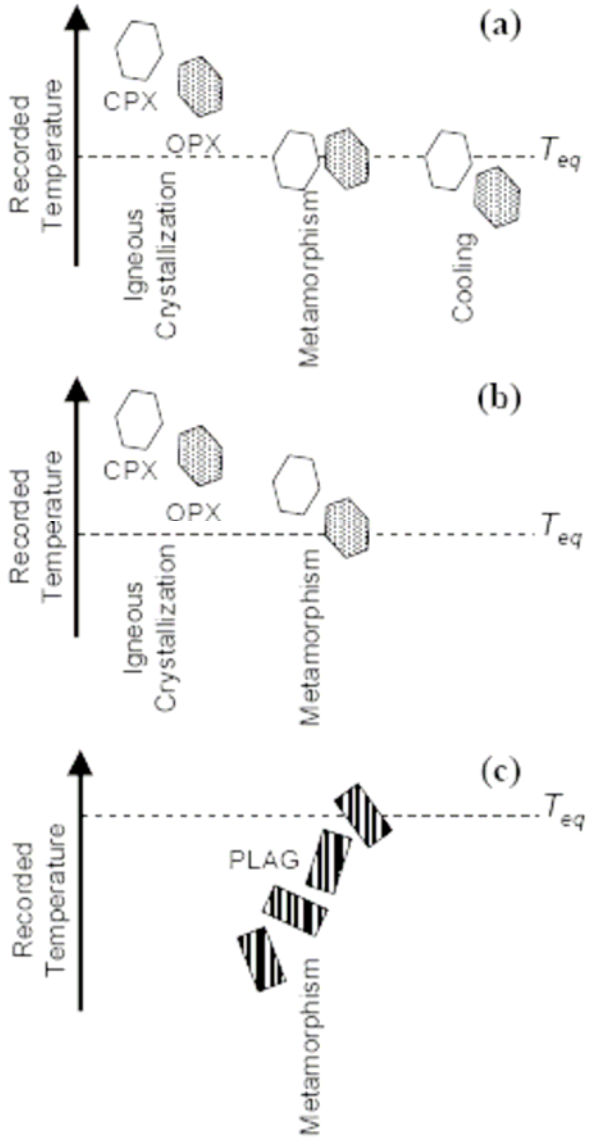
(a)
Recorded Temperature
CPX
OPX
T_{eq}
Igneous Crystallization
Metamorphism
Cooling
(b)
Recorded Temperature
CPX
OPX
T_{eq}
Igneous Crystallization
Metamorphism
(c)
Recorded Temperature
T_{eq}
PLAG
Metamorphism

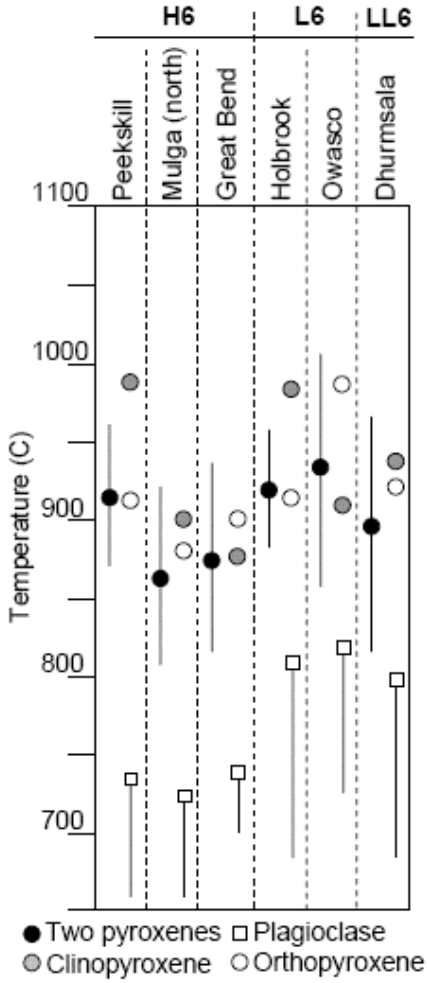

Figure B-2. Peak temperature estimates for pyroxenes (this study) and plagioclase (Nakamuta and Motomura, 1999) determined for the same Type 6 ordinary chondrites. Filled, shaded, and open circles represent two-pyroxene (with error bars), clinopyroxene, and orthopyroxene temperatures, respectively. Open squares indicate peak plagioclase temperatures, and descending bars represent the range of plagioclase temperatures for each meteorite.

Figure B-3. Reflected light photomicrographs of (a) Peekskill-H6, (b) Holbrook-L6, and (c) Dhurmsala-LL6. Fe metal-sulfide boundaries are smooth in every meteorite, suggesting eutectic melting has not occurred. The darker silicate matrix surrounding the Fe metal and sulfide is composed primarily of orthopyroxene and olivine. Sulfide in Dhurmsala appears mottled due to shock.

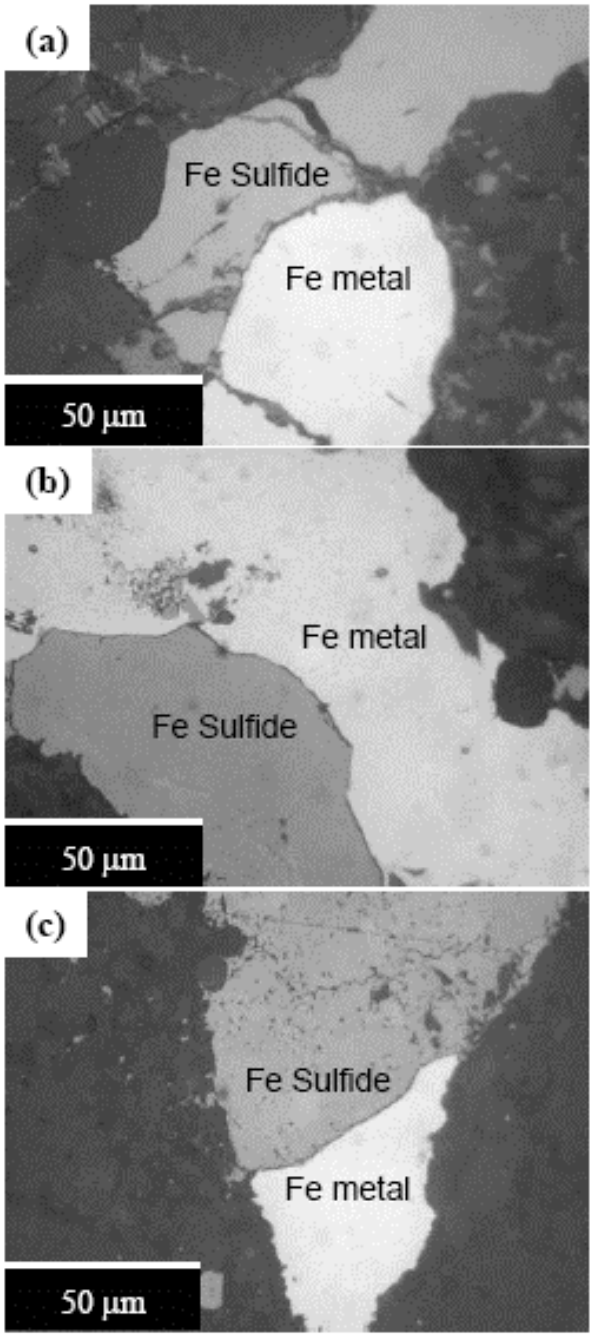
(a)
Fe Sulfide
Fe metal
50 µm
(b)
Fe metal
Fe Sulfide
50 µm
(c)
Fe Sulfide
Fe metal
50 µm

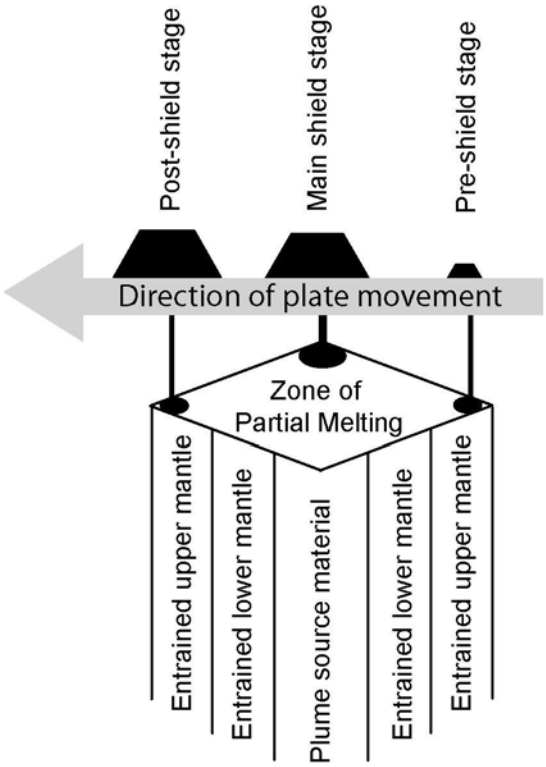

Figure B-4. The geochemistry of Mauna Kea lavas varies as the Pacific plate moves over the underlying mantle plume. During the pre-shield and post-shield stages, lavas are produced from low degrees of partial melting as the volcano samples the peripheral regions of the plume that contain entrained depleted upper mantle. Main shield stage lavas are generated when the volcano is above the region of the plume where a higher degree of partial melting taps a more primitive plume source.

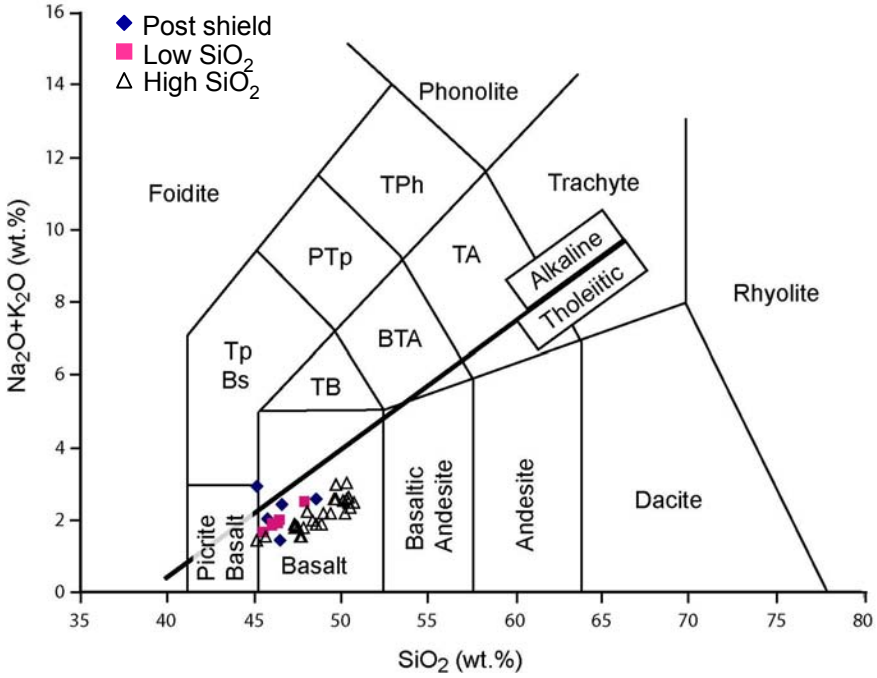

Figure B-5. Total alkalis-silica diagram showing Mauna Kea basalts analyzed in this study. Fields for common rock types are labeled according to Le Bas et al. (1986), and the alkali and tholeiitic boundary determined by Macdonald and Katsura (1964) is also shown. In this and following figures, diamonds represent post-shield lavas, squares represent low-SiO_2 lavas, and triangles represent high-SiO_2 lavas.

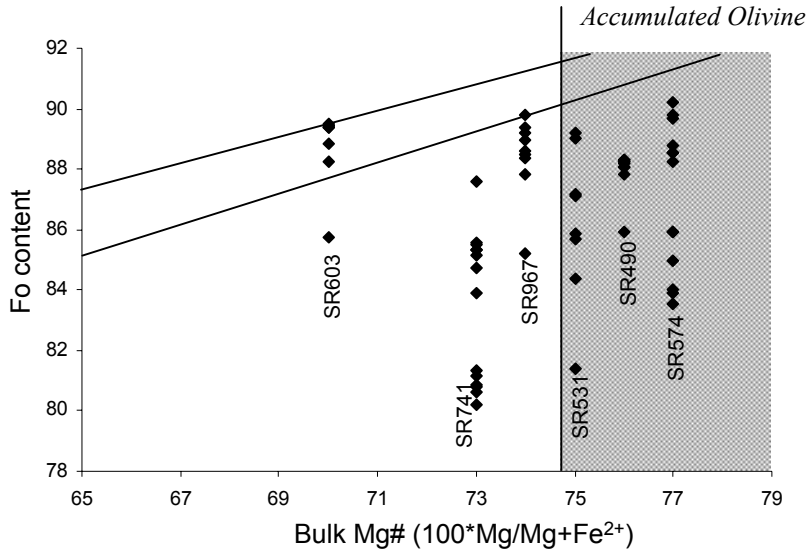

Figure B-6. Bulk Mg# (100*Mg/Mg+Fe^{2+}) compared to the range of olivine forsterite (Fo) contents in selected samples from this study. Diagonal lines represent equilibrium olivine compositions for a given bulk Mg# using a Fe^{2+}/Mg partitioning coefficient of 0.3 (Gee and Sack, 1988). Similar to HSDP-1 lavas examined by Baker et al. (1996), the lack of equilibrium between olivine and host melt in samples with Mg#≥75 suggest they contain accumulated olivine. The observation that the most Fo-rich olivine in SR741 falls below the equilibrium Fo composition suggests the most Fo-rich olivine in SR741 was not analyzed.

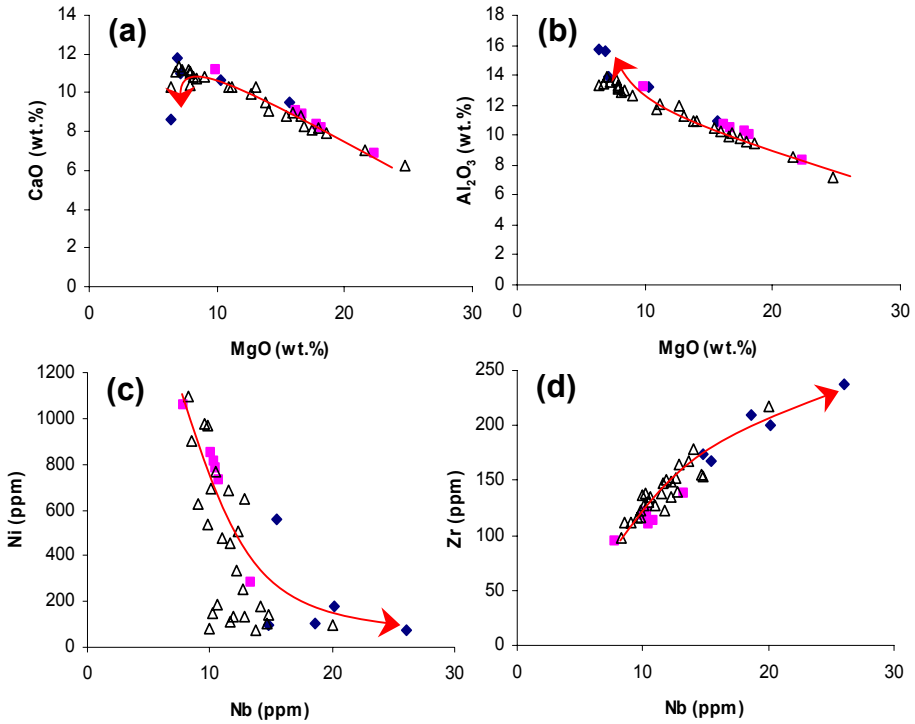

Figure B-7. Strong correlations of MgO with (a) CaO and (b) Al_2O_3 indicate the influence of olivine control in Mauna Kea lavas, except at low MgO values where lower CaO and higher Al_2O_3 indicate fractionation beyond olivine control. Deviations from olivine control are more obvious for post-shield samples when Nb is compared to (c) Ni and (d) Zr. Arrows indicate change in slope from main to post-shield lavas. Symbols as in Figure B-5.

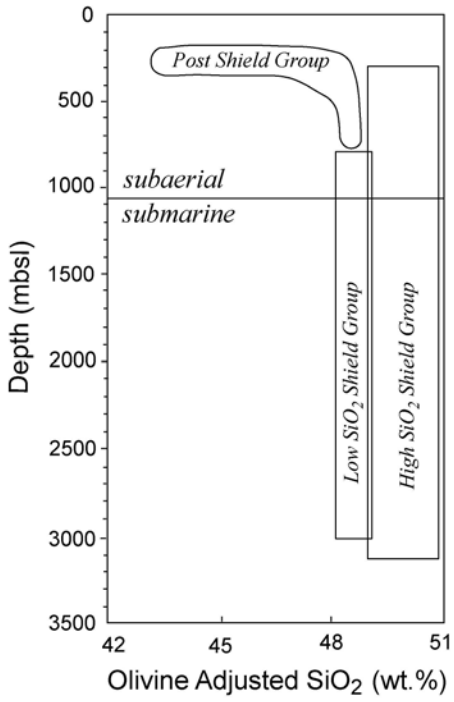

Figure B-8. Based on SiO_2 contents adjusted to 13% MgO (Huang and Frey, 2003), Mauna Kea lavas are divided into low- SiO_2 and high-SiO_2 groups. Subaerial low-SiO_2 samples have higher incompatible element ratios than submarine low-SiO_2 lavas, and represent Mauna Kea's transition from main to post-shield building stages.

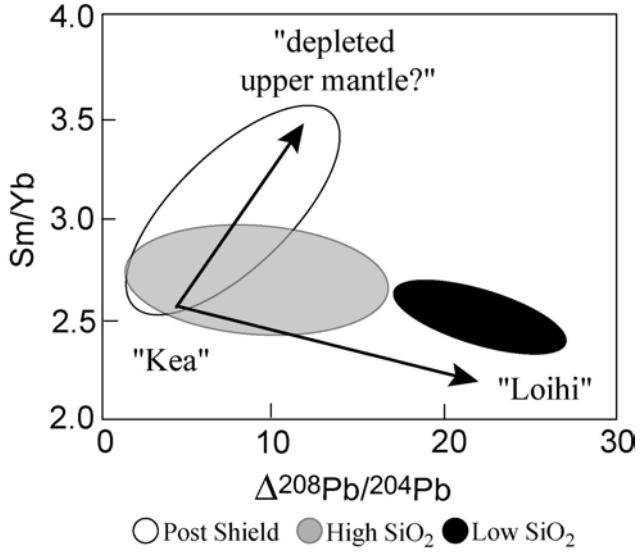

Figure B-9. Mauna Kea lavas define a range of Sm/Yb and $\Delta^{208}Pb/^{204}Pb$ (see text for definition) values that requires three admixed components (from Huang and Frey, 2003). High-SiO_2 lavas (gray) represent "Kea-type" compositions similar to Kilauea, and low-SiO_2 lavas (black) appear to sample a greater proportion of a Loihi-like component. Post-shield lavas (unfilled) sample a more depleted (upper mantle?) component.

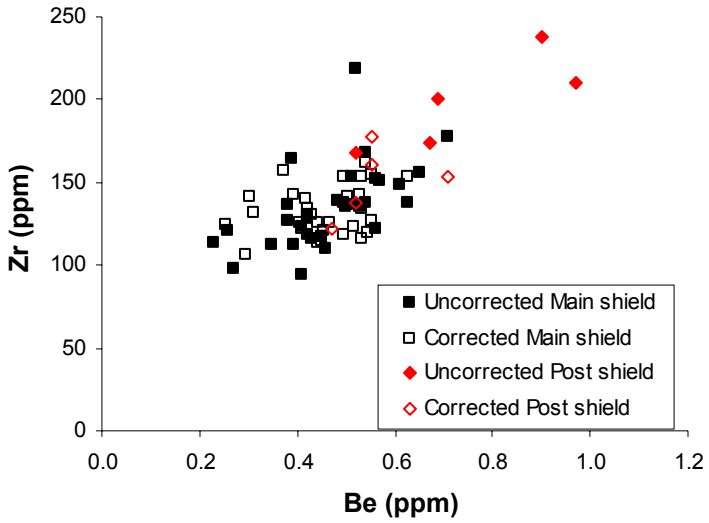

Figure B-10. Be vs. Zr for Mauna Kea samples before (filled) and after (unfilled) correcting for olivine accumulation and fractionation. Main shield lavas (squares) show little change, as expected for incompatible elements. Post-shield lavas (triangles) show significant changes, reflecting fractionation beyond olivine control.

Figure B-11. Li concentrations (ppm) with depth in the HSDP-2 core demonstrate the minimal effect of using variable $D_{Li}^{ol\text{-}melt}$ values of (a) 0.2, (b) 0.35, and (c) 0.45 when correcting for olivine accumulation and fractionation. Li and (d) uncorrected MgO contents follow separate trends, suggesting this correction accounts for the effects of olivine control. Symbols as in Figure B-5.

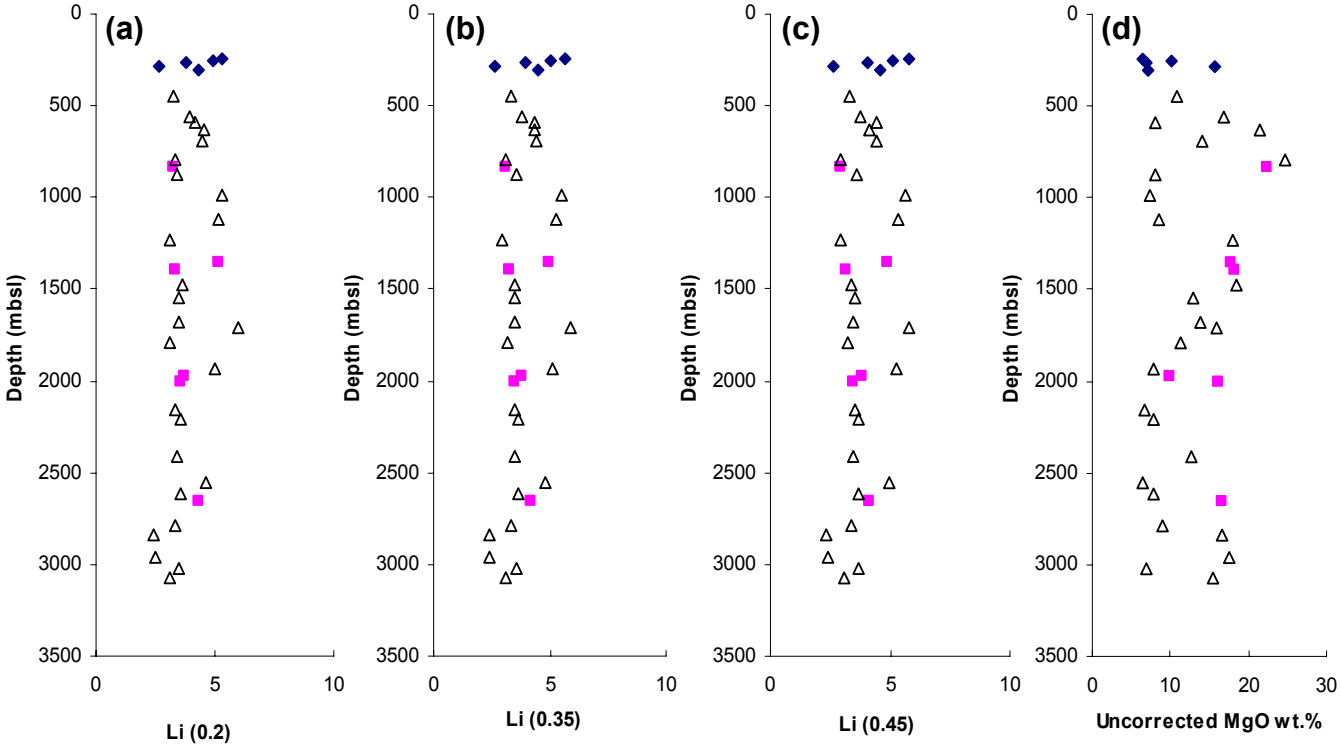
(a)
(b)
(c)
(d)
Depth (mbsl)
0
500
1000
1500
2000
2500
3000
3500
0
5
10
20
30
Li (0.2)
Li (0.35)
Li (0.45)
Uncorrected MgO wt.%

Figure B-12. Li vs. incompatible elements (a) Zr, (b) Nb, and (c) Yb. Correlations observed in post-shield samples (diamonds) are absent in low-SiO_2 (squares) and high-SiO_2 (triangles) lavas, indicating Li modification in the latter two lava types. Sample SR850 has anomalously high abundances of most trace elements. Li/Yb ratios for MORB (1.7) and other ocean island basalts (OIB) (gray regions) are shown for comparison, and the arrow defines the general trend for the large range reported for island arc lavas. Yb data from Feigenson et al. (2003).

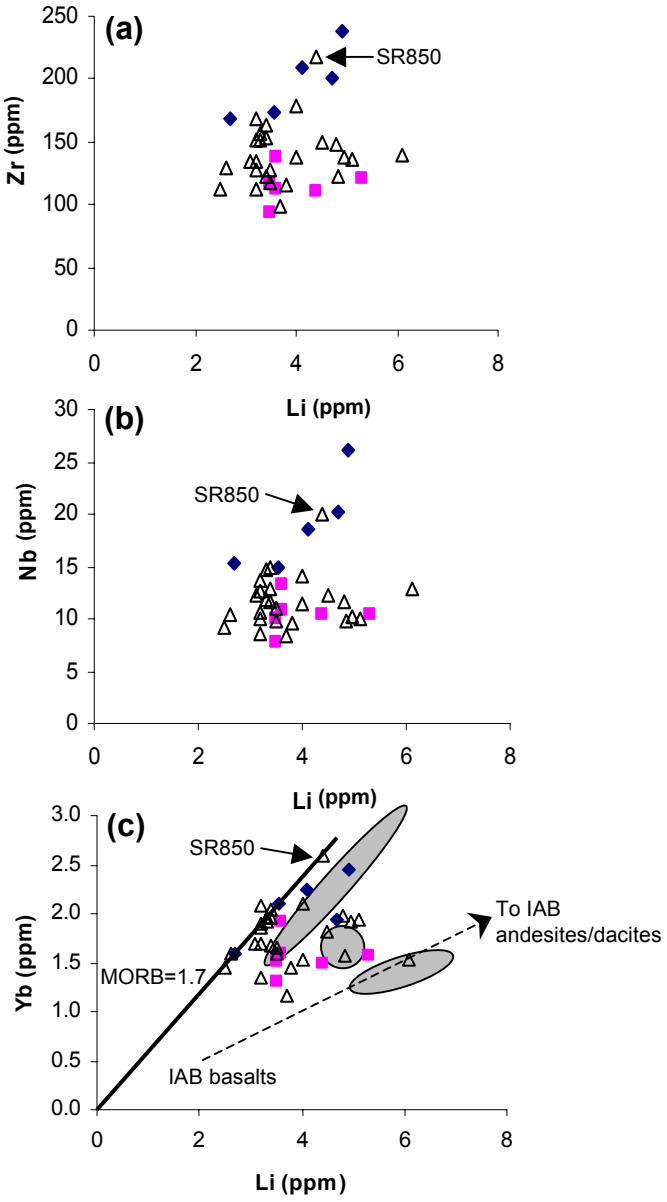
(a)
Zr (ppm)
250
200
150
100
50
0
SR850
0
2
4
6
8
Li (ppm)
(b)
Nb (ppm)
30
25
20
15
10
5
0
SR850
0
2
4
6
8
Li (ppm)
(c)
Yb (ppm)
3.0
2.5
2.0
1.5
1.0
0.5
0.0
SR850
MORB=1.7
To IAB
andesites/dacites
IAB basalts
0
2
4
6
8
Li (ppm)

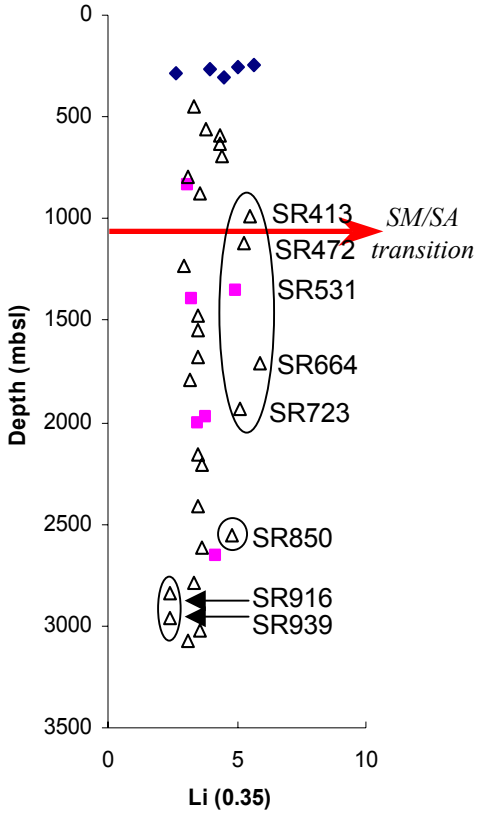

Figure B-13. Variation of Li abundances (ppm) with depth in the HSDP-2 drill core. Bold arrow indicates the submarine/subaerial transition. Individual samples with anomalous Li contents are labeled and described in the text. Symbols are the same as Figure B-5.

Figure B-14. B vs. (a) Be, (b) K, and (c) Nb for Mauna Kea lavas (symbols as described in previous figures). The lack of correlation between these incompatible elements suggests B has been modified so that mantle compositions are no longer represented. B/Be, B/K, and B/Nb ratios for MORB are shown for comparison (bold lines). Other OIB typically have values less than MORB and IAB have values greater than MORB (Ryan and Langmuir, 1993).

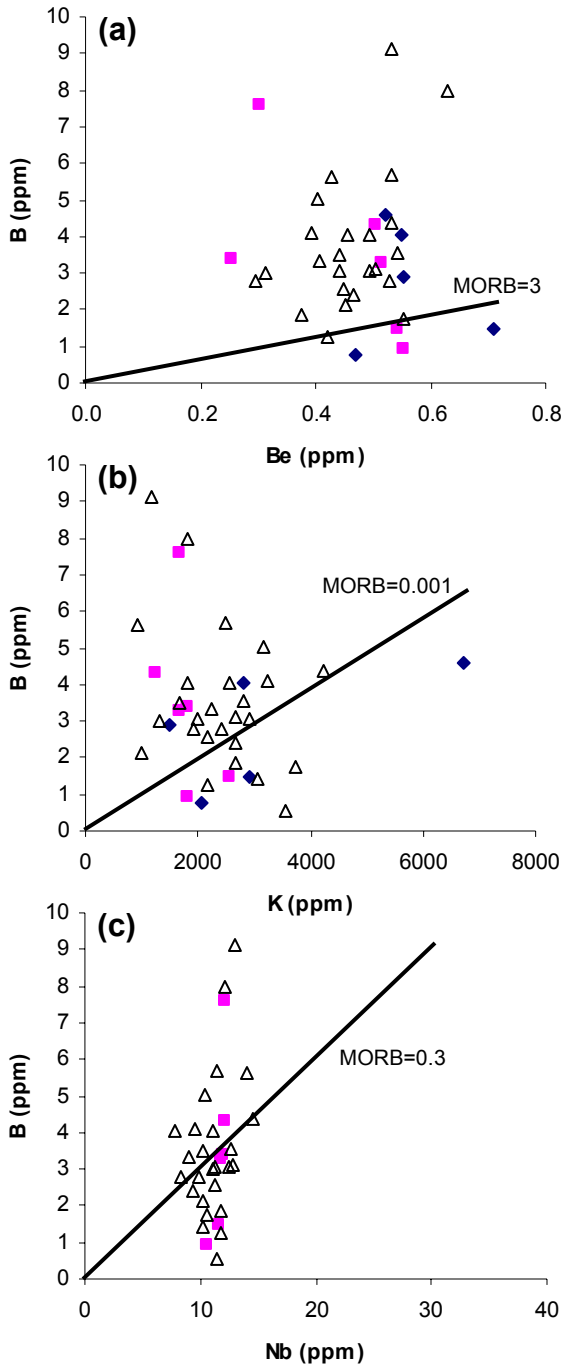
(a)
B (ppm)
Be (ppm)
MORB=3
(b)
B (ppm)
K (ppm)
MORB=0.001
(c)
B (ppm)
Nb (ppm)
MORB=0.3

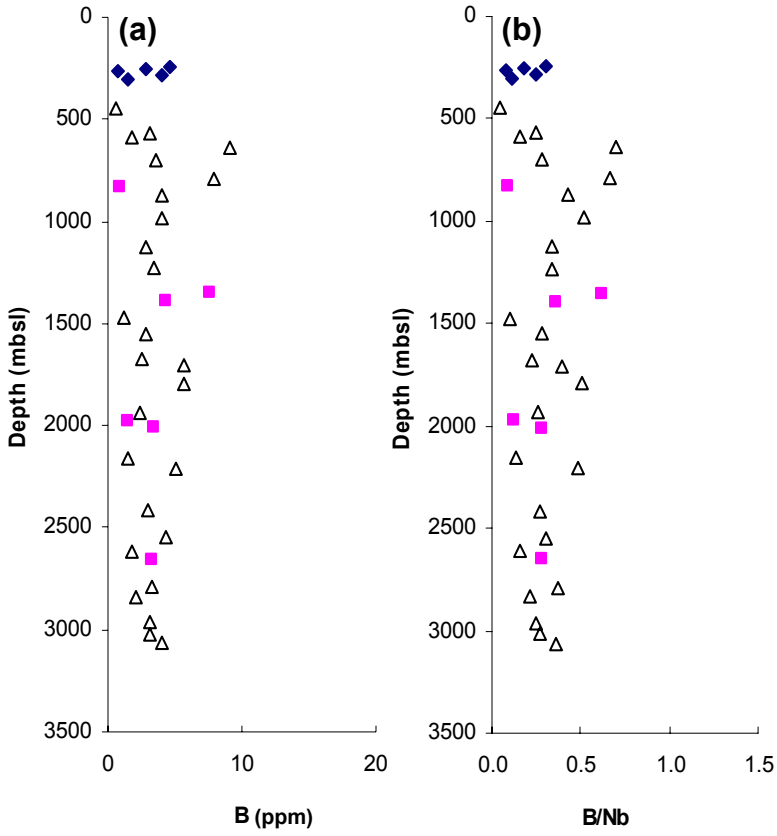

Figure B-15. Depth profiles for (a) B abundances and (b) B/Nb ratios in Mauna Kea lavas (symbols as in Figure B-5).

Figure B-16. Ratios of (a) Li/Dy, (b) Li/V, and (c) Li/Yb with depth in the HSDP-2 core follow similar trends as Li abundances. In low-SiO_2 (squares) and high-SiO_2 (triangles) lavas, Li variations reflect effects alteration whereas variations in post-shield lavas (diamonds) reflect decreasing degrees of partial melting. Dy and Yb data from Feigenson et al. (2003).

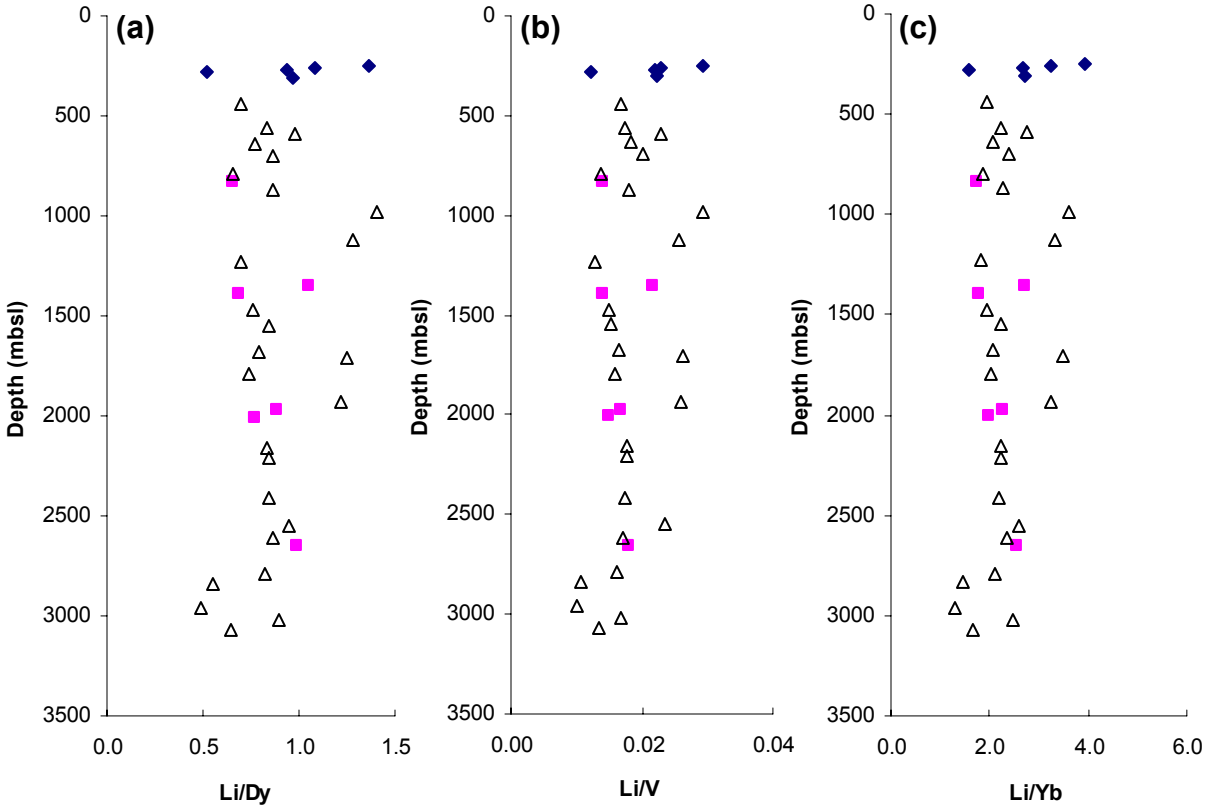
(a)
(b)
(c)
Depth (mbsl)
0
500
1000
1500
2000
2500
3000
3500
0.0
0.5
1.0
1.5
Li/Dy
0.00
0.02
0.04
Li/V
2.0
4.0
6.0
Li/Yb

Figure B-17. Beryllium vs. (a) MgO, (b) Zr, and (c) Nd in post-shield (diamonds), low-SiO_2 (squares), and high-SiO_2 (triangles) lavas. Be/Zr and Be/Nd ratios for other OIB (solid lines), MORB (bold lines), and island arc basalts (IAB) (dashed lines) are shown for comparison (Ryan, 2002). Nd data from Huang and Frey (2003).

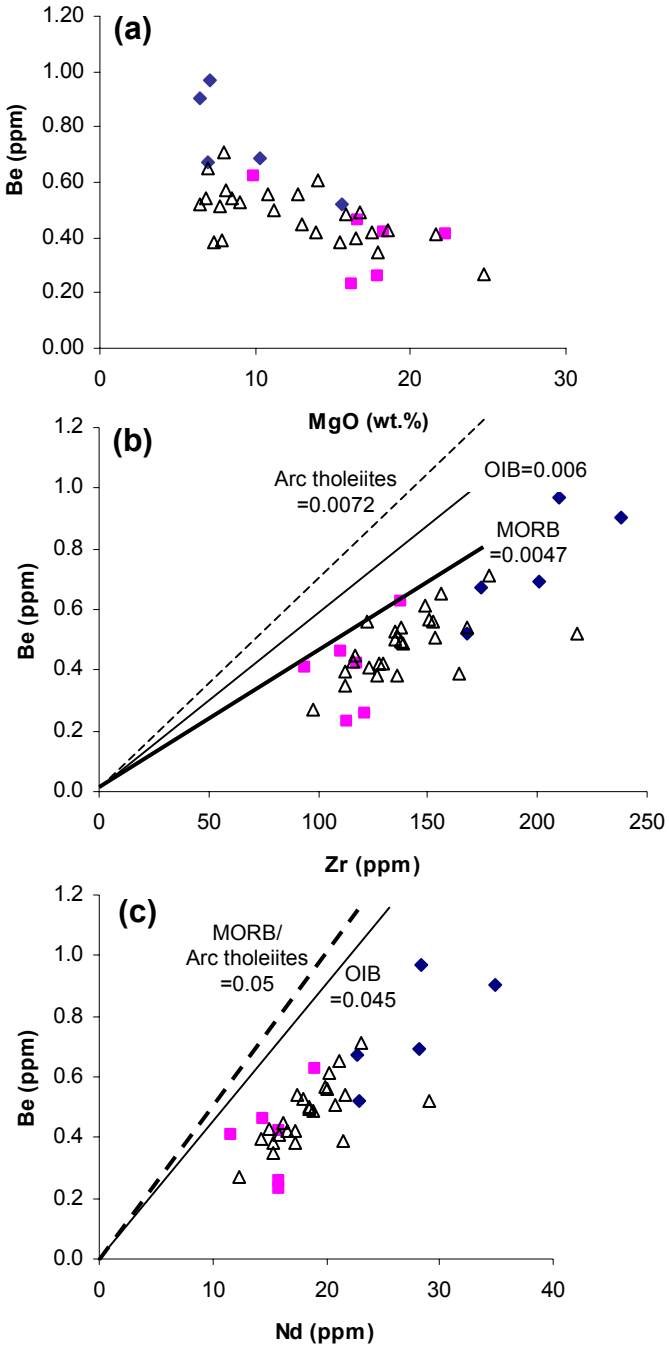
(a)
Be (ppm)
1.20
1.00
0.80
0.60
0.40
0.20
0.00
0
10
20
30
MgO (wt.%)
(b)
Arc tholeiites
=0.0072
OIB=0.006
MORB
=0.0047
Be (ppm)
1.2
1.0
0.8
0.6
0.4
0.2
0.0
0
50
100
150
200
250
Zr (ppm)
(c)
MORB/
Arc tholeiites
=0.05
OIB
=0.045
Be (ppm)
1.2
1.0
0.8
0.6
0.4
0.2
0.0
0
10
20
30
40
Nd (ppm)

Figure B-18. Variations in (a) Be abundances, (b) Be/Nd ratios, and (c) Be/Zr ratios with depth in the HSDP-2 core. Although Be increases in the uppermost late main and post-shield samples (arrow), constant Be/Nd and Be/Zr ratios indicate the variation is a result of decreasing degrees of melting rather than source region variation.

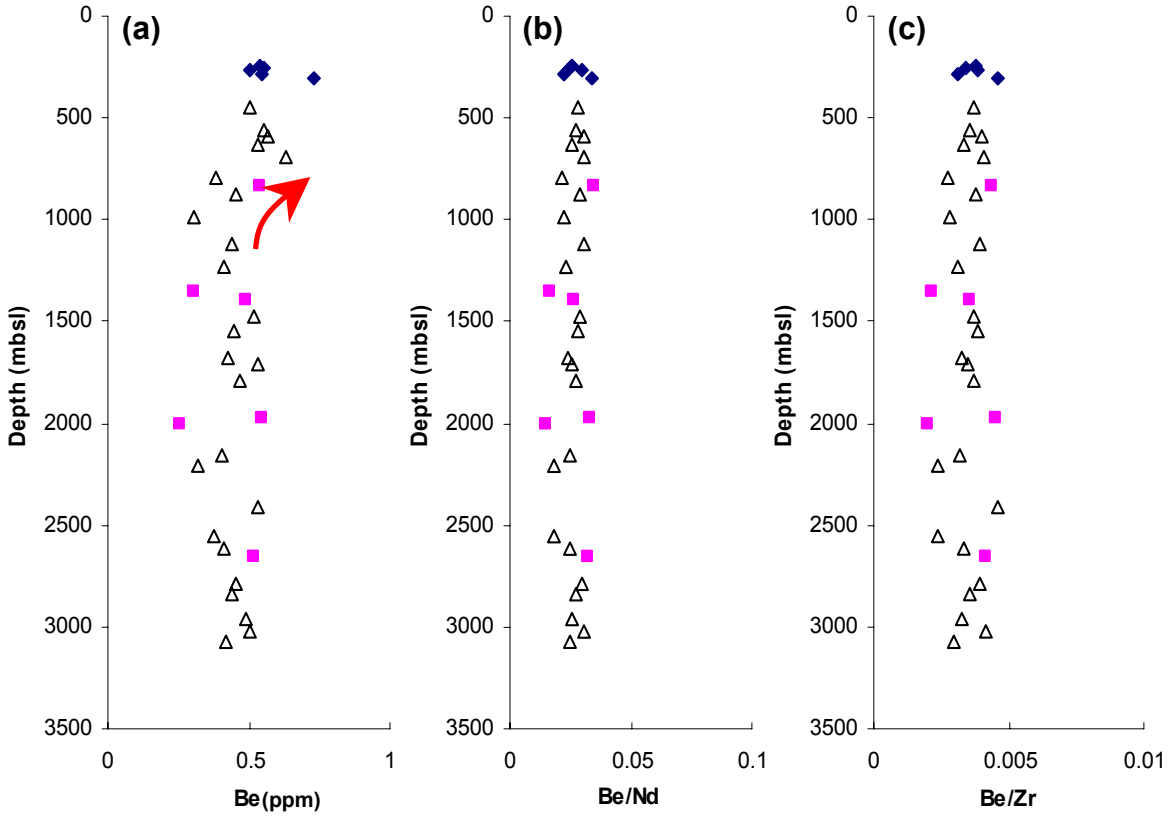
(a)
(b)
(c)
Depth (mbsl)
0
500
1000
1500
2000
2500
3000
3500
0
0.5
1
Be (ppm)
0
0.05
0.1
Be/Nd
0
0.005
0.01
Be/Zr

Figure B-19. Li/Yb and Be/Nd compared to (a, d) Nb/Zr, (b, e) $^{208}Pb/^{206}Pb$, and (c, f) $^{206}Pb/^{204}Pb$ for Mauna Kea lavas. Li/Yb and Be/Nd values overlap, and do not identify distinct lava types described by Huang and Frey (2003). Pb data from Blichert-Toft et al. (2003).

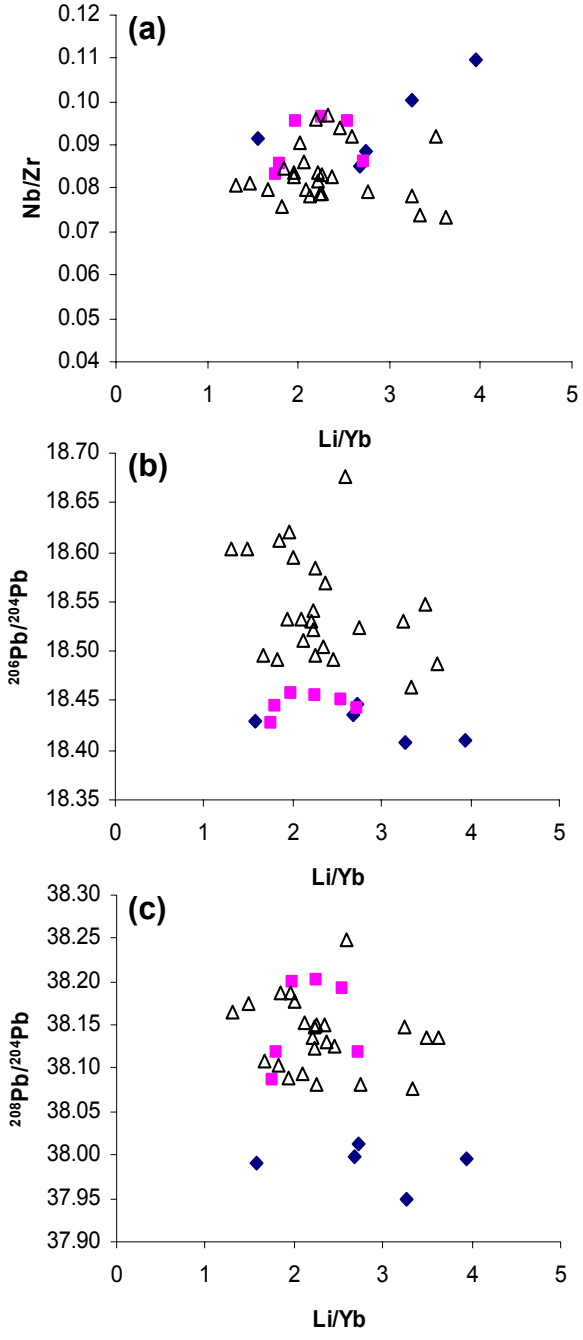
(a)
Nb/Zr
0.12
0.11
0.10
0.09
0.08
0.07
0.06
0.05
0.04
0
1
2
3
4
5
Li/Yb
(b)
$^{206}Pb/^{204}Pb$
18.70
18.65
18.60
18.55
18.50
18.45
18.40
18.35
0
1
2
3
4
5
Li/Yb
(c)
$^{208}Pb/^{204}Pb$
38.30
38.25
38.20
38.15
38.10
38.05
38.00
37.95
37.90
0
1
2
3
4
5
Li/Yb

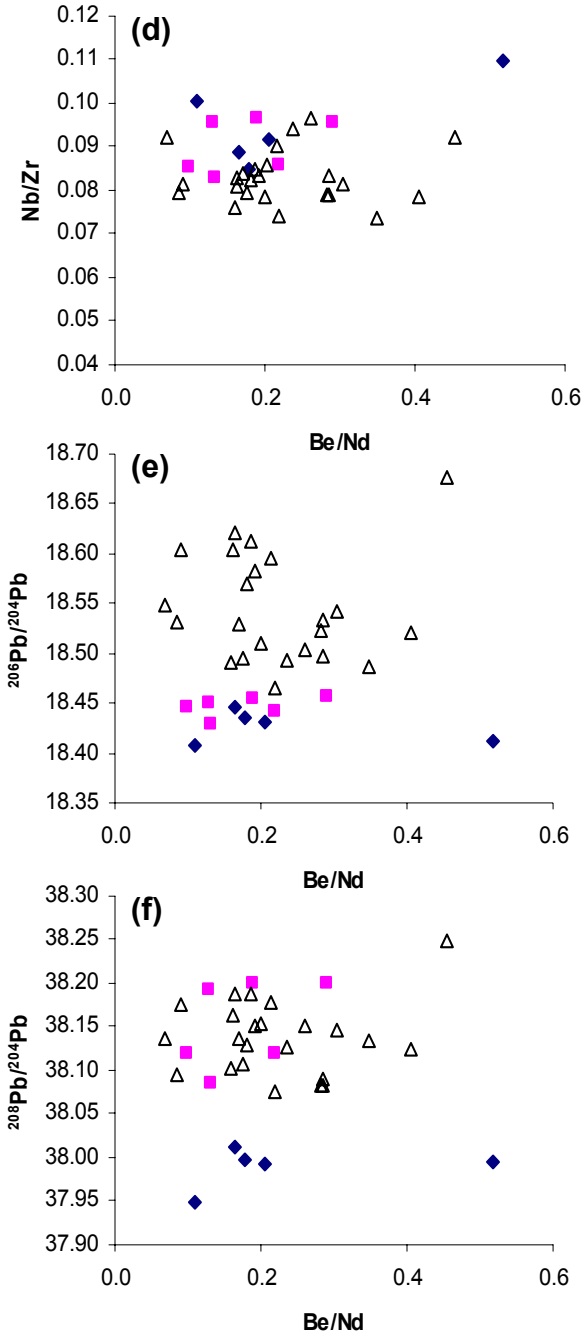
(d)
Nb/Zr
0.12
0.11
0.10
0.09
0.08
0.07
0.06
0.05
0.04
0.0
0.2
0.4
0.6
Be/Nd
(e)
$^{206}Pb/^{204}Pb$
18.70
18.65
18.60
18.55
18.50
18.45
18.40
18.35
0.0
0.2
0.4
0.6
Be/Nd
(f)
$^{208}Pb/^{204}Pb$
38.30
38.25
38.20
38.15
38.10
38.05
38.00
37.95
37.90
0.0
0.2
0.4
0.6
Be/Nd

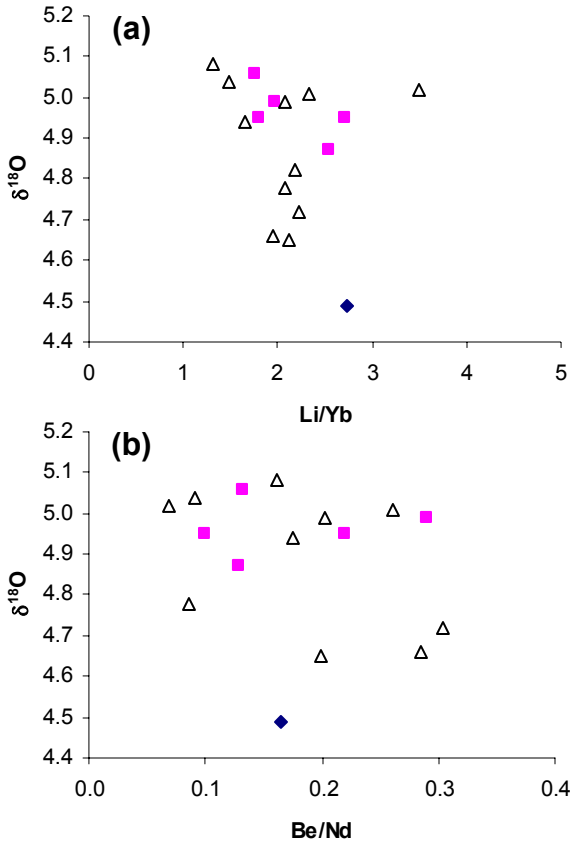

Figure B-20. (a) Li/Yb and (b) Be/Nd compared to $\delta^{18}O$ (data from Wang et al., 2003) for post-shield (diamonds), low-SiO_2 lavas (squares), and high-SiO_2 lavas (triangles). The lack of correlation for any of the geochemical groups suggests Li and Be do not record a crustal component altered at low temperatures in Mauna Kea's source region.

Figure B-21. Correlations between $\varepsilon^{143}Nd$ and (a) initial $^{87}Sr/^{86}Sr$, (b) La/Yb, and (c) oxidation states for basaltic shergottites suggest mixing of primitive (QUE 94201-like) and enriched (Shergotty-like) components (data from Nyquist et al., 1979; Wooden et al., 1982; Borg et al., 1997; Lodders, 1998; Borg et al., 2000; Herd and Papike, 2000; Nyquist et al., 2000; Rubin et al., 2000; Taylor et al., 2002; Borg et al., 2001; Nyquist et al., 2001; Herd et al., 2002). Figure key includes additional meteorites plotted in following figures.

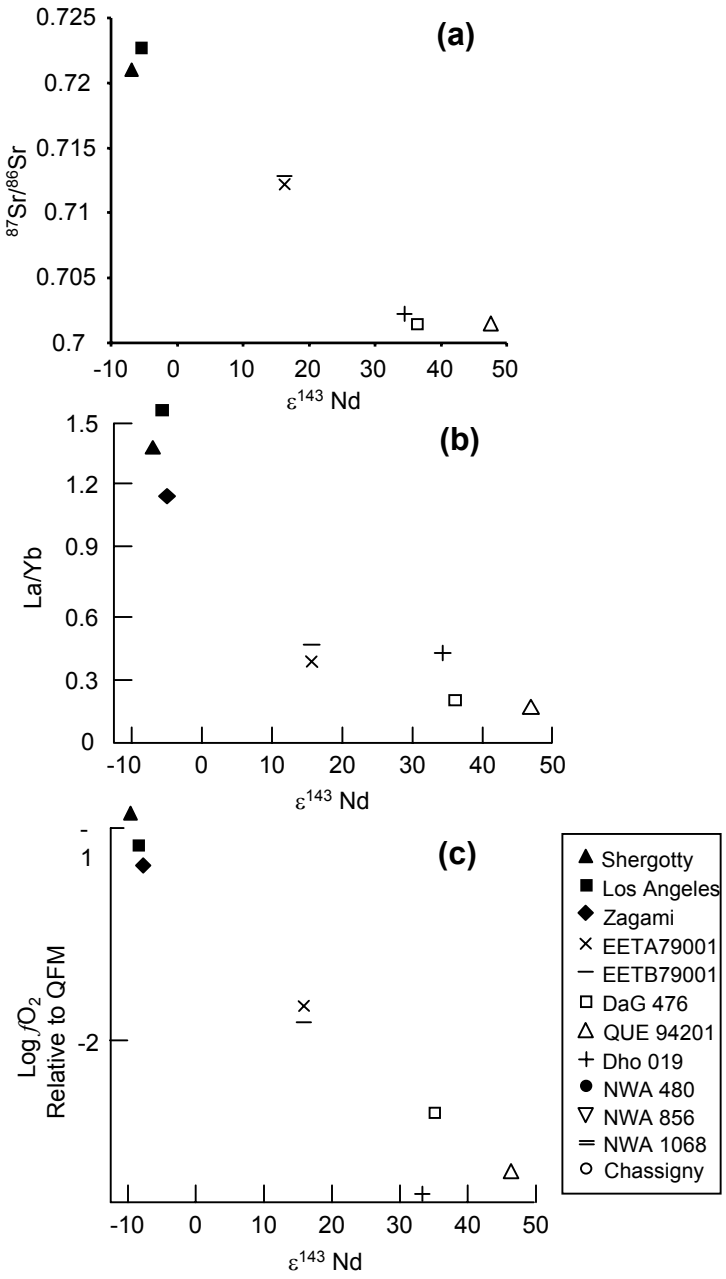
(a)
0.725
0.72
0.715
0.71
0.705
0.7
$^{87}Sr/^{86}Sr$
-10
0
10
20
30
40
50
ε^{143} Nd
(b)
1.5
1.2
0.9
0.6
0.3
0
La/Yb
ε^{143} Nd
(c)
-1
-2
Log fO_2 Relative to QFM
ε^{143} Nd
Shergotty
Los Angeles
Zagami
EETA79001
EETB79001
DaG 476
QUE 94201
Dho 019
NWA 480
NWA 856
NWA 1068
Chassigny

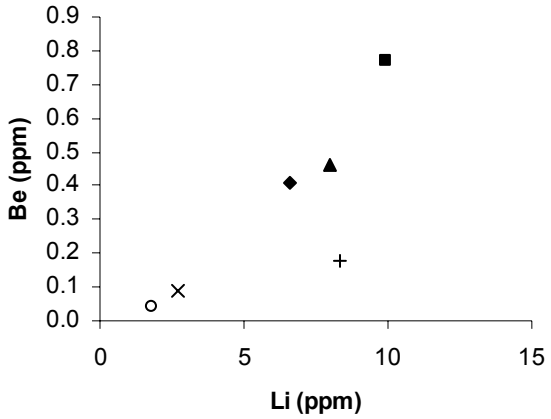

Figure B-22. The linear array defined by Martian meteorites when Li is compared to Be suggests these elements preserve igneous compositions. The elevated Li abundance in Dhofar 019 is attributed to terrestrial alteration minerals (caliche) present in the sample. Symbols as in Figure B-21.

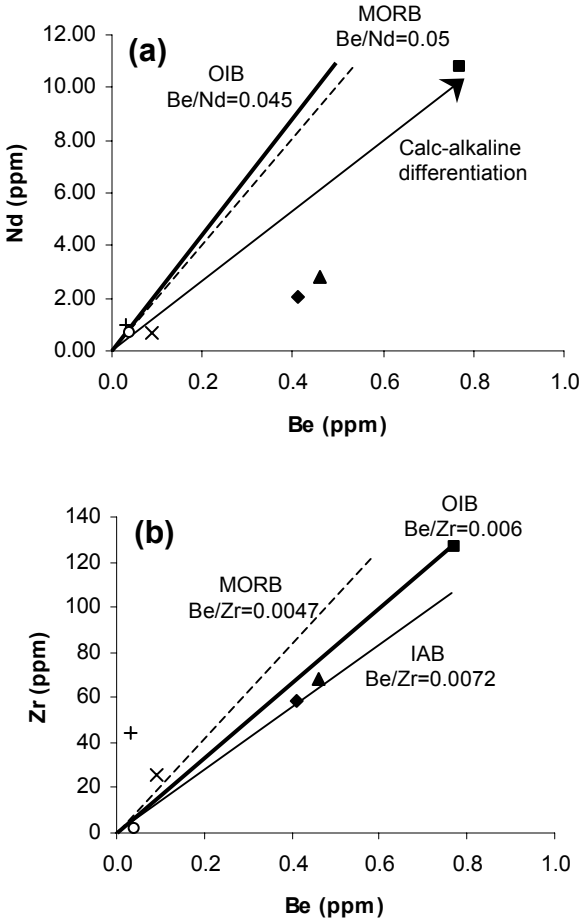

Figure B-23. Lavas generated in different terrestrial oceanic magmatic environments (MORB-dashed, OIB-bold, IAB-arrow) define different slopes when Be is compared to (a) Nd and (b) Zr (Ryan and Langmuir, 1987). Symbols as in Figure B-21. Data for Dhofar 019 from Neal et al. (2001).

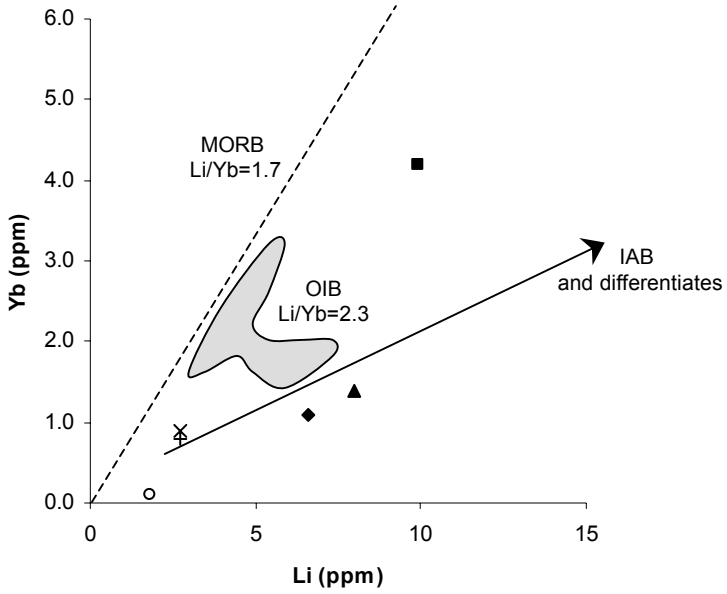

Figure B-24. Li vs. Yb for meteorites in this study. Symbols as in Figure B-21. Li/Yb ratios for MORB (dashed), OIB (shaded region), and IAB (arrow) are shown for comparison (Ryan and Langmuir, 1987). Data for Dhofar 019 from Neal et al. (2001).

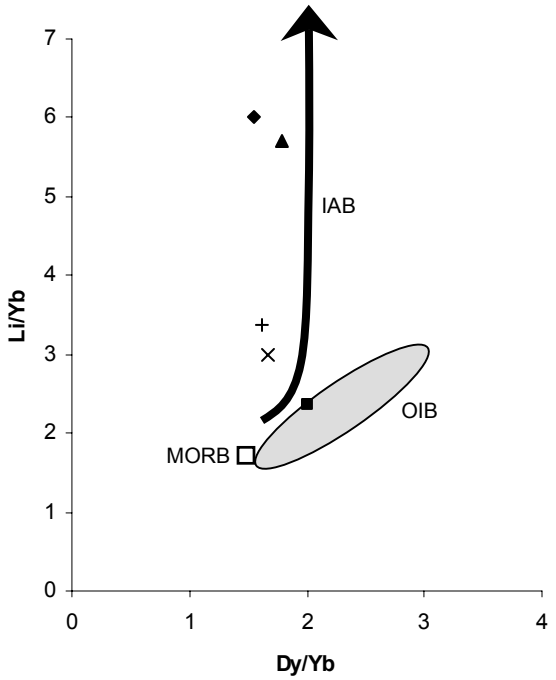

Figure B-25. Li/Yb vs. Dy/Yb for meteorites analyzed in this study. Symbols as in Figure B-21. Values for OIB (shaded), MORB (box), and IAB (arrow) are shown for comparison (Ryan and Langmuir, 1987). Data for Dhofar 019 from Neal et al. (2001).

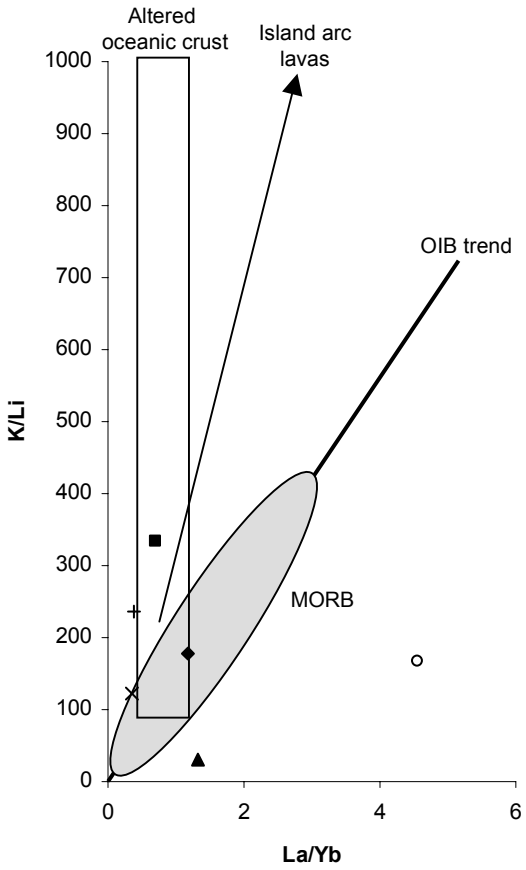

Figure B-26. On a plot of K/Li vs. La/Yb, OIB (bold) and MORB (shaded region) define similar slopes, but arc lavas (arrow) define a distinctly different trend (Ryan and Langmuir, 1987). The steeper slope of arc lavas results from the contribution of altered oceanic crust (box) in the source region. Symbols as in Figure B-21. Data for oceanic crust from Donnely et al. (1980). Data for Dhofar 019 from Neal et al. (2001).

Figure B-27. Li and Be compared to (a,d) $\varepsilon^{143}Nd$, (b,e) initial $^{87}Sr/^{86}Sr$, and (c,f) La/Yb ratios (data references as in Figure B-21). Arrows indicate apparent trends despite greater scatter in some of the data. Li and Be in Los Angeles seem anomalous when compared to La/Yb. Symbols same as Figure B-21. Data for NWA 480 from Barrat et al. (2002b). Data for NWA 856 from Jambon et al. (2002). Data for EETB79001 from Lodders (1998).

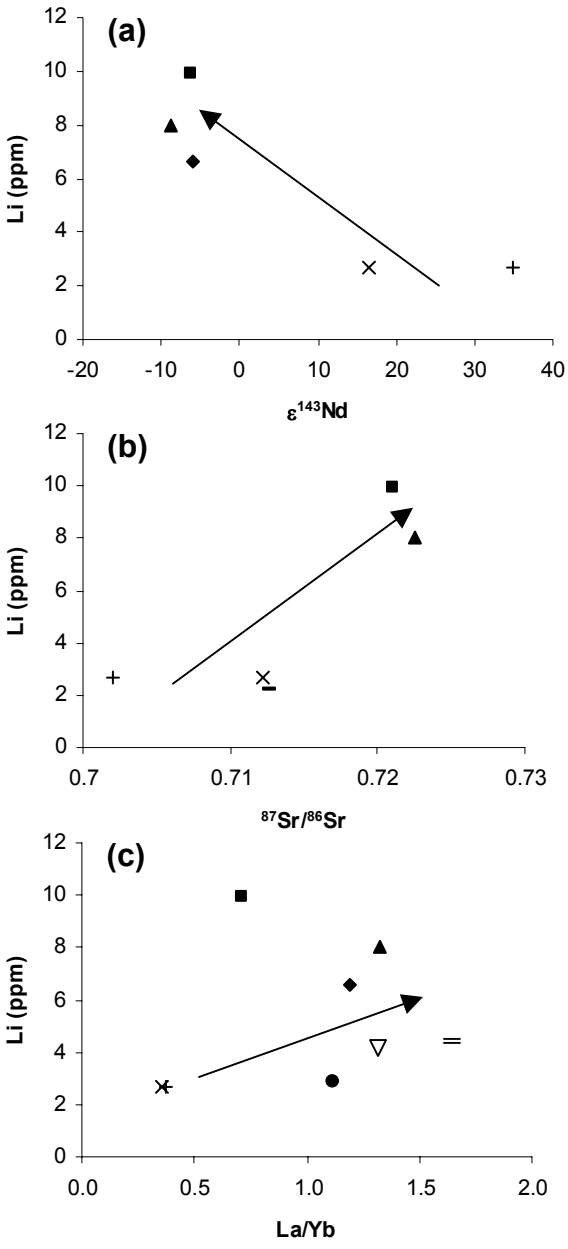
(a)
Li (ppm)
12
10
8
6
4
2
0
-20
-10
0
10
20
30
40
ε143Nd
(b)
Li (ppm)
12
10
8
6
4
2
0
0.7
0.71
0.72
0.73
87Sr/86Sr
(c)
Li (ppm)
12
10
8
6
4
2
0
0.0
0.5
1.0
1.5
2.0
La/Yb

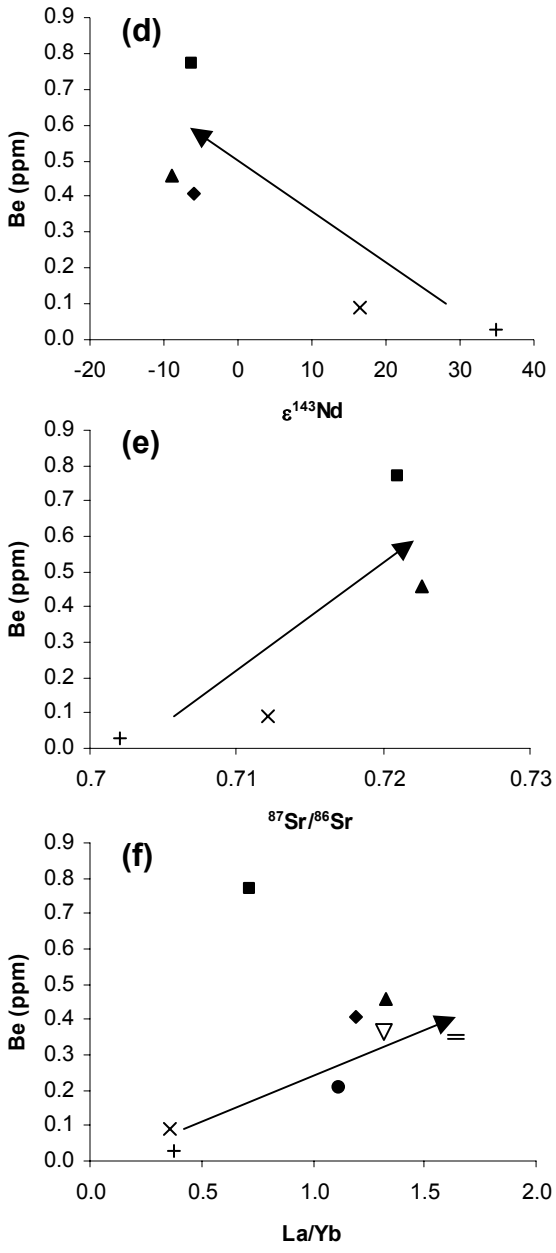
(d)
Be (ppm)
0.9
0.8
0.7
0.6
0.5
0.4
0.3
0.2
0.1
0.0
-20
-10
0
10
20
30
40
ε143Nd
(e)
Be (ppm)
0.7
0.71
0.72
0.73
87Sr/86Sr
(f)
Be (ppm)
0.0
0.5
1.0
1.5
2.0
La/Yb

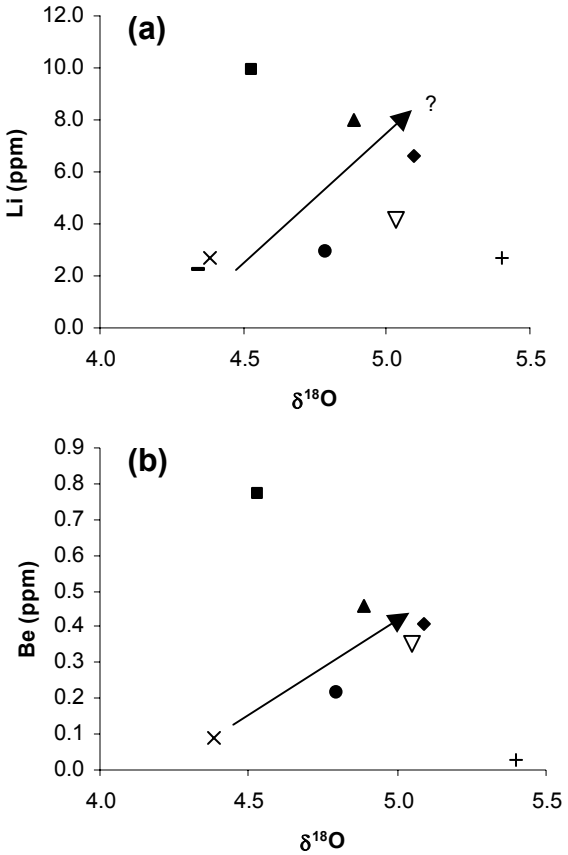

Figure B-28. Oxygen isotopes ($\delta^{18}O$) compared to (a) Li and (b) Be data for basaltic shergottites. Be data show a stronger correlation except for the seemingly anomalous $\delta^{18}O$ composition of Dhofar 019 and Be composition of Los Angeles. Symbols as in Figure B-21. Data for NWA 480 from Barrat et al. (2002b). Data for NWA 856 from Jambon et al. (2002). Data for EETB79001 from Lodders (1998).

VITA

In 1971, Valerie Priscilla Slater was born in Lubbock, Texas to parents Irma and Victor. She moved with her family to Asheville, North Carolina in 1973 where she lived for the next eleven years. After living in Gastonia, North Carolina for one year, she moved to Eden, North Carolina where she graduated from J. M. Morehead High School in May of 1989.

In the Fall of 1989, Valerie enrolled in the University of North Carolina at Wilmington where she received her Bachelor of Science degree in Geology in 1994. After a two-year hiatus from academia, Valerie began graduate school in the University of Tennessee's Department of Geology where she received her Master of Science degree in 1998. Following graduation, Valerie worked as a geologist for an environmental consulting firm for two years. In 2001, Valerie returned to graduate school in the Department of Earth and Planetary Sciences (formerly Geology) at the University of Tennessee where she received her Doctor of Philosophy degree in Geology in August of 2005.

Valerie will be moving to the District of Columbia with her husband and daughter to begin a post-doctoral position at the Smithsonian National Museum of Natural History.